ENHANCED ELECTRICAL TRANSPORT IN MIXED ALKALI HALIDE CRYSTALS

by

Periasamy MANORAVI

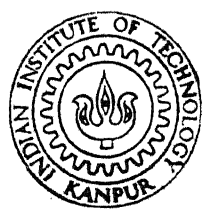

DEPARTMENT OF PHYSICS

INDIAN INSTITUTE OF TECHNOLOGY KANPUR

June, 1991

ENHANCED ELECTRICAL TRANSPORT IN MIXED ALKALI HALIDE CRYSTALS

A Thesis Submitted
in Partial Fulfilment of the Requirements
for the Degree of
DOCTOR OF PHILOSOPHY

by

Periasamy MANORAVI

to the

DEPARTMENT OF PHYSICS

INDIAN INSTITUTE OF TECHNOLOGY KANPUR

June, 1991

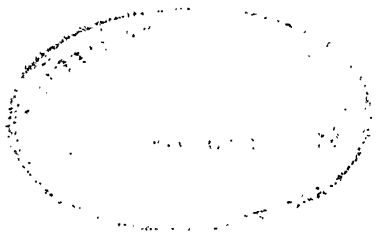

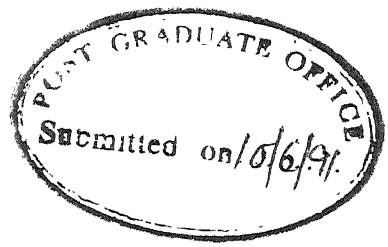

CERTIFICATE

It is certified that the work contained in the thesis entitled "ENHANCED ELECTRICAL TRANSPORT IN MIXED ALKALI HALIDE CRYSTALS", by "P. Manoravi", has been carried out under my supervision and that this work has not been submitted elsewhere for a degree.

June, 1991

(K. SHAHI)

Department of Physics
and Materials Science Program
I.I.T - Kanpur

to

my parants

& my brother

SYNOPSIS

Name of Student: P.Manoravi Roll No: 8610968

Degree for which submitted : Doctor of Philosophy

Department : Physics

Thesis Title : ENHANCED ELECTRICAL TRANSPORT IN MIXED ALKALI HALIDE CRYSTALS

Name of thesis supervisor : Dr. K. Shahi

Month and year of submission : Febrauary, 1991

Mixed ionic crystals, eg., KCl-KBr, KBr-KI etc., have attracted considerable attention in recent times. Several properties (parameters) such as lattice constant (Vegard's law), molar volume etc., are found to vary monotonically between the two end members. However, the behaviour of ionic conductivity (σ) and diffusion coefficient (D) is rather unusual in the sense that the σ (and D) of the mixed crystals is generally higher than either of the end (or parent) members. The magnitude of the enhancement in σ (or D), which of course depends on the mismatch (size difference) between the host and homovalent dopant ions, could be as large as two to three orders of magnitude in certain cases. However, the ionic conductivity studies on mixed crystals are few and far between, and the conduction processes in general are poorly understood at present. The observed enhancements in σ (or D) cannot be explained on the basis of the existing classical doping concept, nor by any law of averages.

The aim of the present work was to (i) study the effect of homovalent dopants on σ and related transport parameters, (ii) develop possible highly conducting solid electrolytes and (iii) propose a model which would explain the mechanism of ionic transport in the mixed crystals.

Chapter 1 reviews the historical background and the various methods employed so far to enhance the σ of normal ionic solids. The existing theory of ionic conduction is briefly presented in Chapter 2. Besides, the concept of lattice loosening (LL) model and the CBΩ model which bear relevance to conduction in mixed crystals are also discussed in this Chapter.

Chapter 3 consists of experimental techniques used in the present work. Since the alkali halides are hygroscopic, all the operations which include the materials preparation and their subsequent electrical characterization, were carried out inside a dry box. The impedance measurements were carried out on well sintered pellets using HP 4192A low frequency impedance analyzer using platinum paint or platinum foil as electrodes. The samples were also characterized by differential thermal analisis (DTA, LINSIS model L62) and X-ray diffraction for the phase diagram studies.

The complex impedance analysis (CIA) technique is presented in Chapter 4. The CIA plots for most of the mixed crystal are found to be semicircular, suggesting that the cell assembly is equivalent to a resistance and a capacitance in parallel. However, the CIA plots for LiBr-rich samples show an additional

tail in the low frequency region which was attributed to electrode/electrolyte interfacial effects.

The phase diagram and the σ results obtained for all the five systems, viz., KBr-NaI, KBr-NaBr, NaBr-NaI, NaBr-LiBr and NaCl-NaBr are presented in Chapter 5. The KBr-NaI system is found to form a complete solid solution only above 400°C. A maximum σ enhancement by a factor of 500 with respect to pure KBr is observed for $K_{0.3}Na_{0.7}Br_{0.3}I_{0.7}$ solid solution. The overall behaviour of the conductivity and the activation energy is consistent with that of the solidus curve. Interestingly, the σ of the two phase mixtures in KBr-NaI system is also found to be orders of magnitude higher than that of the corresponding solid solution.

In KBr-NaBr system, a maximum σ enhancement by a factor of 36 with respect to pure KBr, and 14 with respect to pure NaBr, is observed at 400°C for $K_{0.58}Na_{0.42}Br$ solid solution. The phase diagram solidus curve exhibits a flat minimum between 42 and 73 mole percent (m/o) NaBr which is also reflected in the conductivity - composition (σ-x) plots at constant temperatures. In NaBr-NaI system, the maximum enhancement in σ by a factor of 46 with respect to pure NaBr is observed at 400°C for $NaBr_{0.3}I_{0.7}$ solid solution. While a maximum enhancement in σ by factors of 2.3×10^4 is observed at 400°C in NaBr - 70 m/o LiBr mixed crystal, only a small enhancement (≈ 2 times at 400°C) is observed in NaBr- 40 m/o NaCl with respect to pure NaBr. Both σ-x isotherms and the activation energy (E_a) versus composition plots follow a pattern which is consistent with the melting (solidus)

curve of the phase diagram for all the system studied. The ionic conductivity results are analyzed in view of the LL model, which suggests that the substitution of homovalent dopants introduces strain in the host lattice, weakens the bonding between the ions and reduces the melting point, energies of formation and migration of the defects and hence increases the σ. The agreement between the observed and calculated σ-x curves using LL model is quite satisfactory in all the above systems studied.

Chapter 6 presents a comprehensive discussion on the ionic conductivity results. The validity of the LL model is examined in two different ways. Since the melting (solidus) curve of the phase diagram and the σ-x plot are found to be very well correlated, it has been suggested that a part of the phase diagram, viz, the solidus curve, may be calculated from the conductivity data on mixed crystals.

The CBΩ model is applied to the present mixed crystal systems and its validity is discussed. Finally, a model of (crystal) melting based on creation of vacancies is suggested. According to this model, the crystals start melting when a critical concentration of Schottky defects is attained. Since the concentration of point defects gets enhanced in the mixed crystals, the critical concentration is attained at a lower temperature and hence melting occurs at lower temperatures.

ACKNOWLEDGEMENTS

It is my pleasure to take this oppertunity to acknowledge Dr. K. Shahi, for his excellent guidence throughout my Ph.D programme, without whome it would have been impossible to produce this thesis. I am very grateful to him for his kind encouragements.

I wish to thank prof. A.K. Majumdar and Dr. D. Sahadev for their periodic review and comments on my work and their personnel encouragements.

I am also grateful to my labmates Ms. Sujata, Ms. Shiuli, Dr. Y.P. Yadava, Mr. Padmanaban, Mr. Ashok Kumar, Dr. Ajay Kumar, Mr. Ghosal, Mr. Jacob, Mr. Tyagi, Mr. G.S. Battacharya for their kind co-operation in the lab.

My sincere thanks are due to Mr. J.N. Sharma, Mr. Sairam, Mr. Baskar, Mr. Viswanath Singh, Mr. Jawar Singh, Mr. T. Raj, Mr. V.P. Sharma, Mr. B. Sharma, Mr. B.K. Jain, Mr. Uma Shankar, Mr. Srivastava, Mr. Pal, Mr. Paswan and Mr. Prasad for their continuous help during my work by various means.

I am very fortunate to get friends like Dr. Rathakrishnan and his family, Ilango, Govind, Ramesh and his family, Sampath Kumar, Ponnusamy, Varadarajan, Kaja, Immi, Ranga, Ponds, Kasi, P.S. Pandian, S.R. Pandian, Narayanan, Devanand, Sampath, Chandru, Manzoor, Murali, Bangui, Siddarth, Saravanan, Arul and Kottes, who made my campus life as pleasent and a memorable one.

Finally, I would like to thank Kaja for a neat typing.

CONTENTS page

LIST OF FIGURES

LIST OF TABLES

page

CHAPTER-1

INTRODUCTION

1.1 Historical Developments:

The ionic conduction, i.e., the charge transport by movement of ions, was observed by the great experimentalist Faraday as early as 1830. Based on his classic studies on both liquid and solid ionic conductors, Faraday was able to put forward what is known as "Faraday's law of electrolysis". It states that "purely ionic conduction will result in the liberation of components of the salt which are transported to the electrodes at the rate of one gram-equivalent for every Faraday of electricity (i.e., 96500 Coulombs) passed". The suspected presence of ionic conduction in a solid may be verified by measuring the weight of the products of the electrolytic decomposition deposited at the electrodes, together with the quantity of electricity required to effect the decomposition.

The pioneering work by Tubandt (1920) not only verified the Faraday's law but established it firmly for solid ionic conductors as well. Tubandt demonstrated unambiguously that α-AgI (stable above $147^{o}C$ and now known to be the best superionic conductor) was a predominantly cationic (Ag^{+} ion) conductor while $PbCl_2$ was an anionic conductor, the electronic conductivity being negligible in both cases.

From the crystallographic point of view, a perfect ionic crystal would be an insulator. The movement of ions from one part

of a perfect crystal to another part would be impossible if it were to occur only through direct exchanges between the anions and the cations. The energy which would have to be supplied to effect such a mechanism is so large (≈ 15eV, for example in NaCl) that in one gram-mole of the solid, such an event would occur only once in some ≈ 10^{30} years (Lidiard 1957).

In order to explain the ionic transport in solids, the presence of what is known as "point-defects" was first invoked by Frenkel (1926). He proposed that under the influence of thermal vibrations, the ions may occasionally receive enough thermal energy to leave their normal place of residence (lattice site) and get pushed into a nearby void space (interstitial site), ordinarily not occupied by any ion. Under further thermal excitation, such an interstitial ion may jump from one interstitial position to another, until it finds a vacant normal site and drops into it. In presence of an electric field, the (positive) interstitial ions will jump more frequently in the field direction than in the opposite direction, giving rise to a net movement of charge (ionic conduction). Schottky (1935) developed a model in which there exists an equal number of anion and cation vacancies but no interstitial ions. Both Frenkel and Schottky type of point defects are now well accepted and constitute the basic foundation of the modern theories of ionic transport in solids which is the subject matter for Chapter -2.

The nature of the lattice disorder can be inferred from the simultaneous measurements of the unit cell expansion from the X-ray lattice parameter and the overall thermal expansion

(Lidiard 1957). In case of Frenkel disorder, the relative expansion of the unit cell volume as determined by X-rays, is identical with the relative macroscopic volume expansion. On the other hand, the relative macroscopic volume expansion generally exceeds that determined from the unit cell, if Schottky defects are present.

All silver halides like AgCl, AgBr, β-AgI (<147^{o}C) exhibit Frenkel defect while almost all alkali halides are known to display Schottky defect. AgBr is unique in that it appears to display simultaneously both (Schottky and Frenkel) types of defects, which becomes increasingly obvious at higher temperatures (Teltow 1949; Kurnick 1952; Friauf 1972). Indeed all solids can be said to exhibit both type of defects, it is the question of their relative magnitudes. In alkali halides, Mott and Littleton (1938) have calculated the heat of formation of Frenkel (H_F) and Schottky (H_S) defects. For example, in NaCl, they found H_F = 2.9 eV which is much larger than the value of H_S (1.86 eV), and, as a result, the concentration of Na^+ interstitials is negligible even at temperatures close to the melting point of NaCl. Thus NaCl, indeed all alkali halides, are said to exhibit Schottky type of defect.

1.2 Classification of Solid ionic Conductors:

Figure 1.1 compares the ionic conductivity of various crystalline ionic solids. Ionic solids are often classified into three categories based on their magnitude of conductivities:

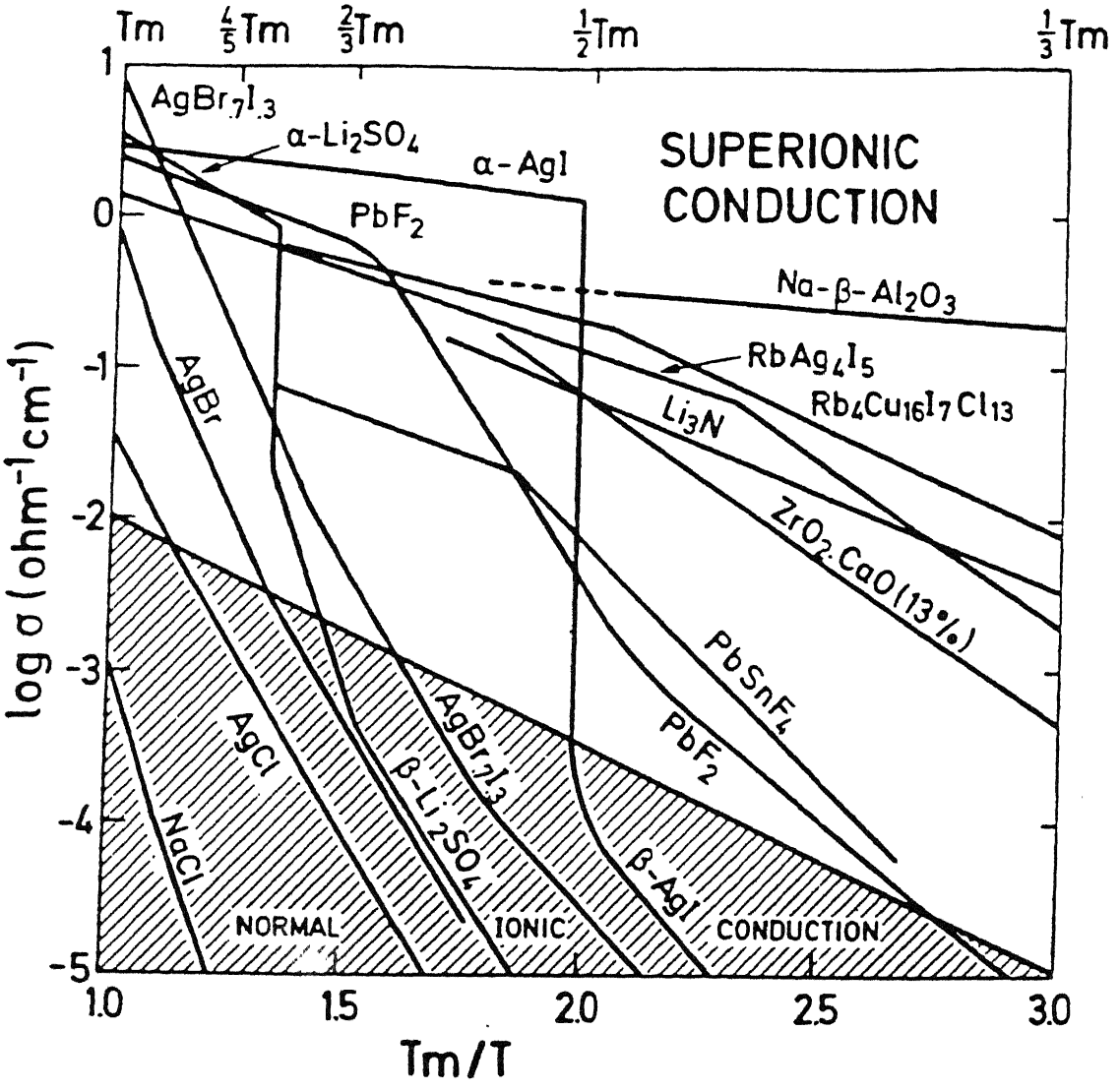

Fig.1.1 Logarithm of conductivity versus inverse of homologous temperature (T_m/ T) for a number of ionic conductors.

(i) poor ionic conductors; ($\sigma \leq 10^{-6}$ ohm^{-1} cm^{-1})*

eg: alkali halides

(ii) Moderate ionic conductors; ($10^{-6} \leq \sigma \leq 10^{-3}$ ohm^{-1} cm^{-1})

eg: AgBr, β-AgI, CaF_2, PbF_2, $CaO.ZrO_2$

(iii) Superionic conductors; ($\sigma \geq 10^{-3}$ ohm^{-1} cm^{-1})

eg: α-AgI, $RbAg_4I_5$, β-alumina, $Rb_4Cu_{16}Cl_{13}I_7$, $LiI-Al_2O_3$ etc.

It would be observed in Fig.1.1 that the ionic conductivity varies by many orders of magnitude from one solid to the other and also as a function of temperature. Thus while conductivity of NaCl is $\approx 10^{-26}$ ohm^{-1} cm^{-1} (Friauf 1972) at room temperature, that of $RbAg_4I_5$ is ≈ 0.1 ohm^{-1} cm^{-1} at about the same temperature. Similarly, the conductivity of NaCl changes from 10^{-11} to 10^{-3} ohm^{-1} cm^{-1} as temperature varies from 300 to 800°C, the melting point of the salt. The large variation of the conductivity with temperature is not very surprising in view of the fact that it is the product of two exponential functions of temperature, i.e.,

$$\sigma = e\, n(T)\, \mu(T)$$
$$= A \exp(-H / 2kT) \exp(-h / kT)$$

where n is the concentration and μ, the mobility of a particular type of defect, H and h, the formation and migration enthalpies respectively, k, the Boltzmann constant and T, the temperature.

---

* It must be emphasized that the above classification by no means can be strictly true. At most it may be regarded as a general guideline.

The conductivity (σ) is related to the diffusion constant (D) through the Nernst-Einstein relation.

$$\sigma = ne^2D/kT$$

where e is the charge of the conducting ion. The first diffusion measurements appear to have been done by von Hevesy and Seith (1929). There are several good review articles on diffusion theory (Süptitz and Teltow 1967; Beniere 1972; Le Claire 1970; Friauf 1972). The diffusion of impurity ions have been studied by Beniere et al (1969 and 1977) in alkali halides and by Laskar (1984 and 1989) in silver halides.

It should be pointed out here that even though both n(T) and μ(T) vary exponentially with temperature, it is the former, i.e., n(T), which is largely responsible for vast variation of the conductivity from solid to solid as well as with temperature. The mobility of the ions in various solids does not seem to change much as the data of Table 1.1 reveals. The mobility for all the normal salts lies in the range 10^{-4} to 10^{-6} $cm^2V^{-1}s^{-1}$

Table 1.1: Mobility (μ) of ions in various normal ionic solids at 600^oK (Friauf 1972)

	LiCl	NaCl	KCl	LiBr	NaBr	KBr
μ cm^2/V-s	10^{-4}	2×10^{-5}	2×10^{-6}	2×10^{-4}	3×10^{-6}	5×10^{-6}

at a moderate temperature of 600^{o}K, which is not very different from that (10^{-5} $cm^{2}V^{-1}s^{-1}$ at 600^{o}K) of Ag^{+} ion in α-AgI, a superionic conductor. Thus it is apparent that the mobility is not the decisive factor in determining the conductivity and the three categories of ionic solids, viz. poor, moderate and superionic conductors, could also be arrived at solely on the basis of concentration of defects (Chandra 1981);

(i) Poor ionic conductor or dilute point defect type ($n \leq 10^{17}$ cm^{-3})

(ii) Moderate ionic conductor or concentrated point defect type ($n \approx 10^{20}$ cm^{-3})

(iii) Superionic conductors ($n \approx 10^{22}$ cm^{-3}).

The materials falling under the last two categories, owing to their potential applications in high energy density batteries and other electrochemical devices, are generally grouped into one and called "Solid Electrolytes" or "Fast ion conductors", besides superionic conductors. The discovery of many such materials in the last two decades (Table 1.2) and the realization of their vast potential in energy conversion and storage devices have not only revived the studies on ionic solids but also given a new thrust to it.

The solid ionic conductors could also be categorized based on the nature of mobile ions; for instance, into cationic and anionic conductors. The cationic conductors can be further subgrouped as

(i) Li- ion conductors

(ii) Cu- ion conductors

(iii) H^+- ion(proton) conductors etc.

Similarly the anionic conductors may be further categorized as

(i) O^{2-}-ion conductors

(ii) F^- -ion conductors

There is yet another way of classification that has been used. According to this, the ionic solids may be put into either of the following group

(i) Crystalline ionic conductors

(ii) Amorphous solid electrolytes

(iii) Polymeric solid electrolytes

(iv) Composite solid electrolytes

1.3 Search for Solid Electrolytes:

Following the discovery of certain highly conducting solid ionic conductors such as Ag_3SI (Reuter and Hardel 1961); β-Al_2O_3 (Yao and Kumar 1967), MAg_4I_5 (M = K, Rb, NH_4; Owens and Argue 1967; Bradley and Green 1967) and the realization of their potential applications in devices, a great deal of effort during the last 2 decades has been made to develop improved solid electrolytes. The various techniques that have been used to enhance the ionic conductivity or to achieve better solid ionic conductors include,

(i) aliovalent doping of a salt

(ii) stabilization of "average" or disordered structure

Table 1.2

A list of significant (class of) solid electrolytes developed in the last 2 - 3 decades

Materials	Reference
ZrO_2 (CaO) ThO_2 (Y_2O_3)	Kiukkola and Wagner (1957 a & b)
Ag_3SI	Reuter and Hardel (1961)
Li_2SO_4	Kvist and Lunden (1965)
$RbAg_4I_5$	Owens and Argue (1967) Bradley and Green (1967)
Na- β- alumina	Yao and Kumer (1967)
$Ag_7I_4PO_4$ and $Ag_{19}I_{15}P_2O_7$	Takahashi et al (1972)
Cu - based solid electrolytes	Takahashi et al (1973)
Polymeric electrolytes	Furton et al (1973) Armond et al (1978)
Composite electrolytes	
$LiI - Al_2O_3$ $AgI - Al_2O_3$ $Na_2SO_4 - Li_2SO_4$	Liang (1973) Shahi and Wagner (1981) Chaklanobis et al (1990)
$Na_{1+x}Zr_2Si_xP_{3-x}O_{12}$ NASICON	Hong (1976)
Li_3N	Boukamp and Huggins (1976) von Alpen et al (1977)
$Li_2P_2S_7 + LiI$ Glassy electrolyte	Malugani et al (1978)
Proton conductors	
Polymolibolic acid NH_4^+ - β- alumina	Nakamura et al (1976) Farrington and Briant (1978)
$Rb_4Cu_{16}I_7Cl_{13}$	Takahashi et al (1979)
Homovalently doped mixed crystals	Shulz (1952) Shahi and Wagner (1983)

(iii) Dispersion of fine insulating particles (eg; Al_2O_3, SiO_2)

(iv) Homovalent doping of a salt.

1.3.1 Aliovalent Doping:

The extraordinary influence of aliovalent dopants on the concentration of point defects, and hence on the charge carriers and conductivity, was first realized by Koch and Wagner (1937), and subsequently demonstrated extensively by Kelting and Witt (1949), Teltow (1949) and others. An impurity ion whose valancy is different from that of the corresponding host ion is referred to as aliovalent ion. Thus when an ionic solid (eg., alkali (M) halide (X), MX) is doped with divalent cations (eg., M^1X_2, M^1= Ca, Cd, etc) or divalent anions such as S^{2-}, CO_3^{2-} etc., the electrical charge neutrality requirement demands generation of excess defects of the compensatory type (cation vacancy or anion vacancy) which in turn increases the conductivity, often quite dramatically. The same principle is applicable to semiconductors. Thus when a semiconductor such as Si, Ge, etc is doped with a group III element (B,Al, etc) or a group V element (P,As, etc), excess of compensating charge carriers (holes or electrons) are generated, leading to a highly conducting , extrinsic (P- or n-type) semiconductor.

Earlier the aliovalent doping was primarily used to control the type of defects (majority charge carriers) and hence to enable the determination of transport parameters associated with individual charge carriers (See Chapter-2). Later the aliovalent doping was also effectively used to enhance the ionic

conductivity. Some examples are: Calcia (CaO) - stabilized ZrO_2 and many other related solid solutions which are well known O^{2-} ion conductors (Tuller 1981), LiI: Ca^{2+} (Schalaikjer and Liang 1971 and 1972), Li_4SiO_4-PO_4^{3-} (Hu et al 1976), Li_2SO_4:Zn^{2+} (Lunden et al 1983) etc. The effect of aliovalent dopants on the concentration of point defects and hence on the ionic conductivity and its role in elucidating the ion transport mechanism(s) are further elaborated in Chapter-2.

1.3.2 Stabilization of Average Structure:

As pointed out earlier, Faraday observed the "conducting power of Ag_2S when hot", i.e., the high ionic conductivity in its high temperature α-phase, as early as 1833. Similarly, the high ionic conductivity in the high temperature α-phase of AgI was also observed quite early and has since been confirmed several times (Tubandt 1920; Kvist 1967; Shahi and Wagner 1981a and 1981b). The exceptionally high ionic conductivity in the high temperature modifications of these and other salts is attributed to their unique structure. For instance, α-AgI is said to have a bcc structure, in which anions (ie., I^- ions) occupy the 8 corner positions as well as the body center position. Thus the bcc lattice is essentially defined by anions alone. The two caions (Ag^+ ions) are distributed over 42 interstitial sites per unit cell. Thus there are many times more possible cation sites than there are ions to occupy them. This leads to a situation in which the statistical occupancy of the sites is much less than unity, ie., the cation which is here one moment is gone the next moment. This situation is variously described as average (not rigid)

structure, or molten sub-lattice (Geller 1977) or even lattice gas (Mahan 1976).

A great deal of effort was subsequently put into stabilizing this "average structure" at lower temperatures. Ag_3SI (Ag_2S+AgI) appears to be the first double salt (Takahashi 1966 a,b; Reuter and Hardel 1966) to possess the average structure and high conductivity. At present there are a large number of such new double salts. Table 1.3 lists some of the prominent superionic conductors which owe their high ionic conductivity to the "disordered" or "liquid-like" (average) structure, alongwith their β-α transition temperatures and conductivities. It is evident that the superionic α-phase in some cases has not only been stabilized near room temperature but even below it.

As Table 1.3 reveals, the superionic conductors with average structure are more numerous with Ag^+ ion transport than any other ion. There are several good review articles on the so-called "Ag^+ based superionic conductors" (Wiedersich and Geller 1970; Owens 1971; Takahashi 1973; Funke 1976; Shahi 1977; Chandra 1981). It should, however, be pointed out that not only copper and silver have similar metallic properties (eg., highest electrical conductivity among various metals) but their salts, particularly halides, also exhibit quite identical properties. It would seem that whatever Cu (Cu-salts) can do, Ag (Ag-salts) can do it better. Consistent with this, there are quite a few Cu-based superionic conductors (Takahashi 1973; Chandra 1981). The one listed in Table 1.3, Viz., $Rb_4Cu_{16}I_7Cl_{13}$, is the one which is

Table 1.3

Some selected superionic conductors with "average" or "molten" sub-lattice structure.

Compound	mobile ion	ionic (β)-(α)superionic transition temperature(^{o}C)	σ (ohm^{-1} cm^{-1}) (at T^{o}C)
α - Ag_2S	Ag^+	175	4.1 (200)
α - Ag_2Se	Ag^+	133	3.1 (200)
α - AgI	Ag^+	147	1.3 (150)
α - Ag_3SI	Ag^+	235	2 (240)
α - Ag_2HgI_4	Ag^+	52	2×10^{-3} (60)
$RbAg_4I_5$	Ag^+	-64	0.21 (22)
KAg_4I_5	Ag^+	-64	0.21 (22)
$Rb_4Cu_{16}I_7Cl_{13}$	Cu^+	-25	0.34 (25)
α - Li_2SO_4	Li^+	575	1.03 (600)
α - Li_2WO_4	Li^+	684	1.43 (700)
α - Na_2WO_4	Na^+	589	1.5×10^{-2} (800)

the best superionic conductor ($\sigma \approx 0.3$ ohm^{-1} cm^{-1} at 25^{o}C, Takahashi et al 1979). Unfortunately, Ag and Cu based solid electrolyte batteries have poor energy densities, and hence have only a limited commercial interest.

α-Li_2SO_4 is another important superionic conductor which has the "average" structure but its β - α transition temperature is too high ($\approx$ 575^{o}C) to permit any useful application. Moreover, all efforts (see for a review; Lunden 1986) to stabilize its double (complex) salts at lower temperatures have failed to produce any result, even though effort in this direction is still on (Lunden 1986; Deshpande et al 1986; Singh et al 1988; Prakash and Shahi 1987; Chaklanobis et al 1990).

1.3.3 Dispersion of Fine Insulating Particles:

Liang (1973) was the first to report orders-of-magnitude enhancement in the conductivity of LiI due to dispersion of fine insulating Al_2O_3 particles. Subsequently, the effect was found to be quite general, not just limited to dispersion of insulting particles such as Al_2O_3, SiO_2, fly-ash etc., but even dispersion of AgBr solid solution in β-AgI (Shahi and Wagner 1983), Na_2SO_4 solid solution in β-Li_2SO_4 (Chaklanobis et al 1990) etc., were found to enhance the conductivity significantly. Such highly conducting materials have shown good promise for high energy density batteries and are now popularly called "composite solid electrolytes". Table 1.2 also lists some of the important composite solid electrolytes.

1.3.4 Homovalent Doping:

The effect of homovalent dopants, ie., substitution of ions having the same valency as the corresponding host ions such as Br^- in AgI, on the ionic conductivity has been relatively poorly studied. The reason for this negligence seems to be the very nominal effect reported in the earliest investigations. For instance, the ionic conductivity of $KCl_{0.5}Br_{0.5}$ mixed crystals, ie., KCl doped with Br^- ion, was found to be only twice as large as that of pure KCl (Schulz 1952; See also Lidiard 1957). However, several recent investigations on mixed crystals have revealed that the effect of built-in wrong size of the homovalent ions depends strongly on the mismatch (size difference between the host and the guest ion). Table 1.4 lists some typical examples of mixed crystals and their conductivities at appropriate temperatures. An inspection of this table would reveal that the conductivity enhancement ranges from a factor of ten to thousand. The substitution of Br^- ions in β-AgI was found not only to increase the conductivities, but also to decrease the ionic-superionic (β-α) transition temperature (Shahi and Wagner 1982). The effect of Cl^- ion substitution in β-AgI was found to be similar but more pronounced (Ihara et al 1984) which reinforces the conjecture that larger the mismatch, more pronounced is the effect of homovalent dopants.

In the meantime, a few tentative models and theories have been suggested to explain the unusual transport properties of the mixed crystals. That the vacancy concentration in KCl-KBr mixed crystals is as high as 1% (Wallace and Flinn 1953) would suggest

Table 1.4

The electrical conductivity (σ_x) of some selected mixed crystals and the conductivity enhancement (σ_x/σ_o) relative to that of pure component (σ_o).

mixed crystals	conductivity ($ohm^{-1}\ cm^{-1}$)	σ_x/σ_o	at T(^oC)	reference
KCl+73 m/o KBr	3.3×10^{-5}	2	645	Schulz (1952)
KCl+70 m/o RbCl	5.5×10^{-5}	5	660	Holt et al (1969)
NaCl+47 m/o NaBr	8×10^{-5}	10	393	Bhima Sankaram & Basigir (1978)
CsCl+70 m/o TlCl	5.6×10^{-2}	7×10^{3}	387	Schiraldi and Pezzati (1978 a)
CsBr+70 m/o TlBr	2.1×10^{-3}	1.7×10^{3}	377	Schiraldi and Pezzati (1978 a)
AgCl+61 m/o AgBr	3×10^{-5}	25	127	Cain and Slifkin (1980)
AgI+4 m/o AgBr	4.3×10^{-6}	16	25	Shahi and Wagner (1982)
AgBr+30 m/o AgI	6.5×10^{-6}	77	25	Shahi and Wagner (1982)
AgI+10 m/o AgCl	7.9×10^{-5}	125	25	Ihara et al(1984)
KBr+50 m/o KI	2.9×10^{-4}	63	500	Shahi and Wagner (1983)
KBr+70 m/o KI	4.5×10^{-5}	9	596	Johannesen and McKelvy (1985)
LiBr+40 m/o LiI	1.8×10^{-6}	34	385	Gupta et al (1988)
LiBr+75 m/o LiI	5×10^{-7}	80	25	Mercier et al (1985)
KCl+50 m/o NaCl	8×10^{-6}	80	500	Erofeev and Hartmann (1988)

that the unusual behaviour of conductivity was essentially due to large change in the density of point defects. However, the above result was found to have been in error (Haven 1955).

According to lattice loosening model (Lidiard 1957; Shahi and Wagner 1983; Johannesen and McKelvy 1985 and 1986), the substitution of a homovalent ion which is either too large or too small (ie., never of the same size as the host ion), introduces strain in the lattice that generally, if not invariably, results in the lowering of the melting point of the salt. The above statement needs no justification; An inspection of a few phase diagrams in the "Phase Diagram for Ceramists" (1964) would suffice. It would be observed that the melting point vs composition (ie., liquidus and solidus) curves generally exhibit a minimum, and only rarely otherwise. The decreased melting point leads to lowering of the formation and migration enthalpies, hence more and more mobile defects and thus an increase in the conductivity. Chapter-2 deals with this semi-quantitative theory which has been found quite reasonable and satisfactory for a few mixed crystal systems.

Varotsos (1981,1986) has proposed a purely thermodynamical theory, called CBα model, which predicts, among other things, the composition of the mixed crystal which exhibits maximum conductivity and diffusion coefficient (D). This model, which works well for some systems, fails to explain the observed behaviour for several other mixed crystals. Besides, a major disadvantage of this model is that it does not predict the

magnitude of σ enhancement. This model is also discussed in Chapter-2 in more detail.

1.4 Statement of the Problem:

It is clear from the preceding discussion that considerable work has been done on aliovalently doped ionic solids, composite electrolytes as well as on superionic conductors with disordered, average structure. However, there are relatively fewer studies on homovalently doped mixed crystals. The aim of the present work, therefore, was to (i) enlarge the available data on mixed crystals, (ii) test/verify the existing lattice loosening and CBΩ models and/or modify them suitably so as to enlarge their acceptability, and (iii) examine the possible existence of intermediate double salts with average structure and high ionic conductivity.

The alkali halides were the obvious choice for this work as they (i) generally do not undergo any solid-solid transitions except cesium halides, and (ii) offer considerable choices with regard to the variation of the size of the homovalent dopants. Thus it has been possible to study the effect of homovalent cation and anion doping separately as well as simultaneously, and hence examine the role of wrong size, and the lattice loosening model critically. In addition, the phase diagrams of various binary systems have also been investigated as these, particularly the solidus (melting) temperatures, have a direct bearing on the ionic transport properties of the mixed crystals.

An important, though unintentional, achievement of this work has been the demonstration that the enhancement in the conductivity of composite electrolytes is not limited to dispersion of insulating particles like Al_2O_3 or SiO_2 only. Most of the mixed alkali halide solid solutions are known to precipitate, on cooling , into two phase mixtures at lower temperatures. It was found that this process of precipitation was generally accompanied by a sudden increase in the conductivity, contrary to the dictates of decreasing temperature, which could only be attributed to some dispersion-like effect. Thus it is possible to have what may be termed as "aluminaless" composite solid electrolytes.

Lastly, it has been demonstrated that the excellent correlation between the conductivity and the change (lowering) in the melting point permits the calculation of part of the binary phase diagram (solidus curve) from the known conductivity vs composition data.

CHAPTER-2

THEORY OF IONIC CONDUCTION

2.1 Ionic Conductivity of Pure Crystals:

The electrical conductivity (σ) is usually expressed as

$$\sigma = \sum_{k} n_k q_k \mu_k \qquad (2.1)$$

where n is the concentration, μ the mobility of the charge carriers, q the charge associated with the carrier and the summation is over all possible charge carriers (eg., vacancies, interstitials, electrons, holes etc.). However, in most ionic solids the contribution of electrons and holes to the overall conductivity is negligible compared to that of ions.

2.1.1 Concentration of Point Defects:

As pointed out earlier, to explain the presence of ionic conduction, the concept of point defects was invoked. At absolute zero degree Kelvin ($T = 0^{o}K$), every crystal is free of point defects. At $T > 0$, there is always a certain (finite) concentration of defects owing to thermal fluctuations. A large number of solids exhibit Schottky type of defect (cation and anion vacancies in equal number; for example, in monovalent salts like alkali halides), Frenkel type of defect is usually exhibited by silver halides, many oxides, rare earth fluorides, etc.

(a) Schottky Defects:

The production of Schottky defects, for example in alkali halides (MX), can be represented by the following reaction

equation†

$$\text{Crystal (MX)} \longleftrightarrow V_M' + V_X^{\cdot}$$

The condition of electroneutrality requires Schottky disorder to occur with the formation of equal number of cation (n_c) and anion (n_a) vacancies, ie., $n_c = n_a = n_s$ (say). This increases the configurational entropy (S_{cf})

$$S_{cf} = k \ln \left\{ \frac{(N + n_s)!}{N!\, n_s!} \right\}^2 \qquad (2.2)$$

where k is the Boltzmann constant, and the term inside the bracket gives the number of ways in which the n_s Schottky defects can be arranged over N lattice sites. The free energy change (ΔG) associated with the formation of Schottky defects is then given by (Lidiard 1957)

$$\Delta G = n_s g_s - kT \ln [(N+n_s)!/(N!\, n_s!)]^2 \qquad (2.3)$$

The equilibrium concentration of defects is then obtained by the usual procedure of minimizing the free energy change ($\partial \Delta G/\partial n = 0$). In the approximation $n_s << N$, we get

---

† The symbols have been used according to Kröger (1970) where V_M' means a vacancy at the site of M (cation) with an effective negative (') charge and $V_X^{\cdot}$ means a vacancy at the anion (X) site with an effective positive (·) charge.

$$\left[\frac{n_c}{N}\right]\left[\frac{n_a}{N}\right] = \exp(-g_s/kT) \qquad (2.4)$$

In terms of enthalpy (H_s) and entropy (S_s) of formation of Schottky defects ($g_s = H_s - TS_s$), the concentration of vacancies is given by

$$n_c = n_a \approx N \exp(S_s/2k) \exp(-H_s/2kT) \qquad (2.5)$$

Eq.(2.4) is often considered to be an expression of law of mass action, ie., the product of the concentration of anion vacancies and of cation vacancies is a constant, equal to $\exp(-g_s/kT)$, at a given temperature. Eq.(2.4) is valid even if the two concentrations are unequal, as in case of a salt like PbI_2 and in aliovalently doped crystals.

(b) **Frenkel Defects:**

In MX type solids, the formation of (cationic) Frenkel defect is expressed as

$$\text{Crystal} \longleftrightarrow V_M' + M_i^{\cdot}$$

where V_M' stands for a negatively charged vacancy at the cation site and $M_i^{\cdot}$ denotes the M ion (cation) with an effective positive charge, denoted by the superscript, (·), located at an interstitial site, denoted by the subscript (i). The Gibbs free energy of the crystal containing n_F Frenkel defects is increased by an amount $n_F g_F$ (g_F = free energy of formation of a Frenkel pair of defect), and simultaneously decreased by the configurational entropy arising from the disorder in the position of the interstitials and vacancies. For Frenkel defects, the

equivalent of Eq.(2.3) is

$$\Delta G = n_F g_F - kT \ln \{ \frac{N!}{(N-n_F)!n_F!} \quad \frac{N_1!}{(N_1-n_F)!n_F!} \} \qquad (2.6)$$

where N_1 is the number of interstitial sites per unit volume. The usual minimization procedure gives (for $n_F << N, N_i$)

$$\left[\frac{n_i}{N_i} \right] \left[\frac{n_c}{N} \right] = \frac{n_F^2}{NN_1} = \exp(-g_F/kT) \qquad (2.7)$$

Once again, the product of the two concentrations is a constant at a fixed temperature. Substituting $g_F = H_F - TS_F$, where H_F and S_F are enthalpy and entropy of formation respectively, and $N_1 = 2N$ for solids with rocksalt structure, we get

$$n_i = n_c = n_F = 2^{1/2} N \exp(S_F/2k) \exp(-H_F/2kT) \qquad (2.8)$$

2.1.2 Mobility of Defects:

During the diffusion and ionic conduction processes, the ions must move through the lattice from one site to another by jump process. The jump frequency w is expressed as (Glyde 1967)

$$w = v \exp(-g_m/kT) \qquad (2.9)$$

where v is the vibrational (attempt) frequency of the ions vibrating harmonically around their equilibrium positions and the migration energy g_m is the height of the barrier separating the two equivalent, adjacent sites.

Consider a solid with NaCl-structure. An interstitial position will be available for the cation at a distance a/2 where

a is the interionic distance. In presence of a dc electric field (E), the jump in the direction of the field takes place with an increased probability w^1 (Lidiard 1957; Chandra 1981)

$$w^1 = \nu \exp \{- (g_m - \tfrac{1}{2} eaE)/ kT\}$$

and a jump against the field will take place with a reduced probability w^{11} given by

$$w^{11} = \nu \exp \{- (g_m + \tfrac{1}{2} eaE)/ kT\}$$

The net number of ions moving per unit volume in the direction of field (assuming $eaE \ll kT$) is given by

$$n(w^1 - w^{11}) = nweaE/ kT \qquad (2.10)$$

where n is the number of charge carriers per unit volume. The amount of charge passing per unit area per unit time, ie., the current density is given by

$$j = n a^2 e^2 wE/ kT \qquad (2.11)$$

Comparing Eq.(2.11) with $j = \sigma E = ne\mu E$, we get the following expression for mobility

$$\mu = a^2 ew / kT$$

For vacancy conduction in NaCl-type solids, the charge carrier has to jump a distance 2a in the field direction. Hence the mobility term will contain an additional numerical factor 4.

$$\mu = \frac{4a^2 e}{kT} \nu \exp (s/ k) \exp (- h/ kT) \qquad (2.12)$$

where h and s are enthalpy and entropy of migration respectively.

2.1.3 Ionic Conductivity:

For ionic solids with rocksalt structure in which the dominant type of defects are cation and anion vacancies (Schottky defect), the ionic (electrical) conductivity, ie., Eq.(2.1) becomes

$$\sigma = e\,(n_c\mu_c + n_a\mu_a)$$

Substitution for the concentrations n_c and n_a (Eq.2.5) and the mobilities μ_c and μ_a (Eq.2.12) leads to

$$\sigma = \frac{4Na^2e^2}{kT}\left[v_c \exp\left(\frac{S_s}{2k} + \frac{s_{sc}}{k} \right) \exp\left\{ - \left(\frac{H_s}{2} + h_{sc} \right) / kT \right\} \right]$$

$$+ \frac{4Na^2e^2}{kT}\left[v_a \exp\left(\frac{S_s}{2k} + \frac{s_{sa}}{k} \right) \exp\left\{ - \left(\frac{H_s}{2} + h_{sa} \right) / kT \right\} \right] \qquad (2.13)$$

where e is the electronic charge and the subscripts s, c and a denote Schottky type, cation vacancy and anion vacancy respectively.

The above equation can be written in a simpilified form as

$$\sigma T = A_c \exp(-E_{ac}/kT) + A_a \exp(-E_{aa}/kT) \qquad (2.13a)$$

Thus if more than one defect types are involved in the conduction, the σ vs T dependence cannot be used to obtain any of the relevant transport parameters because of the complexity of Eq.(2.13a). Fortunately, for most ionic solids, a particular type

of defect dominates over the others (Friauf 1972) and, in that case, Eq.(2.13a) for a single conduction mechanism, can be written as

$$\sigma T = A \exp(-E_a/kT) \qquad (2.14)$$

For all alkali halides except for fluorides and cesium halides, the cation vacancies are the dominant charge carriers, and hence the parameters (A and E_a) in Eq. (2.14) can be assigned exclusively to cation vacancies.

2.2 Ionic Conductivity of (Aliovalently) Doped Crystals:

2.2.1 Concentration of Defects:

The principle of doping the pure crystal with aliovalent impurities was first realized by Koch and Wagner (1937) and subsequently illustrated by Kelting and Witt (1949); Teltow(1949) and others. Consider a solid whose intrinsic defect is either Schottky or Frenkel type. Let $x_c = n_c/N$ and $x_a = n_a/N$ be the molar fractions of the two complementary defects (cation and anion vacancies).Eq.(2.4) can then be rewritten as

$$x_c x_a = x_{os}^2 = \exp(-g_s/kT) \qquad (2.15)$$

where x_{os} is the molar fraction of Schottky defects in the pure (undoped) solid. If C is the molar fraction of the aliovalent dopant (say, Ca^{2+} in a monovalent salt like NaCl), the condition for electroneutrality demands that

$$x_c = C + x_a$$

Eq.(2.15) then becomes

$$x_c (x_c - C) = x_{os}^2$$

which is a quadratic equation in x_c. The solution is

$$x_c = \frac{C}{2}\left[\left(1 + \frac{4x_{os}^2}{C^2}\right)^{1/2} + 1\right] \qquad (2.16)$$

Substituting this value of x_c in Eq. (2.15), we get

$$x_a = \frac{C}{2}\left[\left(1 + \frac{4x_{os}^2}{C^2}\right)^{1/2} - 1\right] \qquad (2.17)$$

When the concentration of the dopant (C) is large compared to that of thermally produced (intrinsic) defects (ie., $C >> x_{os}$) which is generally the case at lower temperatures, Eqs.(2.16) and (2.17) lead to

$$x_c \approx C$$

and

$$x_a \approx x_{os}^2/C \quad << 1$$

Thus the concentration of one type of defects (cation vacancies, say) becomes nearly the same as that of the dopant (divalent cations, in the above example), and the concentration of the other (complementary) defect is made relatively negligible. The effect of doping was demonstrated most spectacularly in $AgBr:Cd^{2+}$ system by Teltow (1949).

At higher temperatures $x_{os} >> C$ (intrinsic region), the Eqs. (2.16) and (2.17) yield

$$x_c = x_a = x_{os} = \exp(-g_s/2kT)$$

which is the same as that for pure (undoped) crystal (Eq.2.4).

2.2.2 Ionic Conductivity of Doped Crystals:

Since the mobility of the defects remains almost unaffected due to the presence of a small quantity of aliovalent impurity, the conductivity expression for a doped ionic solid exhibiting Schottky defects can be written as

$$\sigma = \frac{4Na^2e^2}{kT} v_c \frac{C}{2}\left[\left(1 + \frac{4x_{os}^2}{C^2}\right)^{1/2} + 1 \right] \exp\left(\frac{s_{sc}}{k}\right) \exp\left(-h_{sc}/ kT\right)$$

$$+ \frac{4Na^2e^2}{kT} v_a \frac{C}{2}\left[\left(1 + \frac{4x_{os}^2}{C^2}\right)^{1/2} - 1 \right] \exp\left(\frac{s_{sa}}{k}\right) \exp\left(-h_{sa}/ kT\right) \qquad (2.18)$$

For $C >> x_{os}$ (extrinsic region), the σ can be approximated by

$$\sigma T = \frac{4Na^2e^2}{k} v_c C \exp\left(s_{sc}/ k\right) \exp\left(-h_{sc}/ kT\right) \qquad (2.19)$$

2.2.3 Estimation of Transport Parameters:

Eq.(2.19) is in a much simpler form and thus permits the determination of transport parameters (h_{sc} and s_{sc}) associated with the cation vacancies, from the conductivity data on divalent cation doped samples. Likewise, ionic conductivity measurements on divalent anion doped solid yields information associated with anion vacancies. Thus σ vs T data on pure, divalent cation doped and divalent anion doped solid leads to complete characterization of ionic transport processes.

The conductivity at high temperatures (intrinsic region, Eq.2.14) can be written as

$$\sigma_1 = A_1 \exp\left(-E_1/ kT\right) \qquad (2.20)$$

$$\text{where } A_1 = \frac{4Na^2e^2}{kT} v_c \exp\left(\frac{S_{sc}}{2k} + \frac{s_{sc}}{k}\right)$$

In the low temperature (extrinsic) region, the conductivity (Eq.2.19) can be expressed as†

$$\sigma_2 = A_2 \exp(-E_2/kT) \qquad (2.21)$$

$$\text{where } A_2 = \frac{4Na^2e^2}{kT} v_c C \exp\left(\frac{s_{sc}}{k}\right)$$

Thus the slope of log σ_2 vs 1/T plot directly gives the activation energy E_2, ie., the enthalpy of migration of defects (h) and hence the mobility can be calculated from σ_2 ($= \sigma_{ext}$). Similarly, Eq.(2.20) gives the activation energy $E_1 = \frac{1}{2} H + h$ and hence H, the enthalpy of formation of the defects, can be obtained. By having a knowledge of v_c, the pre-exponential factors A_1 and A_2 will give the formation and migration entropies of the defect. The knee temperature in the log σ vs 1/T plot occurs at the temperature at which the concentration of intrinsic (thermally produced) defects (x_{os}) equals that of divalent dopants ($x_{os} = C$).

In general the solubility of aliovalent impurities is always limited, particularly at lower temperatures. Thus, when a doped sample is cooled, the impurity phase may precipitate out at lower temperatures. In addition, a divalent cation impurity tends to

---

† The change in T is very small (by a factor of 2 to 3) compared to the change in σ, which is of several orders of magnitude. Hence it is customary to write Eq.(2.14) in form of Eq.(2.20).

form what is called impurity- vacancy pairs with the cation vacancies owing to their mutual attraction. Both the concentrations of the impurity-vacancy pairs and the solute (impurity phase) are temperature dependent. Thus the log σ vs 1/T plot for a typical salt like alkali halides is a curve of constantly changing slope. The modern data analyses employ computer fit methods (Chandra and Rolfe 1970 a and b) to obtain the best and most consistent set of transport parameters.

2.3 Theory of Ionic Conduction in Mixed Crystals:

2.3.1 The Lattice Loosening Model:

If the dopant has the same charge as the corresponding host ion, eg., NaCl doped with KCl, the classical doping concept (see Sec.2.2) cannot be used to explain any change (generally enhancement) in the conductivity. Eventhough a formal theory is yet to emerge, a semi-quantitative "lattice loosening model", based on certain empirical correlations observed in ionic solids, has been proposed by Shahi and Wagner (1983) and tested by Johannesen and McKelvy (1986; 1987) in KBr-KI and KCl-KBr systems.

According to the above model, the substitution of a wrong size ion generally introduces strain in the host lattice, and thereby weakens the bonding that eventually results in lowering of the melting point of the salt. That the phase diagrams of various binary systems generally exhibit a minimum in the melting point versus composition-(liquidus/ solidus) curves may be taken as evidence for it. Since the formation and the migration enthalpies of defects are correlated to the melting temperature

of the solid (Barr and Lidiard 1970; Kostopoulos et al 1975; Bollman 1980; Uvarov et al 1989; Bollman et al 1989; Varotsos and Alexopoulos 1986), the effect of wrong-size dopants ultimately is to decrease the formation and migration enthalpies of the point defects, and thus to increase both the concentration and the mobility of the point defects leading to enhanced ionic conductivity.

(i) Concentration of Defects in Mixed Crystals:

Whether the enhanced conductivity of the mixed crystals is due to increased concentration of charge carriers (defects) or due to enhanced mobility of the defects or due to a combined effect of both, has been a matter of investigation. Wallace and Flinn (1953) reported as much as 1% of vacancies in KCl-KBr mixed crystals from X-ray density measurements. However, such a large defect concentration was found inconsistent with the conductivity results which led Haven (1955) to conclude that the above measurements must be in error. However, Holt et al (1969) have investigated the pure and (divalent) cation-doped KCl-RbCl mixed crystals, and reported an enhanced concentration of vacancies.

A semi-quantitative expression for the concentration of point defects in mixed crystals can be arrived at in view of the existing good empirical correlation between the enthalpy of formation (H_s) of Schottky defects and the melting point (T_m) of ionic solids. Table 2.1 lists the formation enthalpy (H_s) and melting point data for alkali, thallium and lead halides. As first pointed out by Barr and Lidiard (1970), H_s and T_m are linearly related

Table 2.1

Enthalpy of formation and migration of some ionic solids

(Barr and Lidiard 1970; Friauf 1972; and Catlow et al 1979)

Salt	Melting point (°C)	Enthalpy of formation (eV)	Enthalpy of migration cation vacancies (eV)	anion vacancies (eV)
LiF	842	2.34-2.68	0.65-0.73	1.1, 0.67
LiCl	606	2.2	0.41	——
LiBr	550	1.8	0.39	——
LiI	452	1.34	0.38	——
NaF	992	2.42-3.0	0.52-0.95	1.46
NaCl	800	2.18-2.38	0.66-0.76	0.9-1.1
NaBr	755	1.72	0.8	1.18
NaI	661	1.46-2.27	0.47-0.78	——
KF	846	2.64-2.72	0.84-1.02	1.35-1.65
KCl	768	2.26-2.31	0.71	0.67-1.04
KBr	728	2.3-2.53	0.62-0.67	0.87-0.95
KI	680	0.6-2.2	0.6-1.21	0.5-1.5
RbI	647	2.1	0.6	1.6
CsCl	636	1.86	0.6	0.34
CsBr	636	2.0	0.58	0.27
CsI	621	1.9	0.58	0.3
TlCl	427	1.3	0.5	0.2
$PbCl_2$	500	1.56	——	0.35
$PbBr_2$	373	1.4	——	0.29

$$H_s = \alpha T_m \qquad (2.22)$$

where α is the proportionality constant and has a value of $\approx 2.14 \times 10^{-3}$ eV K^{-1}. Eq. (2.22) is an expression of the plain fact that stronger the bonding, higher is the melting point and hence more energy is required to displace the ions to form vacancies. Eq.(2.22) may be rewritten for mixed crystals as

$$H_{sx} = \alpha \; T_{mx}$$

(or) $$(H_{sx} - H_{so}) = \Delta H_{sx} = \alpha \; \Delta T_{mx} \qquad (2.23)$$

where x refers to the concentration of the mixed crystal, and H_{sx} and H_{so} the formation enthalpies of mixed and pure crystals respectively. Eq.(2.23) expresses that the change in the formation enthalpy of the mixed crystal ($\Delta H_{sx} = H_{sx} - H_{so}$) with respect to that of pure crystal is proportional to the change in the melting point (ΔT_{mx}) of the mixed crystal (T_{mx}) with respect to that of pure crystal (T_{mo}).

The expression for the concentration of Schottky defects (Eq.2.5) for mixed crystals can be rewritten as ††

$$n_x = B_x \exp(-H_x / 2kT) \qquad (2.24)$$

where B_x is a constant. Thus the ratio of the concentration of Schottky defects (n_x) in the mixed crystal to that in the pure crystal is given by

---

†† Since the mixed crystals dealt with in this thesis exhibit Schottky defects only, the subscript (s) is dropped henceforth.

$$\frac{n_x}{n_o} = \frac{B_x}{B_o} \exp \{ - (\frac{H_x - H_o}{2kT}) \} \qquad (2.25)$$

Substituting the value of $H_x - H_o = \Delta H_x = \alpha \Delta T_{mx}$ from Eq.(2.23) in Eq.(2.25)

$$\frac{n_x}{n_o} = \frac{B_x}{B_o} \exp \{ - \alpha \Delta T_{mx} / 2kT \} \qquad (2.26)$$

Thus the concentration of defects in the mixed crystals relative to that in pure crystal may be calculated from a knowledge of the change in the melting point (ΔT_{mx}) of the mixed crystal, provided the ratio of the pre-exponential factors

$$(B_x/B_o) = \exp [(S_x - S_o)/ 2k]$$

can be calculated. We are not aware of any such calculation in mixed crystals. However, the entropies of formation of vacancies in the mixed crystal (S_x) and that in the pure crystal (S_o), in general, will not be very different, and hence their difference ($S_x - S_o$) is likely to be negligible. Thus B_x/B_o may be taken to be of the order of unity (Shahi and Wagner 1983; Johannesen and McKelvy 1988), and Eq.(2.26) may then be written as

$$n_x/n_o \approx \exp (- \alpha \Delta T_{mx}/ 2kT) \qquad (2.27)$$

which expresses the relative concentration of vacancies as a function of the change in the melting point (ΔT_{mx}) of the mixed crystal. Since the melting point of the mixed crystal is generally less than that of the pure component, ie., ΔT_{mx} is negative, Eq.(2.27) predicts an enhanced concentration of

Schottky vacancies in the mixed crystal compared to that in the pure crystal.

(ii) Mobility of Defects:

The first experimental evidence to suggest that the mobility of the ions also increases in the mixed crystal was put forward by Bonpunt et al (1983) who carried out the tracer diffusion coefficient measurements on KI-RbI mixed crystals. A semi-empirical expression for the mobility of the ions in the mixed crystals can be obtained in a manner similar to that for the concentration (Eq.2.27), by utilizing the existing correlation between the migration enthalpy and the melting point (Barr and Dawson 1971). Table 2.1 also lists the enthalpy of migration (h) of vacancies in alkali and other halides. The h vs T_m behaviour is also found to be reasonably linear, and can be expressed by

$$h = \beta T_m - r \qquad (2.28)$$

where β (= 0.84 $\times 10^{-3}$ eV K^{-1}) and r(= 0.2 eV) are constants. For mixed crystals, Eq.(2.28) may be rewritten as

$$h_x = \beta T_{mx} - r$$

(or)
$$h_x - h_o = \Delta h_x = \beta \Delta T_{mx} \qquad (2.29)$$

The ratio of the mobility of cation vacancies in the mixed crystals to that in pure component may be written as (see Eq.2.12)

$$\frac{\mu_x}{\mu_o} = \frac{v_x}{v_o} \exp\left(\frac{s_x - s_o}{k}\right) \exp\left(-\frac{h_x - h_o}{kT}\right)$$

where v_x and v_o are the basic vibrational frequencies, and s_x and s_o, the migration entropies in the mixed and pure crystal respectively. To a first order approximation, we assume $v_x \approx v_o$ and $s_x \approx s_o$, so that

$$\frac{\mu_x}{\mu_o} \approx \exp\left(-\frac{h_x - h_o}{kT}\right) \qquad (2.30)$$

Substituting the value of $h_x - h_o = \Delta h_x = \beta\ \Delta T_{mx}$ from Eq.(2.29) in Eq.(2.30), one obtains

$$\frac{\mu_x}{\mu_o} \approx \exp\left(-\frac{\beta\ \Delta T_{mx}}{kT}\right) \qquad (2.31)$$

which predicts an enhanced mobility of vacancies as well in the mixed crystals as ΔT_{mx} is generally negative. The depression in the melting point at most is of the order of $100^{o}K$, ie., $\Delta T_{mx} = -100^{o}K$, hence $-\beta\ \Delta T_{mx}/\ kT \approx 1.6$ at $600^{o}K$. Thus the maximum enhancement in the mobility of the defects in the mixed crystals is expected to be of the order of 5 or so.

(iii) Ionic Conductivity in Mixed Crystals:

The ratio of the mobility of cation to that of anion vacancies in the mixed crystals remains almost the same as that in the component crystals over the entire composition range, as inferred from the diffusion coefficient measurements in KBr-KCl (Beniere and Haribabu 1987) and in KI-RbI (Bonpunt et al 1983) mixed crystals. Thus, if the cation vacancies are the more mobile species in the pure component, they are likely to remain so in the mixed crystals as well. Thus assuming that the cation vacancies are the dominant charge carriers, the ionic

conductivity in mixed alkali halide crystals (σ_x) relative to that of pure crystal (σ_o) may be expressed as

$$\frac{\sigma_x}{\sigma_o} = \frac{n_x}{n_o} \frac{\mu_x}{\mu_o}$$

Substituting the values of (n_x/n_o) and (μ_x/μ_o) from Eqs. (2.27) and (2.31), we get

$$\frac{\sigma_x}{\sigma_o} \approx \exp \{ - \frac{(\frac{1}{2} \alpha + \beta) \Delta T_{mx}}{kT} \} \qquad (2.32)$$

which on substituting the values of the constants α and β and the Boltzmann constant $k = 8.62 \times 10^{-5}$ eV K^{-1}, yields

$$\sigma_x / \sigma_o = \exp \{ -22.17 \Delta T_{mx} / T \} \qquad (2.33)$$

The above equation which is based on the lattice loosening (LL) model and the empirical correlations between the enthalpies of formation and migration vs T_m (Eqs.2.22 and 2.28), expresses the enhancement in σ_x of the mixed crystals relative to that of the pure crystal (σ_o) as a function of the change in the melting point due to the substitution of homovalent ions. An inspection of various binary alkali halide phase diagrams (Phase Diagram for ceramists 1964) reveals that the lowering in the melting point (ΔT_m) ranges between 50 and 125^{o}C. Eq.(2.33) would thus suggest that the enhancement in the conductivity of various mixed crystals may be expected to be in the range $\approx$ 10 to $\approx$ 250 at $\approx$ 500^{o}K and $\approx$ 6 to $\approx$ 100 at 600^{o}K. The data given in Table 1.4 are, by and large, in broad agreement with this prediction Eq.(2.33) and the LL model will be further examined in Chapter-5.

2.3.2 The Maximum Conductivity Composition:

(a) Lattice Loosening Model:

The LL model contained in Eq.(2.32) predicts the conductivity enhancement as a function of the depression in the melting point (ΔT_{mx}). Thus, if ΔT_{mx} is known as a function of composition, Eq.(2.32) can be used to predict the conductivity at any desired composition. It is obvious that within the LL model, the maximum conductivity composition would be the same as that at which the melting point is minimum. In other words, the maximum in the σ_x vs x plot would coincide with the minimum in the T_m vs x plot of the phase diagram. The available experimental results, though very few, do support the above prediction.

(b) The CBα Model:

Varotsos (1981) has proposed a purely thermodynamic theory to predict the composition corresponding to the maximum enhancement in σ and the diffusion constant (D) in the binary mixed crystal systems. This so-called CBα theory is briefly outlined below.

Let v_o and v_1 be the volume per molecule of the pure component-I and II respectively (assuming $v_1 > v_o$) and let V_o and V_1 denote their respective molar volumes such that

$$V_o = Nv_o$$

and

$$V_1 = Nv_1$$

where N is the Avogadro's number. If we define the defect volume v^d as the increase in volume V_o by replacing one molecule of component-I by one molecule of component-II

ie., $$v^d = v_1 - v_o \qquad (2.34)$$

then the addition of one molecule of component-II to a crystal containing N molecules of component-I will increase its volume by $v^d + v_o$ (Varotsos 1981; Varotsos and Alexopoulos 1986).

Now, the volume V_{N+n} of a mixed crystal containing N molecules of component-I and n molecules of component-II is given by

$$V_{N+n} = V_o + n\,(v^d + v_o)$$

(or) $$V_{N+n} = V_o + (Nv^d + V_o)\, n/N \qquad (2.35)$$

In terms of the molar fraction, $x = n / (N+n)$ of component-II, the molar volume V of the mixed crystal can be written as

$$V = (1-x)\, V_o + x\, V_1 \qquad (2.36)$$

The molar volume V of the mixed crystal and V_{N+n} are related as

$$V_{N+n} = (1 + n/N)\, V \qquad (2.36a)$$

Differentiating Eq.(2.35) with respect to pressure at constant T, we get

$$kV_{N+n} = k_oV_o + (k_dNv^d + k_oV_o)\, n/N \qquad (2.37)$$

where k, k_o and k_d refer to compressibility of the mixed crystal, pure crystal-I and the defect volume ($k_d = -1/v^d \; dv^d/dP$) respectively.

The compressibility ratio, k_d/k_o, can be derived from Born's model (Smith 1968; Smith and Roberts 1968)

$$\frac{k_d}{k_o} = 1 + \frac{4}{9}\frac{(n^B + 3)}{(dB_o/dP) - 1} \qquad (2.38)$$

where n^B and dB_o/dP are the Born's exponent and the pressure derivative of isothermal bulk modulus for the pure crystal-I respectively.

If we define $\lambda = (V_1/V_o)-1$, Eqs.(2.35),(2.36) and (2.37) lead to (Varotsos and Alexopoulos 1986)

$$\frac{B}{B_o} = \frac{1 + x\lambda}{1 + x\lambda\,(k_d/k_o)} \qquad (2.39)$$

Let Ω and Ω_o refer to the mean volume per atom of the mixed and pure crystal-I (ie., $V/V_o = \Omega/\Omega_o$). Multiplying Eq (2.36) and (2.39) , we get

$$\frac{B\Omega}{B_o\Omega_o} = \frac{(1 + x\lambda)^2}{1 + x\lambda\,(k_d/k_o)} \qquad (2.40)$$

where B (=1/k) and B_o (=1/k_o) are the isothermal Bulk modulus of the mixed and pure crystal-I.

Let us assume that a single mechanism dominates the conduction process, as usual. Varotsos et al (1978) have proposed an empirical theory that the Gibbs free energy of formation (g_f) and migration (g_m) of a defect can be written as

$$g_f = c_f B \Omega \qquad (2.41a)$$

and

$$g_m = c_m B \Omega \qquad (2.41b)$$

where c_f and c_m are constants (independent of temperature and pressure) which depend only on the kind of defect (or defect

mechanism) involved. Therefore the ratio of the conductivity (or diffusion coefficient) of a mixed crystal to that of pure crystal is †

$$\frac{\sigma}{\sigma_o} \text{ (or) } \frac{D}{D_o} = \exp\left(- \frac{g_f + g_m - g_{fo} - g_{mo}}{kT} \right)$$

which in combination with Eqs. (2.41a) and (2.41b) yields (Varotsos and Alexopoulos 1986)

$$\frac{\sigma}{\sigma_o} \text{ (or) } \frac{D}{D_o} = \exp\left[- \frac{C_o B_o \alpha_o}{kT} \left(\frac{CB\alpha}{C_o B_o \alpha_o} - 1 \right) \right] \qquad (2.42)$$

Where C and C_o are constants corresponding to the mixed and pure crystals respectively. Eq.(2.40) can be substituted in Eq.(2.42) which basically reflects the variation of the conductivity (or diffusion coefficient) with the composition. The variation in 'C' with respect to x is very small, and Eq.(2.42) predicts a maximum in (σ/σ_o) or (D/D_o) at a molar concentration (x_m) of component-II given by (Varotsos and Alexopoulos 1986).

$$x_m = \frac{(k_d/k_o) - 2}{\lambda (k_d/k_o)} \qquad (2.43)$$

The Eq.(2.43) has been found to predict 'x_m' correctly for several systems, viz, NaCl-NaBr, KI-RbI, KI-NaI, KCl-RbCl and KBr-KI. The CBα model will be re-examined further in Chapter-5.

---

† The ratio of pre-exponential factor is taken as unity, as assumed in the previous sections.

2.4 Enhanced Ionic Conduction in Multiphase Systems:

The enhancement in ionic conductivity by several orders of magnitude due to dispersion of fine insulating Al_2O_3 particles in LiI was first observed by Liang (1973). A number of systems which have since been investigated include AgI-Al_2O_3 (Shahi and Wagner 1981), CuCl-Al_2O_3 (Chang et al 1979), HgI_2 - Al_2O_3 (Pack1979), AgCl-Al_2O_3 (Dudney 1987), AgBr-Al_2O_3 (Mercier 1985), $PbCl_2$-Al_2O_3 (Brune and Wagner 1987) and LiBr-Al_2O_3 (Nakamura and Goodenough 1982, Gupta et al 1988) etc. Besides, other dispersoids such as SiO_2, Fly-ash etc. have also been tried in AgI (Shahi and Wagner 1982). All these studies suggest that the enhancement in ionic conductivity due to dispersion of fine insulating particles into another matrix is a rather general phenomenon and that the enhancement in the conductivity ranges between one and three orders of magnitude.

While the classical doping theory cannot explain the observed features, Jow and Wagner (1979) proposed that the dispersoids may possess a surface charge which, when embedded in another matrix, generate excess of compensating defects around its immediate neighbourhood and thereby enhance the σ. They showed that the σ enhancement is proportional to $(V_f/\ 1-V_f)\ 1/r$ for lower concentration of dispersoids, where r is the radius of the dispersoids and V_f, their volume fraction. Dudney (1985) has made further investigations on the possible formation of space-charge layer of finite thickness in the boundary regions between the dispersoid and the host matrix. Maier (1985 a,b) has suggested an enhanced concentration of defects in the space-

charge region. For dispersoids of smaller size, more surface area is available, and hence the conductivity enhancement would be larger, as observed experimentally (Shahi and Wagner 1981).

There exists yet another model called "random resistor network (RRN) model" (Bunde et al 1985; Roman et al 1986, Roman and Yussouff 1987) based on the calculations by means of Monte-Carlo simulations. This RRN model assumes the existence of three types of resistors (regions); (a) insulating resistors (regions) which are randomly distributed in the host matrix which represent the conduction through the insulating particles, (b) highly conducting resistors (regions) which represent the interfacial space charge regions, and (c) normally conducting resistors which represent the conduction through the host matrix. This model not only predicts an increase in the σ due to dispersion of a second phase but also successfully explains the effect of the size of the dispersoids on the conductivity (Roman and Yussouff 1987).

In the case of binary systems such as AgBr-AgI, NaI-KBr, etc. which do not form solid solution especially at lower temperatures, a somewhat similar effect is observed in which the σ of the two phase mixture is significantly higher than that of either single phase. A number of binary systems examined in this work have been found to exhibit a similar effect. These results which are to be discussed in Chapter -5 suggest that the enhancement in σ is not confined to dispersion of fine insulating particles like Al_2O_3 or SiO_2 alone, but is a rather general phenomenon, viz, a dispersion of almost any phase into another leads to enhanced ionic conductivity.

CHAPTER-3

EXPERIMENTAL DETAILS

3.1 Materials:

All starting materials (alkali halides) except KBr were obtained from Aldrich chemicals (USA), while KBr was obtained from E. Merck, Germany. The purity of the chemicals was 99.9% or better. Since almost all alkali halides are hygroscopic, it was found quite difficult to process them in open atmosphere and obtain reproducible results. All starting materials therefore were stored inside a dry box and all subsequent processing such as weighing, grinding, melting, pelletization as well as measurements were carried out within the dry box, without exposing the samples to outside environment even for a short time. This posed considerable challenge but there was no alternative.

3.2 Glove Box:

The controlled atmosphere glove box (model GB-80, Mecaplex, Switzerland) that was used extensively in the present work is shown in Fig.3.1. Beneath the dry box (Fig.3.1) is a gas purification system (Model: 2-667/2) that was also procured from Mecaplex, Switzerland. The commercial grade nitrogen gas with a nominal purity of 99% (Indian Oxygen Ltd., Kanpur) was used to fill the dry box. A three phase blower (Fig.3.2) constantly circulates the interior gas through the adsorbers of the gas purification system that was fully automatic and electronically controlled. The removal of moisture was effected by molecular

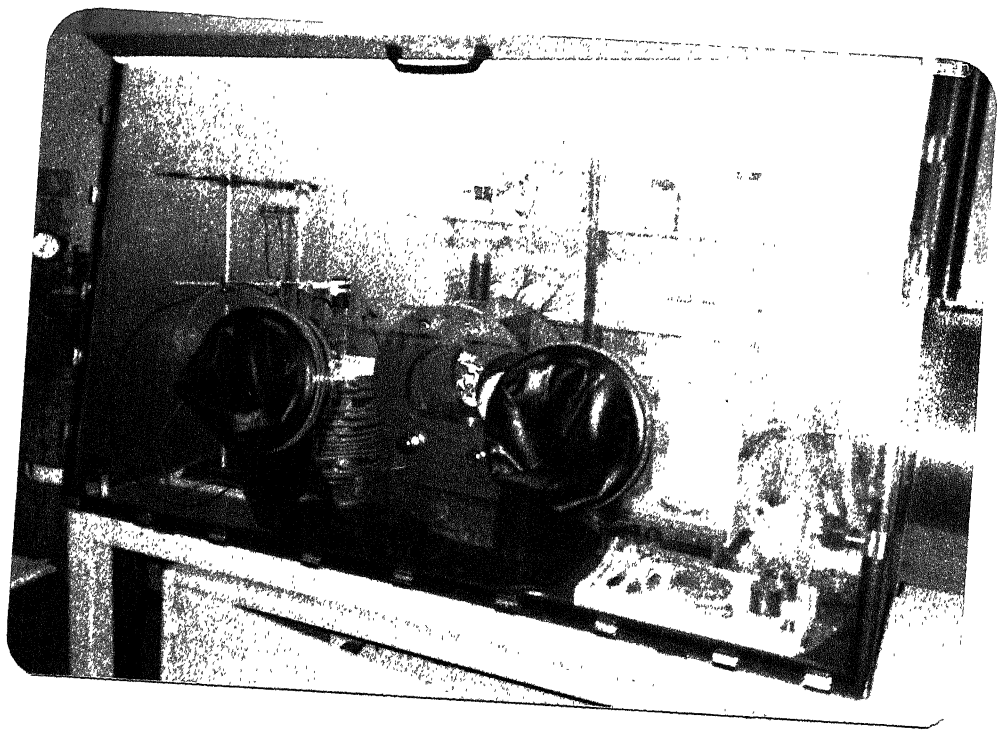

Fig.3.1 The controlled atmosphere glove box (Model: GB-80, Mecaplex) which is equipped with a water cooled furnace, hydraulic press, digital balance and other tools useful for entire materials preparation and electrical characterization.

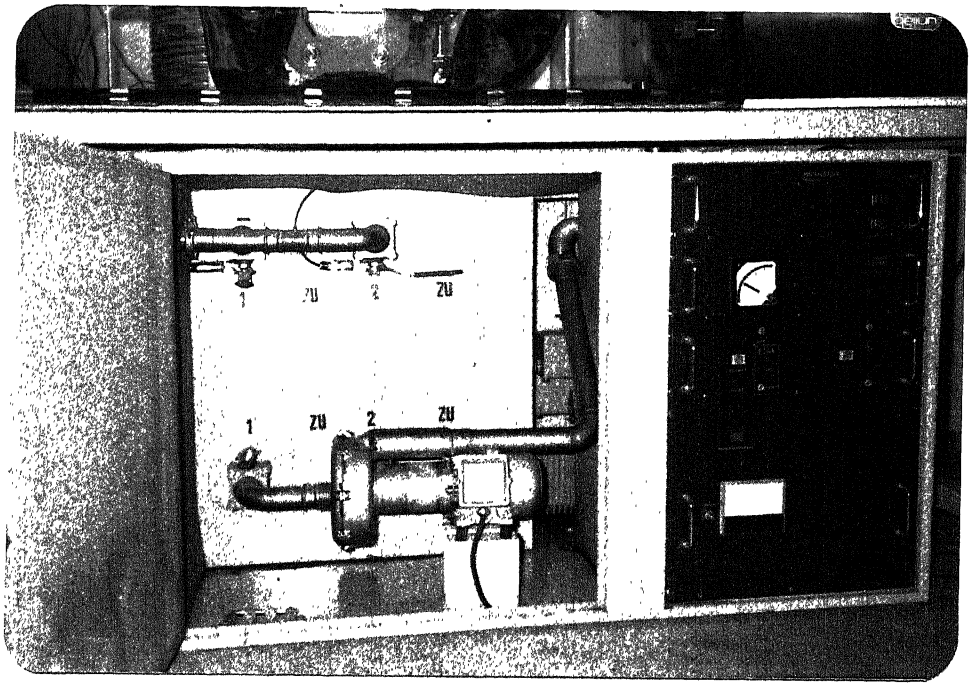

Fig.3.2 The gas purification system (Model: 2-667/2, Mecaplex) maintains the moisture and humidity inside the glove box at a few ppm level.

sieves and that of oxygen by means of copper turnings kept at 400^{o}C. Both the moisture and the oxygen content inside the dry box were maintained at a few ppm level. To ensure the uninterrupted use of the dry box, the gas purification system is equipped with a pair of adsorbers arranged in parallel such that one can switch over to the other as soon as the first one gets saturated. In the meantime, the saturated adsorber can be regenerated/reactivated by the following three successive steps which can be carried out automatically on setting the regeneration-program key on :

(i) The entire adsorber unit is heated for 4 hours to remove the bulk of water from the sieves (water converted into steam).

(ii) The adsorber unit is rinsed with the so called regenerative H_2-N_2 (92% Nitrogen + 8% Hydrogen) gas mixture for 2 hours. During this process not only the water (present in the form of steam) is flushed out but also the oxidized copper turnings are reduced back to copper.

$$CuO + H_2 \longrightarrow Cu + H_2O\ (g) \uparrow$$

(iii) Finally the left-over moisture inside the adsorber is sucked by a three phase vacuum pump (Alcatel, model No. 1012A with Pfeiffer oil mist filter ONF 025) for three hours.

The gas pressure inside the dry box can be kept at a desired level by a mechanical pressure controller via electronically triggered magnetic valves. The moisture level inside the dry box can be monitored through a humidity sensor (Shaw, Red spot type). The sensor consists of a metal core,

coated with a hygroscopic dielectric and covered with a porous gold film. As the dielectric layer is only a few microns in thickness, it rapidly achieves equilibrium with the surrounding vapour pressure. The corresponding capacitance value is displayed in the calibrated dial. The sensor response is logarithmic in parts per million range.

An air-lock chamber attached with the dry box facilitates the take-in/take-out operation without letting the outside gas mix with the inside. The various items such as materials, die, pestle/mortar, tissue paper etc, which are to be taken-in are first kept inside the air-lock chamber which is evacuated and then filled with the purified gas of the glove box. Now the inside door is opened and the items transferred inside the dry box. A somewhat similar operation is performed to take any item out of the dry box.

The workspace inside the glove box is equipped with a hand operated hydraulic press (AIM-315, AIMIL, maximum load capacity ≈ 250 K Newton) and a single pan digital balance (Metler, model: AE 160, with an accuracy of 0.1 m gms), a locally designed water-cooled furnace and other necessary accessories for materials processing and handling.

3.3 Furnace:

The limited space inside the dry box (115 x 85 x 65 cm^3) required custom-built furnace, hydraulic press and other accessories. Fortunately, the commercially available ring shaped hydraulic press (AIM-315) and the single pan digital balance

(Metler, AE 160) were just right size for us. But a furnace had to be designed that not only satisfied our space constraint, but also did not heat-up the interior significantly. Such a furnace was fabricated locally. It comprises a mullite tube (dia ≈ 1.5 inch) over which nichrome wire (22 gauge) was wound uniformly. A high temperature cement was applied over the nichrome windings to fix them in place. This heating element was enveloped with a cylindrical stainless steel (ss) vessel (dia ≈ 18 cm, length ≈ 25 cm). The space between the mullite tube and the ss vessel was filled with MgO powder. Since the furnace was to be housed inside the glove box which also housed a digital balance and a host of other things requiring near-normal environment, it was necessary to devise a cooling arrangement so that the interior temperature did not greately exceed room temperature. This was achieved by welding coiled copper tubes on to the outer ss cover of the furnace and circulating water through it. Care had to be taken to ensure against any leakages, otherwise the whole idea of controlled (moisture-free) atmosphere would be defeated. Thus water was allowed in and out through special airtight valves.

The temperature controller (Indotherm, model:401D-PID type) was located outside the glove box and a chromel-alumel thermocouple was used to control the furnace temperature. All the electrical connections were provided via air tight feed-throughs.

3.4 Sample Holder:

Figure.3.3 shows the sample holder for electrical conductivity measurements as a function of frequency and

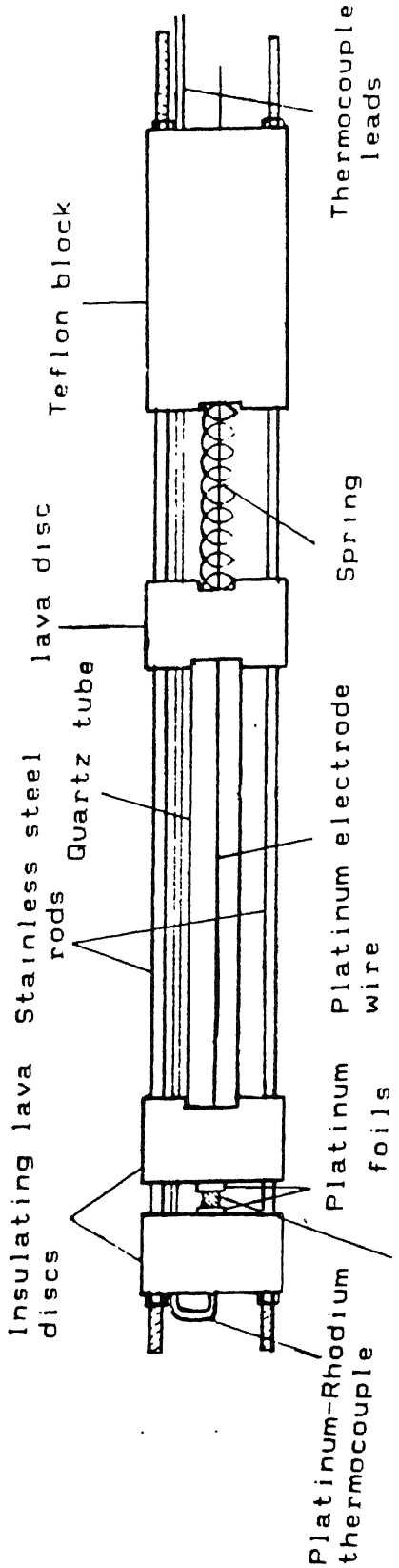

Fig.3.3. Sample holder for electrical conductivity measurements.

temperature. The three lava discs which were machined to the required size (dia ≈ 2.5 cm and thickness 1 cm) and sintered at 1100°C for 4 hours, provide the necessary mechanical support to the sample holder. These discs could be moved smoothly along the two parallel stainless steel (ss) rods. The spring which is so located that it remains outside the furnace, applies uniform pressure to the lava discs to ensure a firm contact between the electrodes and the sample. A quartz tube is used to transmit the spring pressure on to the lava discs. Thin platinum discs were used as electrodes. One of these discs had a platinum wire spot-welded on to its back to serve as lead wire. A platinum/platinum -13% rhodium thermocouple was spot welded on to the back of the other platinum disc which served both as a temperature sensor and lead wire for impedance measurement. Since the cold (reference) junction was kept at the ambient temperature, the temperature near the cold junction was constantly monitored and accounted for in the calculation of actual temperature of the sample.

3.5 Sample Preparation:

Since most of the alkali halides are hygroscopic, all the starting materials used in this work were dried under vacuum at temperature of ≈ 200°C for ≈ 20 hours. Samples of the mixed crystals were prepared by weighing the appropriate amounts of the respective pure materials and mixing them together. This mixture was transferred to a quartz tube, melted and then cooled down to room temperature. The materials so obtained were in the form of tiny crystals which were ground into fine powder in an agate

mortar and pestle and once again transferred into a quartz tube and kept at a suitable high temperature (≈ 3/4 th of its melting points) in order to homogenize the mixture. The solid chunk obtained in this manner was repowdered and pelletized in a high-carbon high-chromium (HCHC) steel die. Typical pressure applied to make the pellet was ≈ 4 tones/cm^2. All the above operations right from drying of starting materials, weighing, mixing, melting, grinding, pelletization etc were carried out inside the glove box (dry nitrogen environment).

3.6 Impedance Measurement:

Fig.3.4 shows the block-diagram of the impedance measurement set-up. As pointed out earlier, the furnace was kept inside the dry box and all the electrical leads were taken out through air-tight electrical feed-throughs. HP 4192A Low frequency impedance analyzer along with HP-16047A test fixture was used for the complex impedance (modulus, Z and the phase angle, θ) measurements in the frequency range 5 to 5 x 10^6 Hz (auto balancing bridge, with test signal level 5 mV to 1.1 V_{rms}).

The flat faces of the cylindrical pellets were polished to obtain smooth surfaces before applying platinum paint electrodes to provide good contact. In some cases thin platinum foils instead of platinum paint were used as electrodes. The pellets provided with thin platinum foils/platinum paint electrodes were sandwiched between the (thick) platinum disc electrodes of the sample holder and kept overnight at temperatures close to their respective melting points in order to;

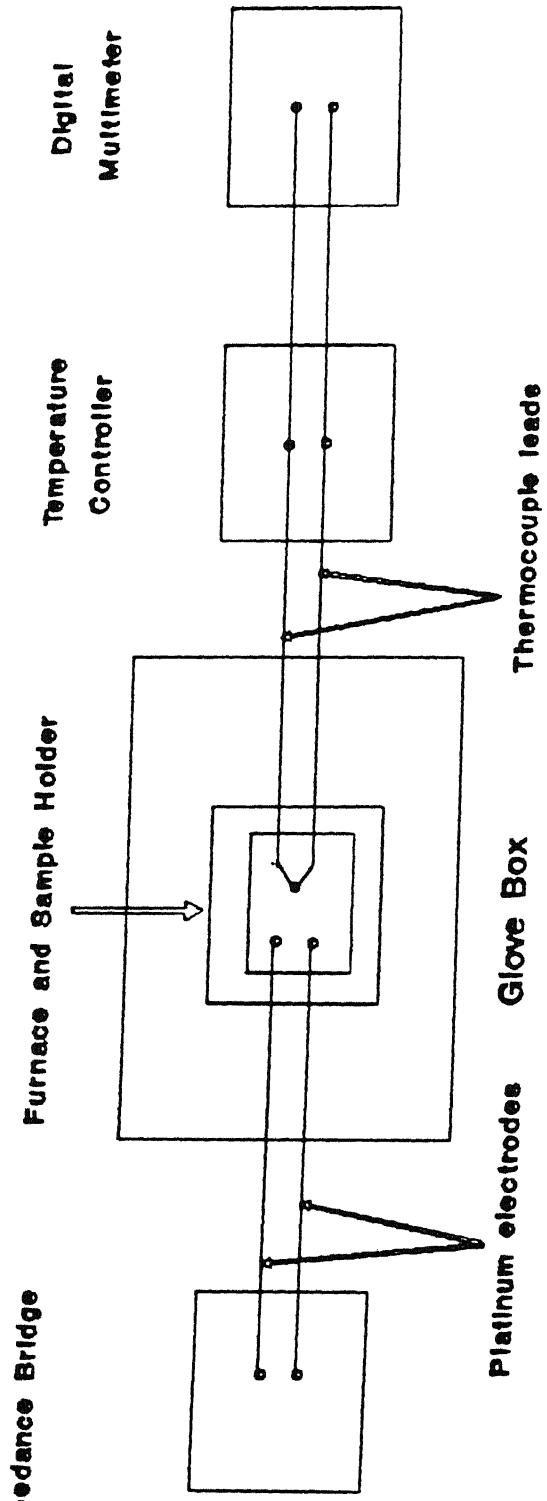

Fig.3.4. Block-diagram of the impedance measurement set-up.

(i) relieve them from any stresses that may have built during pelletization

(ii) minimize the grain boundary effect

(iii) homogenize the charge carriers, and

(iv) obtain good electrical contacts between the pellet and the electrodes.

The impedance measurements were often carried out in the cooling cycle at 10 to 15^{o}C temperature intervals. The samples were kept at each temperature for ≈ 1 hour before the measurements were taken to ensure equilibrium and thus reproducibility of the results. Several samples corresponding to each compositions were investigated to check the reproducibility.

The dc resistance (R_{dc}) of the samples were obtained from the complex impedance analysis as discussed in Chapter 4. The electrical conductivity was subsequently obtained from

$$\sigma = (1/R_{dc})\ L \qquad \text{ohm}^{-1}\ \text{cm}^{-1}$$

where L is the ratio of thickness to the area of the cross section of the cylindrical pellets.

3.7 Differential Thermal Analysis (DTA):

Any phase transformation or chemical reaction accompanied by absorption/evolution of heat can readily be detected by DTA. Fig.3.5 shows the LINSEIS model L62 DTA used in the present investigations. This machine employs a helics-shaped SiC heating element of very small heat capacity which permits a fast and efficient heating/cooling rate over a wide temperature range

(30°C-1500°C). Platinum/Platinum-13% Rhodium thermocouples are employed to measure the temperatures of the test (T_{test}) and reference (T_{ref}) samples, and hence the temperature difference $\Delta T = T_{test} - T_{ref}$. The reference junctions of the thermocouples were kept at the bottom of the furnace where a constant temperature was maintained by water circulation.

Platinum rather than alumina crucibles were used to load both reference and the test samples to obtain a better thermal sensitivity. Al_2O_3 powder was used as a reference material. In order to achieve a good thermal contact with the crucible, the powdered materials were pre-melted after loading into the crucibles. Because of the considerable error involved at large heating/cooling rates, and the poor resolution obtained at the lower heating/cooling rates, the heating/cooling rate was optimized at 5°C/min for best results after making several trial runs. The DTA equipment was standardized by means of several high purity materials of known melting points, though it was ultimately concluded that an error of ± 5°C was unavoidable in the temperature range of 500 to 800°C at a 5°C/min heating/cooling rate.

Most of the materials investigated in this work were hygroscopic and thus they readily absorbed water while taking them out of the glove box and loading into the DTA crucible. The presence of water generally showed up in form of a small endothermic peak in the DTA, particularly in the first heating cycle. Subsequently each sample was dried at a suitable temperature (130-180°C) while loaded in the DTA crucible itself,

and the DTA carried out thereafter.

The melting points of the mixed crystals were, in general, characterized by an endothermic double peak corresponding to the liquidus and solidus temperatures. These double peaks were generally well resolved in the DTA carried out in the cooling cycle. However, the final liquidus and solidus temperatures were obtained by taking the average of their values in the heating and cooling cycles. The single phase/two phase demixing temperatures (boundary points) could not be obtained from the DTA because of the low thermic effect associated with this process.

3.8 X-Ray Diffraction:

Pure starting materials as well as their mixed crystals were characterized by XRD technique at room temperature. The presence of additional peaks in the XRD patterns which were probably associated with the respective hydrate(s), confirmed that even a short exposure of the samples to the atmosphere was undesirable. To overcome this difficulty, acrylic spray paint (KRYLON) was sprayed over the samples before taking them out of the glove box. The XRD patterns were recorded using a Rich Seifert (ISO-DEBYFLEX, 2002) counter diffractometer with a filtered Cu Kα radiation (wavelength = 1.542 Å). The generator was operated at 30 kV and 20 mA, the chart speed was fixed at 1.5 cm/min and the scanning speed was 1.2^{o}/min in 2θ.

Attempts were also made to obtain the single phase-two phase demixing temperatures by measuring the precision lattice constant as suggested by Cullity (1956). The materials were

annealed for ≈ 12 hours in quartz tubes at a temperature at which the XRD was supposed to be taken, followed by quenching by dropping the quartz tube in water. Subsequently, the powdered material was spread on to a glass plate over which the "KRYLON" paint was sprayed immediately. However, the XRD analysis carried out on many such samples suggested that the quenching did not freeze the high temperature phase(s). Rather the samples had already dissociated into the corresponding equilibrium phases to a large extent, if not completely.

CHAPTER - 4

COMPLEX IMPEDANCE ANALYSIS

The electrochemical processes cannot always be represented by a simple combination of ideal resistances , and hence simple dc measurements cannot yield the dc resistance of the samples because of the choice of electrodes and the polarization at the electrode-electrolyte interfaces. Most of the early ionic conductivity measurements which were carried out at a fixed frequency in the range 1 - 10 kHz can only be taken as approximately correct. Ac impedance spectroscopy (complex impedance analysis) technique was first applied to solid electrolytes by Baurele (1969).

The complex impedance technique involves applying a sinusoidal signal of low amplitude across a solid electrolyte cell. The output signal which is also a sine wave (Hooper, 1985, Badwal,1988) is compared with the input signal to determine the impedance modulus and the phase shift corresponding to the cell assembly, ie., sample + electrode + leads, which represents a complex impedance involving a network of resistances and capacitances. The data is then displayed in the complex plane in the form of real and imaginary components.

The complex impedance $Z(w)$ at an applied frequency (w) can be expressed as

$$Z(w) = Z_R(w) + j\, Z_I(w) \qquad (4.1)$$

(or) $$Z(w) = Z\, e^{j\theta}$$

where the magnitude of the complex impedance $Z = (Z_R^2 + Z_I^2)^{1/2}$, and $\theta = \tan^{-1}(Z_I/Z_R)$ is the phase angle, and Z_R & Z_I are the real and imaginary parts of the impedance respectively . The following cases represent the basic configurations.

(i) For a pure resistance, we have

$$Z_R(w) = R, \quad \text{and } Z_I(w) = 0$$

Hence a plot of Z_R vs Z_I at various frequencies (CIA plot) would give an invariant point (at $Z_R = R$) on the Z_R axis.

(ii) For a pure capacitance, we have

$$Z_R(w) = 0, \quad \text{and } Z_I(w) = -1/wc$$

The CIA plot would give a straight line parallel to the (negative) Z_I axis at $Z_R = 0$.

(iii) For a resistance and capacitance in series, we have

$$Z(w) = R - j/wc$$

ie., $$Z_R(w) = R, \quad \text{and } Z_I(w) = -1/wc$$

the corresponding CIA plot will be similar to that of case (ii) at $Z_R = R$.

(iv) For resistance and capacitance in parallel, we have

$$Z(w) = \frac{R(1/\ jwc)}{R + (1/\ jwc)}$$

$$= \frac{R}{1 + w^2c^2R^2} + j\,\frac{-R^2\,wc}{1 + w^2c^2R^2} \qquad (4.2)$$

ie., $$Z_R^2 + Z_I^2 = R\, Z_R$$

(or) $$(Z_R - R/2)^2 + Z_I^2 = (R/2)^2 \qquad (4.3)$$

which is the equation of a circle of radius R/2 with its centre at (R/2,0).

Figure 4.1 displays a typical set of complex impedance plots for KBr + 30 m/o NaI at various temperatures. These semicircular plots are in a form suggested by Eq. (4.3) and hence the cell assembly is equivalent to a resistance and a capacitance in parallel. Since the resistance of the lead is negligible compared to that of the sample, the dc resistance obtained from these plots directly give the dc resistance of the sample. Almost the entire conductivity data reported in this thesis are obtained by employing the complex impedance analysis. To obtain σ of one sample at one temperature, impedance (Z,θ) measurements at some 10 to 15 frequencies are required , and hence to obtain a log σ vs 1/T plot, the conductivity data for at least 20 different temperatures are necessary, and hence for each sample some 200 to 300 impedance (Z,θ) data are required which was accomplished over a period of several days or even weeks. In all, five different systems, viz. KBr-NaI, KBr-NaBr, NaBr-NaCl, NaBr-NaI,and NaBr-LiBr, involving some 50 different compositions (samples) have been investigated. The complex impedance plots of most systems were found semicircular, ie., similar to that for KBr-NaI system (Fig.4.1).

The complex impedance plots (Z_R vs Z_I) for NaBr-LiBr system were, however, found to be somewhat different from that

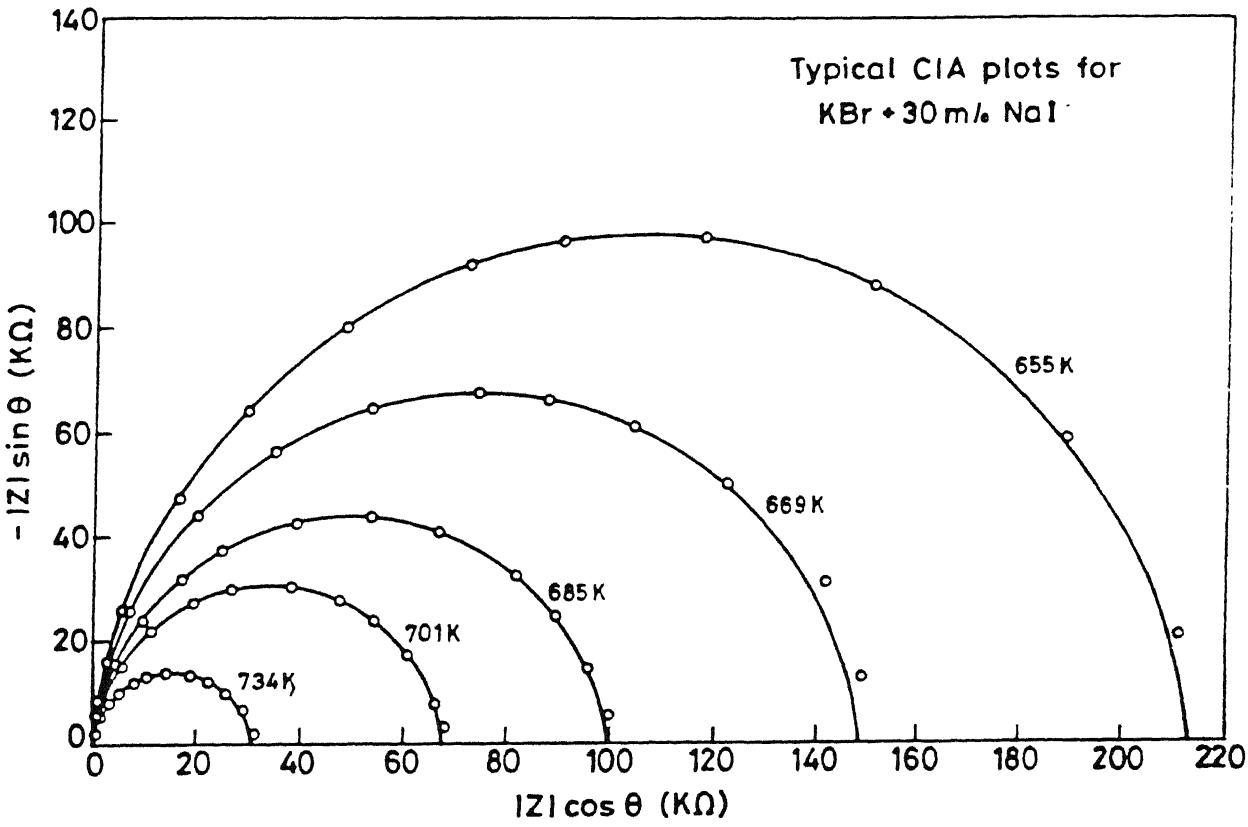

Fig.4.1 Typical complex impedance plots for KBr + 30 m/o NaI at various temperatures.

for other systems. Figure 4.2 shows a typical plot for NaBr-80 m/o LiBr which is characterized by a tail in the low frequency region besides a circular behaviour at higher frequencies (> 1 kHz). The presence of the tail was distinct particularly for LiBr-rich compositions.

A similar behaviour was also reported for LiBr-LiI (Patnaik 1987) and LiBr-Al_2O_3 (Gupta 1988; Gupta et al 1988) systems which suggests that the observed behaviour (Fig.4.2) is a characteristic feature of the lithium salts. The tail could be attributed to the electrode/electrolyte interfacial effects because

(i) the electrode processes relax at lower frequencies (Badwal 1988) and

(ii) the surface of the platinum electrodes were found to have reacted slightly with the material.

Figure 4.3 shows a typical plot of logarithm of conductivity vs 1/T (Arrhenius plot) for KBr + 20 m/o NaBr at different frequencies, measured using HP-4192A low frequency impedance analyzer with HP-16047A test fixture. It is noted that the dc conductivity obtained from the complex impedance analysis agrees well with that at 1 kHz at higher temperatures. However, the two results are quite different at lower temperatures which suggests that the measurements at a fixed (say 1 kHz) frequency cannot always be regarded as frequency independent (dc) conductivity.

All the impedance data were acquired manually but the subsequent analysis and curve fittings were done by using a

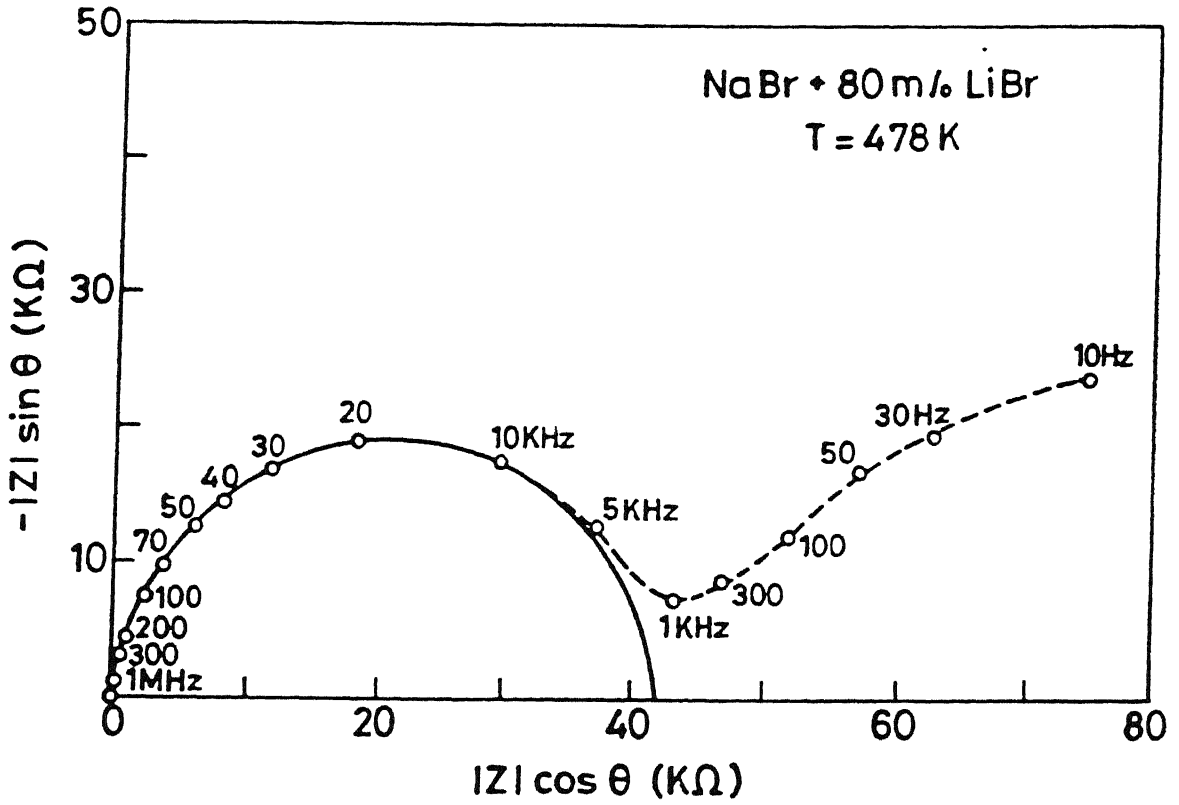

Fig.4.2. Complex impedance plots for NaBr + 80 m/o LiBr.

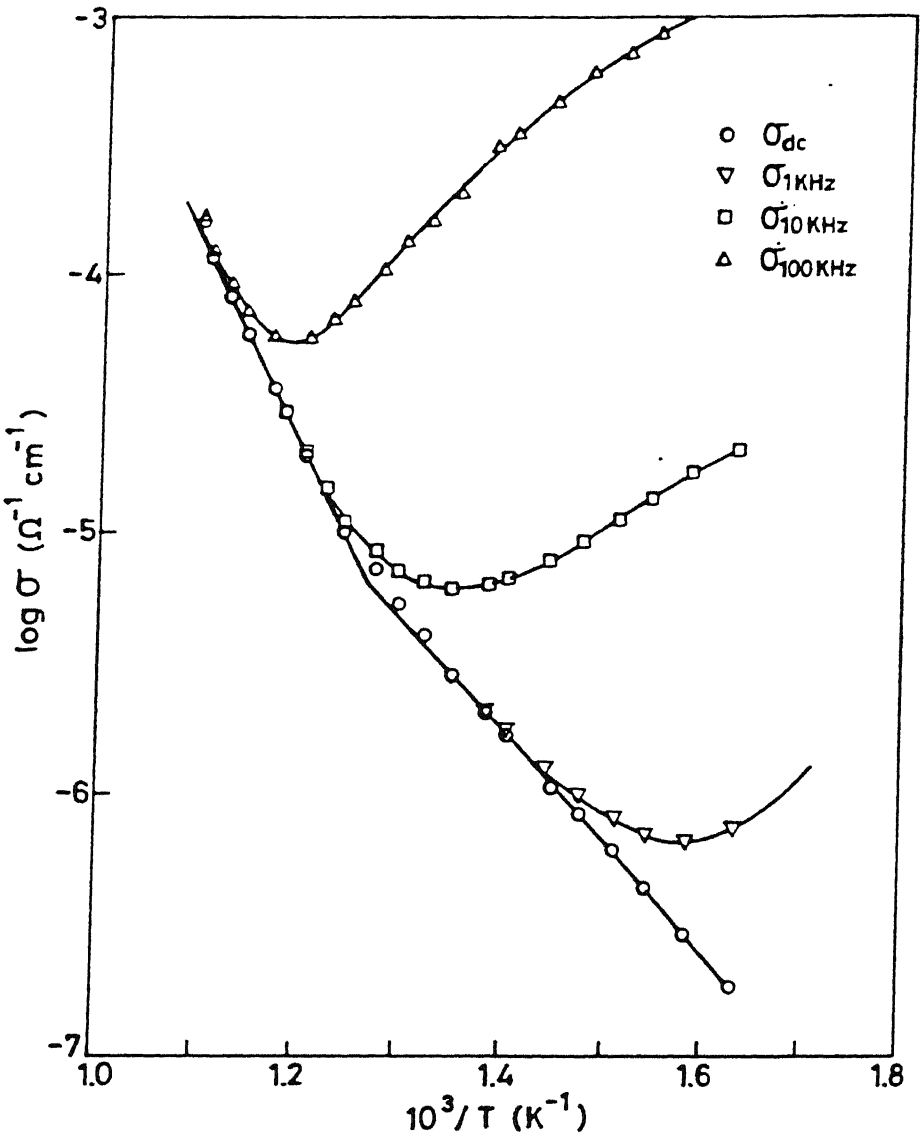

Fig.4.3. Logarithm of conductivity vs inverse temperature for KBr + 20 m/o NaBr at different frequencies.

CHAPTER-5

RESULTS AND DISCUSSION

5.1 KBr-NaI MIXED CRYSTAL SYSTEM

5.1.1 Phase Diagram:

(a) Solid Solution / Two Phase Demixing Curve:

Figure 5.1.1 shows the temperature vs composition (T-x) plot (phase diagram) for KBr-NaI pseudo-binary system. The demixing curve which corresponds to the $K_{1-x}Na_xBr_{1-x}I_x$ solid solution (ss) / [KBr (ss) + NaI (ss)] demixing boundary (shown by the open circle) is also obtained from the DTA results which has been extrapolated on either side (dashed line) down to 20 and 80 m/o NaI as guided by XRD results at room temperature. Due to non-availability of high temperature XRD facilities, the XRD studies were limited to room temperature. This dome-shaped curve that appears to be symmetrical about the x = 0.5 line separates the two-phase region from the solid solution region. These results suggest that complete solid solubility exists only above 380°C. It is worthwhile to compare this phase diagram with those of similar binary systems. For KCl-NaCl (Barret and Wallace 1954), the demixing curve has the shape of a dome (or a parabola) that is somewhat asymmetrical, tilted towards the NaCl -rich region. The peak of the curve appears at 65 m/o NaCl. In KI-NaI (Haget et al 1975), the peak occurs at ≈ 63 m/o NaI, while that in NaBr-NaCl (Fineman and Wallace 1948) it occurs at ≈ 55 m/o NaCl. The extent of asymmetrical tilt apparently depends on the mismatch between the lattice constants of the two components.

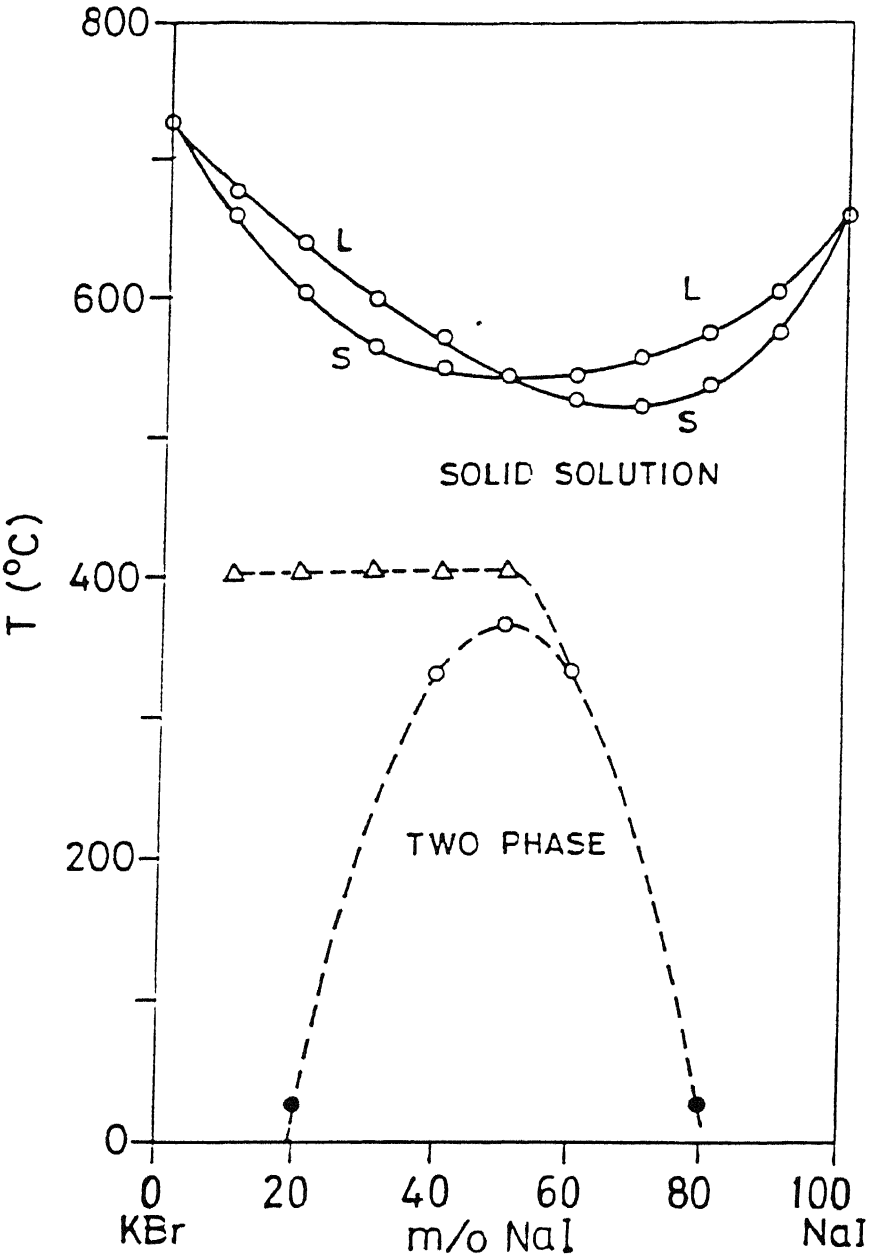

Fig.5.1.1. Phase diagram of KBr-NaI system as determined by various studies; o - DTA studies, Δ- σ studies and ● - XRD study on samples after making DTA studies.

These results clearly imply that a solid having larger lattice constant is soluble to a smaller extent in a solid having a smaller lattice constant at any given temperature. This also means that at any given temperature, it is more difficult to replace a smaller ion with a larger ion than the reverse.

In the present KBr-NaI system, since the difference in the lattice constants of the two components is quite small, there is little or no tilting of the demixing curve (Fig. 5.1.1) which appears reasonable and consistent with the other phase diagrams (Barret and Wallace 1954; Haget et al 1975; Fineman and Wallace 1948) determined using DTA. However, the results inferred from the conductivity measurements are at variance with those inferred from the DTA. During the conductivity measurements in the cooling cycle, the temperature at which the thermodynamically non-equilibrium value of conductivity starts (see Sec.5.1.5), was taken as the boundary of the demixing curve. According to the σ vs T studies, not even 10 m/o NaI is soluble in KBr at $T < 400^{o}C$, while up to 20 m/o KBr is found to be soluble in NaI even at room temperature.

In a bid to resolve the disagreement between the results obtained from conductivity and DTA studies, attempts were made to obtain the solid solution/two-phase demixing boundary by measuring the precision lattice constants by means of X-ray diffraction on samples quenched from high temperatures (Cullity 1956). The powdered materials were annealed for 12 hours in a quartz tube at a temperature at which the XRD was supposed to be

taken by quenching the sealed quartz tube containing the sample in water. The quenched powder was then spread on to a glass plate and the acrylic spray paint (KRYLON), which is transparent to the X-rays, was sprayed immediately. However, the XRD analyses carried out on many such samples suggested that the quenching did not freeze the high temperature phases(s) completely. The results from the conductivity vs temperature studies, which are also shown in Fig. 5.1.1, may be considered more reasonable than the DTA results as the former were obtained at a much slower cooling rate (< 0.1^{o}C /min) and hence may be considered much closer to the equilibrium situation. Interestingly, the results of σ vs T, room temperature XRD and the DTA studies were found consistent in the NaI-rich samples.

(b) Melting Curves:

The solidus (T_S)and the liquidus (T_L) curves shown in Fig.5.1.1 were obtained from the DTA studies alone. The behaviour of the solidus and the liquidus curves is as expected for a binary system, except for a minor anomaly in the former at intermediate compositions. The liqidus temperature decreases as the concentration (x) of NaI in KBr increases, exhibits a clear minimum at $x = 0.5$, and increases with further addition of NaI in KBr. The solidus temperature, on the other hand, exhibits a pair of weak minima at $x \approx 0.3$ and 0.7, separated by a minor maximum at $x \approx 0.5$. Though this kind of behaviour is not uncommon in the binary phase diagrams, it is often indicative of the existence of a new phase (intermediate compound) which, however, could not be detected in the present system. This anomaly in the solidus

curve, howsoever small in the T-x diagram, is more prominently reflected in the σ-x studies to be discussed later (Sec.5.1.2). It is possible that there is at least some sort of ordering of the host and guest ions in the intermediate composition range ($0.4 \leq x \leq 0.6$). Table 5.1 lists the solidus and liquidus temperatures as a function of x along with the ionic transport parameters.

5.1.2. Conductivity vs Composition:

The complex impedance analysis method (Chapter 4) was routinely used to obtain dc conductivity from the measured ac impedance (Z,θ) data. Figure 5.1.2 shows the lagarithm of conductivity (log σ) as a function of composition (m/o NaI in KBr) at 400 and 500°C where complete solid solubility exists. The dashed portion of the curve corresponds to the conductivity obtained by extrapolating the linear log σ vs 1/T plot in the intrisic region down to appropriate temperatures. The conductivity of $K_{1-x}Na_xBr_{1-x}I_x$ increases sharply as the concentration (x) of NaI in the mixed crystal increases upto $x \approx 0.4$. As x increases beyond $x = 0.4$, the σ continues to increase, though the rate of increase slows down and peaks around $x = 0.7$ and then starts decreasing. The conductivity isotherm at 400°C is similar to that at 500°C except in the composition range $0.4 \leq x \leq 0.5$ where σ exhibits a minor local maximum at $x \approx 0.4$ and a minimum at $x \approx 0.5$. The maximum enhancement in conductivity is obtained for KBr + 70 m/o NaI; at 500°C, the magnitude of conductivity enhancement is a factor of 500 with respect to KBr, and 8 with respect to NaI.

TABLE 5.1

Melting points and the ionic transport parameters of KBr-NaI mixed crystals

Mole fraction of NaI	Temperature range(^{o}C) (intrinsic)	E_a intrinsic eV	E_a extrinsic eV	A intrinsic (ohm^{-1} cm^{-1})	T_L (^{o}C)	T_S (^{o}C)
0.0	595-720	1.58	0.83	9.55×10^3	729	729
0.1	540-650	1.43	1.06	7.59×10^3	677	660
0.2	480-595	1.20	—	1.0×10^3	640	605
0.3	405-560	1.29	—	8.32×10^3	600	565
0.4	400-540	1.20	—	3.39×10^3	569	551
0.5	400-540	1.34	—	3.80×10^4	545	545
0.6	330-522	1.37	—	1.1×10^5	545	525
0.7	390-520	1.31	1.03	8.7×10^4	556	522
0.8	410-527	1.34	1.16	8.51×10^4	575	537
0.9	400-570	1.35	1.05	5.37×10^4	605	575
1.0	445-615	1.38	1.03	2.89×10^4	661	661

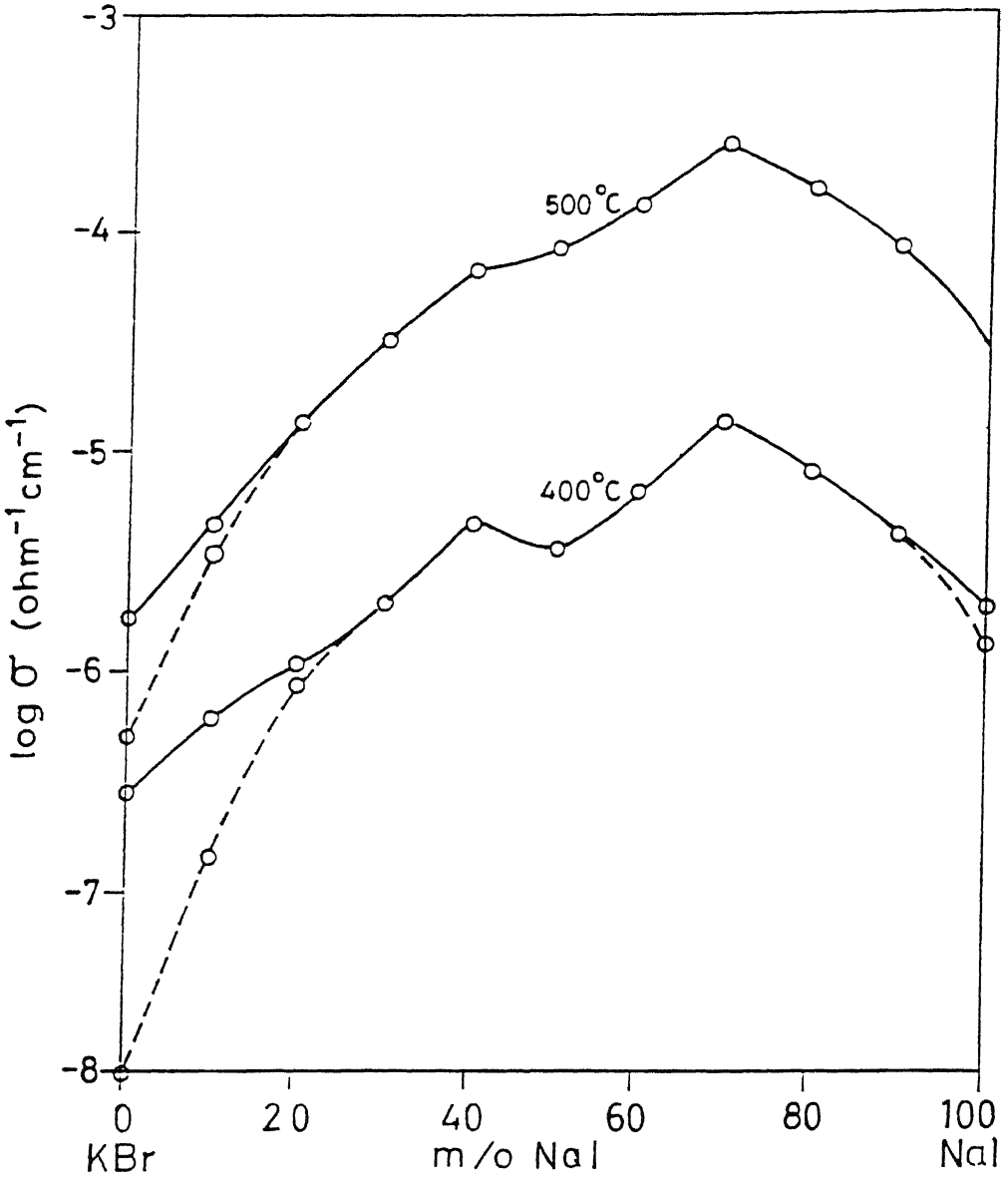

Fig.5.1.2. Logarithm of conductivity vs composition of NaI (m/o) in KBr at 400 and 500°C. Dashed lines correspond to the conductivity obtained by extrapolating log σ vs 1/T plot in the intrinsic region to appropriate temperatures.

5.1.3. Conductivity vs Temperature (Solid Solutioin Region):

Figures 5.1.3 and 5.1.4 show log σ as a function of inverse temperature (K^{-1}) for the $K_{1-x}Na_xBr_{1-x}I_x$ solid solutions. It is observed that the log σ vs $10^3/T$ plots usually consist of two linear segments; the high temperature intrinsic region associated with a higher slope, and the low temperature extrinsic region associated with a lower slope. The conduction parameters E_a and A defined by

$$\sigma = A \exp(-E_a/kT)$$

are listed in Table 5.1 for all the 11 different compositions studied.

It should be noted that the value of $E_a = 1.58 \pm 0.02$ eV obtained for the sintered pellets of pure KBr is in fair agreement with the two recent results on polycrystalline samples, viz., 1.52 eV (Shahi and Wagner 1983) and 1.5 eV (Johannesen and Mckelvy 1985). However, the activation energies obtained for single crystalline samples are generally higher, 1.87 eV (Phipps and Partridge 1929), 1.91 eV (Dawson and Barr 1967), 1.94 eV (Johannesen and Mckelvy 1985), 2.04 (Johannesen and Mckelvy 1986) and 2.07 eV (Chandra and Rolfe 1971). Becuase of the limited solid solubility in the mixed crystal system at lower temperature, it was not possible to grow and handle the single crystals, and hence all the conductivity studies were carried out on sintered pellets.

An activation energy of 1.65 ± 0.02 eV is obtained for the sintered pellets (polycrystalline) of pure KBr using platinum

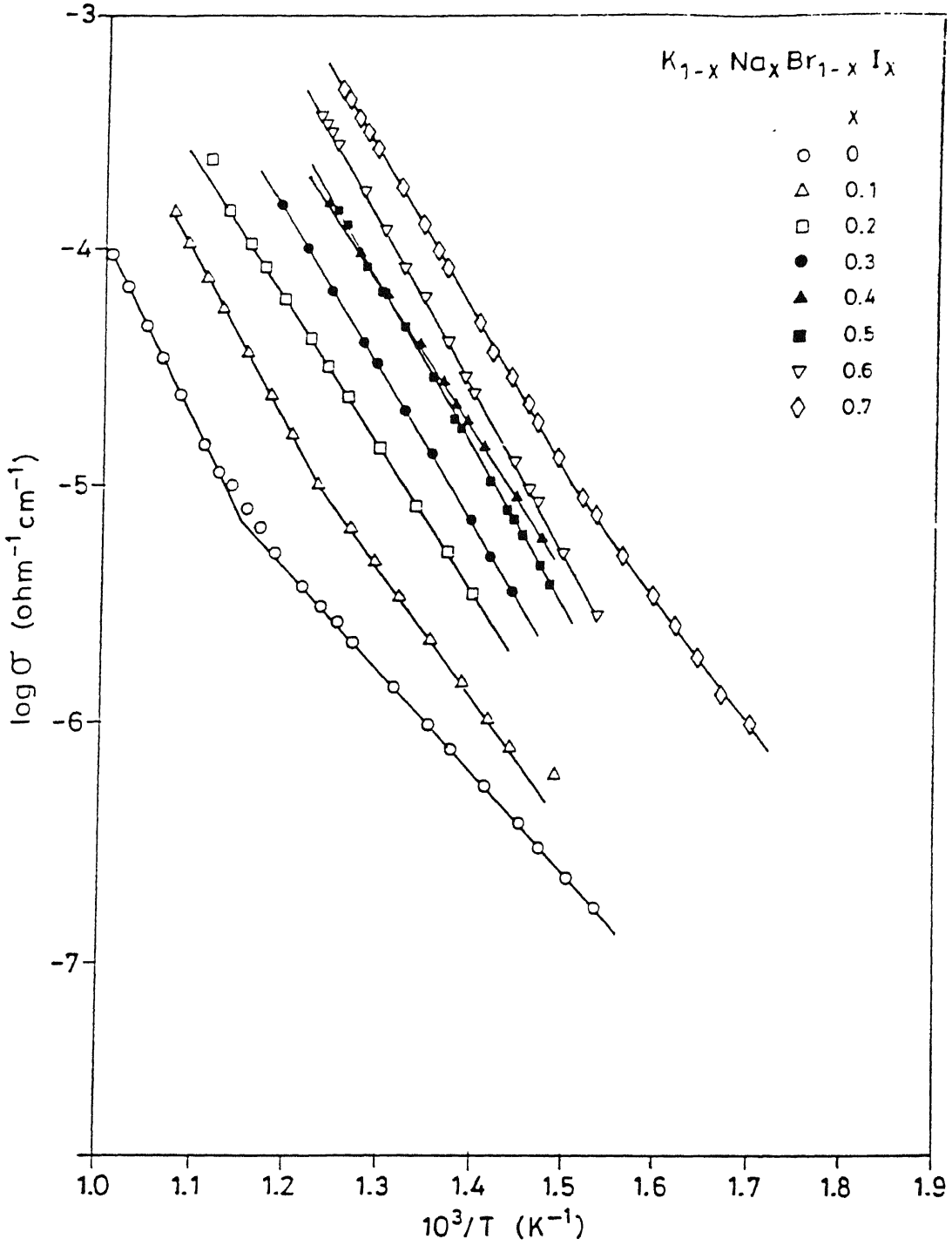

Fig.5.1.3. Logarithm of conductivity vs inverse temperature for $K_{1-x}Na_xBr_{1-x}I_x$ ($0 \leq x \leq 0.7$) solid solutions.

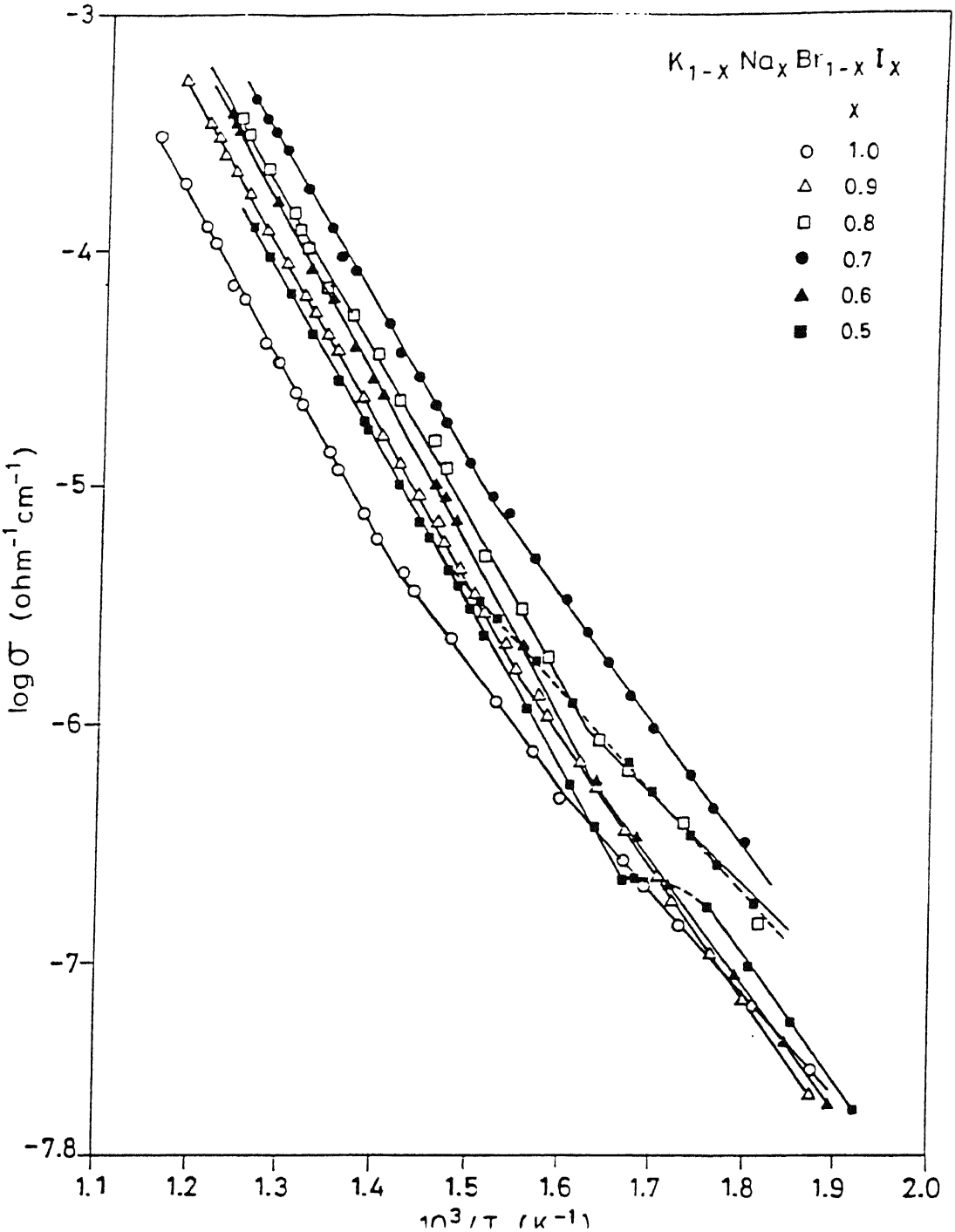

Fig.5.1.4. Logarithm of conductivity vs inverse temperature for $K_{1-x}Na_xBr_{1-x}I_x$ ($0.5 \leq x \leq 1$) solid solutions.

paint electrodes, which differs slightly with that of 1.58 ± 0.02 eV for KBr using thin platinum foil electrodes. The ratio of the conductivity of pure KBr with platinum paint electrodes to that of pure KBr with thin platinum foil electrodes is found to be 1.26 at ≈ 630°C, suggesting that the contact between the pellet and the electrodes shows improvement with the platinum paint electrodes. A similar observation was made by Johannesen and Mckelvy (1985) in their studies on KBr-KI mixed crystals, who, however, found that the graphite paint contact tends to deteriorate at high temperatures after prolong use.

Similarly, an activation energy of 1.38 ± 0.02 eV is obtained for pure NaI pellets using thin platinum foil electrodes. The activation energy for the single crystals of NaI is reported to be 1.6 eV (Hoodless et al 1971) and 1.49 ± 0.03 eV (Kostopoulos et al 1975). Even though the platinum paint electrodes yielded a 20-30 % higher conductivity and ≈ 10 % higher activation energy, it was not preferred vis-a-vis thin platinum foil because of the lack of reproducibility of the σ data over several heating/hooling cycles.

From Figs. 5.1.3 and 5.1.4, it is evident that as the concentration of homovalent dopants, for example, of NaI in KBr or of KBr in NaI, increases, the conductivity increases considerably. Moreover, the enhancement in conductivity is accompanied by a more or less proportionate decrease in the activation energy. For the composition range 20-60 m/o NaI, the demixing occurs before the onset of extrinsic region in the

cooling cycle and hence no transport parameters (enthalpy of migration, etc) could be determined in the extrinsic region.

5.1.4. Activation Energy vs Composition:

Figure 5.1.5 displays the activation energy (intrinsic region) vs composition characteristics. As the concentration (mole fraction x) of NaI in the mixed crystal increases, the enthalpies of formation and migration of defects and hence E_a (= H/2 + h), decrease sharply and go through a minimum at ≈ 30 m/o NaI. As x increases further, E_a increases and goes through a maximum at ≈ 55 m/o NaI followed by another minimum at ≈ 70 m/o NaI. This E_a vs x behaviour, viz., a pair of minima separated by a maximum, is consistent with the melting (solidus) temperature vs composition dependence (Fig. 5.1.1).

5.1.5. Conductivity vs Temperature (Two Phase Region):

The ionic conductivity in the two-phase region ($T < 400^{\circ}C$) is found to be very sensitive to the heating/cooling rate of the sample. Figure 5.1.6 shows the log σ vs $10^3/T$ plot for KBr + 40 m/o NaI at three different cooling rates. In the solid solution region, a fairly reproducible single curve is obtained corresponding to all three different cooling rates. However, as soon as the demixing occurs, the log σ vs $10^3/T$ curves take different shapes corresponding to different cooling rates. The curves 1,2 and 3 in Fig.5.1.6 represent the data corresponding to fast cooling (≈ $5^{\circ}C$ /min), slow cooling (≈ $0.3^{\circ}C$ /min) and very slow cooling (≈ $0.1^{\circ}C$ /min) cycles. It is quite interesting to note that as soon as the demixing process sets on, the decreasing trend of σ is not just arrested but actually reversed, i.e., σ

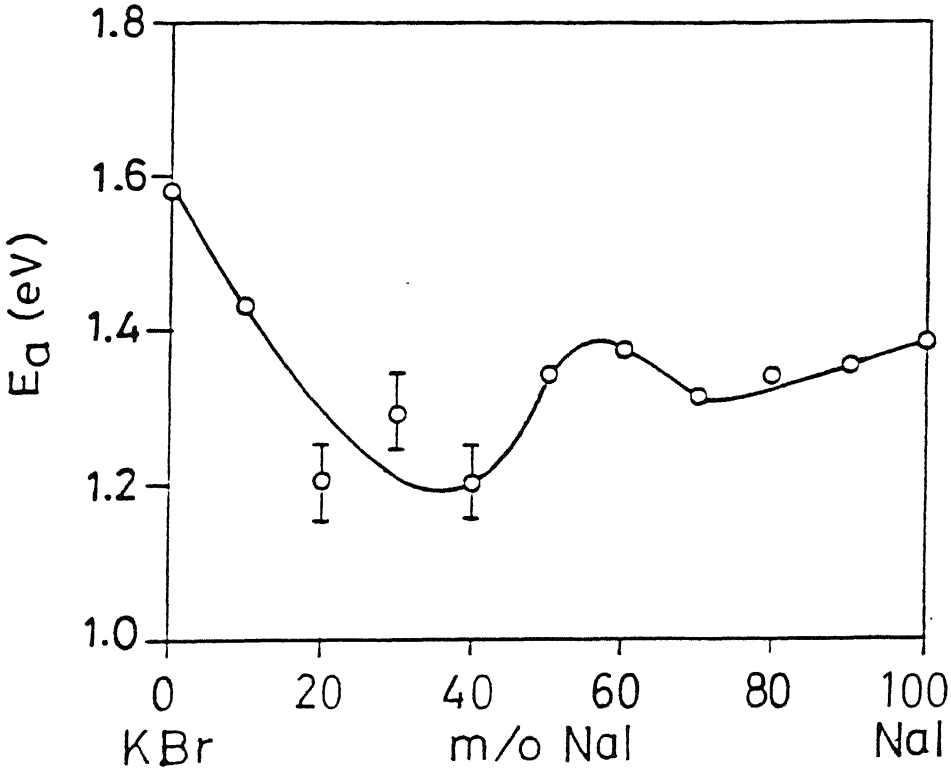

Fig.5.1.5. Activation Energy (intrinsic region) vs composition for $K_{1-x}Na_xBr_{1-x}I_x$ mixed crystals.

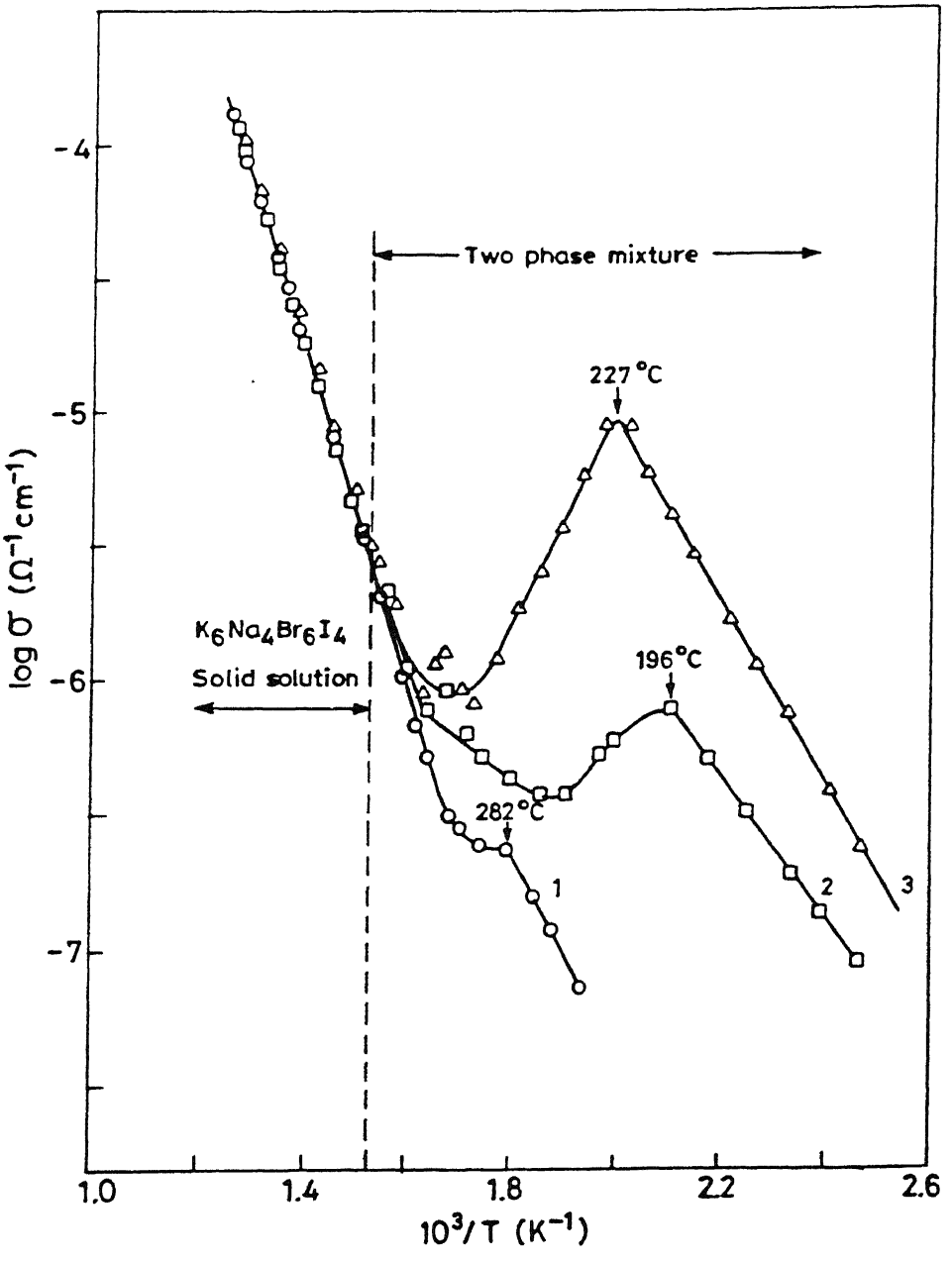

Fig.5.1.6. Logarithm of conductivity vs inverse temperature for KBr + 40 m/o NaI at three different cooling rates. Curve 1, 2 and 3 corresponds to the cooling rate of 5°C / min, 0.3°C / min and 0.1°C / min respectively.

starts increasing while the temperature continues to decrease. Eventually σ goes through a maximum and then starts decreasing, more or less in the usual Arrhenius manner. It should be obvious that the σ data in the two-phase region ($T < 400^{o}C$) are not equilibrium values, perhaps not even those corresponding to the slowest cooling rate ($0.1^{o}C$ /min). The varying log σ vs $10^{3}/T$ plots corresponding to different cooling rates may be qualitatively explained in terms of (i) nucleation and grain growth (phase separation) of the two phases (KBr ss* and NaI ss) from the parent phase, and (ii) the pre-assumption that the conductivity of the uniformly interpersed particles (grains) of the two phases, is higher than the conductivities of either KBr ss or NaI ss or the parent phase $K_{1-x}Na_xBr_{1-x}I_x$. It should be pointed out that at any temperature $T < T_e$†, the rate of nucleation and grain growth will be proportional to (i) the temperature difference (T_e-T) and (ii) the diffusion coefficient D of the ions in the parent phase

$$D \propto \exp(-g_d/kT) \qquad (5.1.1)$$

where g_d is the free energy of diffusion. As the temperature decreases, (T_e-T) increases and hence the rate of phase separation will increase. However, the decreasing temperature decreases the diffusion coefficient (D) in view of Eq. (5.1.1) which adversely affects the rate of phase separation. Thus, the

---

†The temperature at which the three phases, viz, the $K_{1-x}Na_xBr_{1-x}I_x$ solid solution, KBr (ss) and NaI (ss) coexist together is called the equilibrium temperature, T_e. Its value for KBr+ 40 m/o NaI is $400^{o}C$ according to the phase diagram Fig.5.1.1.

*KBr ss stands for KBr containing some dissolved NaI.

decreasing temperature drives the two processes working for and against the phase separation.

When the sample is cooled quickly below T_e = 400^{o}C ($\approx$ 5 ^{o}C /min, curve 1), there is not enough time for the precipitation of the two phases, and hence the sample which is still a largely single phase solid solution of KBr and NaI exhibits a linear log σ vs 1/T behaviour, more like a normal solid down to $10^3/T$ = 1.67 K^{-1} or T = 326 ^{o}C. However, when the temperature has decreased considerably below T_e = 400^{o}C, i.e. (T_e-T) has become large, some phase separation occurs and the sample now consists of three phases, KBr ss and NaI ss particles dispersed in the metastable parent phase. Since the dispersion of second phase particles in general is known to increase the conductivity (Shahi and Wagner 1981, 1982 a,b; Liang 1973; Maier 1985 a,b, 1988, 1989; Chaklanobis et al 1990), it results in retarding the rate of decrease in conductivity in the range 1.67 $\leq 10^3/T \leq$ 1.8 K^{-1}. As the temperature continues to decrease, the diffusion coefficient decreases to the extent that further phase separation is hampered. Thus at $10^3/T \geq$ 1.8 K^{-1} (or T $\leq$ 282^{o}C) once again a linear log σ vs 1/T behaviour with E_a = 0.7 eV is obtained that must correspond to a three phase metastable mixture, viz., KBr ss and NaI ss fine particles dispersed in the $K_{0.6}Na_{0.4}Br_{0.6}I_{0.4}$ solid solution.

Now consider the curve 3 corresponding to the very slow cooling mode of the conductivity measurement. Coooling at a very slow rate (0.1^{o}C /min) allows sufficient time for ions to diffuse and hence for the phases to separate in sufficient quantitity so

as to not only offset the decrease in the conductivity due to the decrease in temperature but actually to cause a net increase in the conductivity. As the slow cooling continues, more and more of the two phase mixture is formed, while the temperature has decreased a little, causing a net increase in the conductivity. Finally, the phase separation is completed (at $10^3/T \approx 2\ K^{-1}$ or $T = 227^oC$) and beyond that a linear log σ vs 1/T plot with E_a = 0.66 eV is obtained.

For the curve 2, corresponding to an intermediate slow cooling rate of 0.3^oC /min, the behaviour is more or less as expected in view of the above discussion. The appearance of the maximum in this curve at a lower temperature than in the curve 3 may be understood in the following way: since the cooling rate for curve 2 is faster than that for curve 3, the process of phase separation continues for a longer time and the maximum in the conductivity appears at a lower temperature (196^oC).

A comparison of the curves 1 and 3 corresponding to fast and very slow cooling rates reveals that the conductivity of 10^{-5} ohm^{-1} cm^{-1} corresponding to the maximum in the curve 3 is more than two orders of magnitude higher than that of the curve 1 at the same temeprature. Thus, an important conclusion is that the two-phase mixture has orders of magnitude higher conductivity than the corresponding solid solution of the same composition. This suggests a new means to achieve highly conducting solid electrolytes.

5.1.6 Discussion:

The observed conductivity vs composition behaviour (Fig. 5.1.2) may be explained semi-quantitatively on the basis of the lattice loosening model (Sec. 2.3). A crude inspection of the phase diagram (T-x plot, Fig.5.1.1) and the conductivity-composition (σ-x plot, Fig.5.1.2) reveals that the conductivity of the mixed crystals follows the solidus rather than liquidus temperature.

The log σ vs 1/T studies on the KBr-NaI mixed crystals (Sec. 5.1.3) reveal that as the doping concentration increases, the melting point decreases, the formation and migration enthalpies decrease and the conductivity increases. It is obvious from the results shown in Figs. 5.1.3 and 5.1.4 that the mixed crystals $K_{1-x}Na_xBr_{1-x}I_x$ ($x > 0$) attain a certain fixed conductivity at a lower temperature (T_x) than the pure salt ($x = 0$) does. In order to illustrate this correlation qualititatively, the temperature (T_σ) at which the mixed crystal $K_{1-x}Na_xBr_{1-x}I_x$ attains a fixed conductivity (σ) is ploted as a function of composition x (m/o NaI) in Fig.5.1.7. The curves marked $T_{\sigma 1}$ and $T_{\sigma 2}$ correspond to two different (fixed) conductivities $\sigma_1 = 5 \times 10^{-5}$ and $\sigma_2 = 10^{-5}$ ohm^{-1} cm^{-1}. These T_σ vs x curves are constructed by drawing lines parallel to 1 / T -axis at $\sigma_1 = 5 \times 10^{-5}$ and $\sigma_2 = 10^{-5}$ ohm^{-1} cm^{-1} in Figs.5.1.3 and 5.1.4, and reading off the temperatures (T_σ) corresponding to the intersection with the log σ vs 1/T curves. Also shown in Fig.5.1.7 is T_{mx} which is the solidus curve (T_S) of the phase diagram (Fig. 5.1.1). It is readily seen that the variation of T_σ

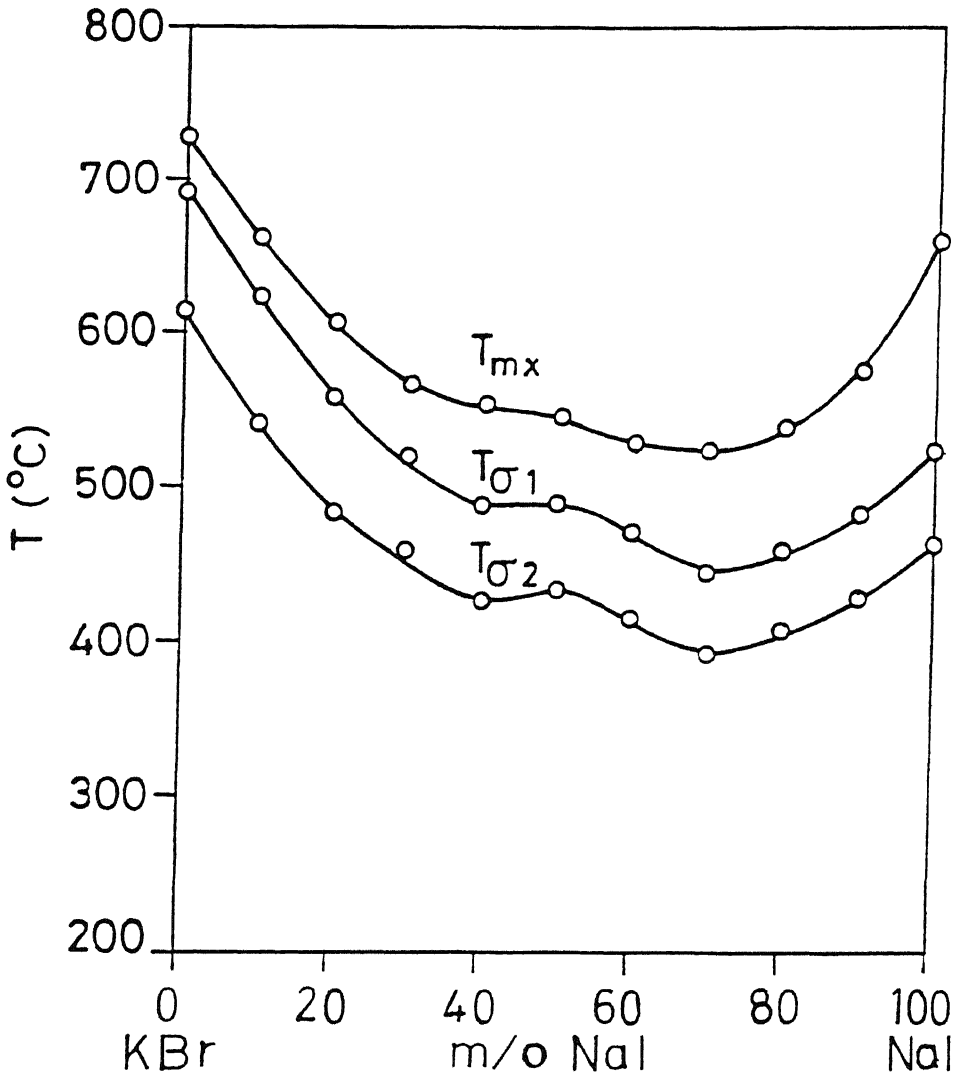

Fig.5.1.7. Temperature (at which a mixed crystal attains a fixed conductivity) as a function of the composition of NaI in KBr. $T_{\sigma 1}$ and $T_{\sigma 2}$ curves corresponds to two different fixed conductivities $\sigma_1 = 5 \times 10^{-5}$ and $\sigma_2 = 10^{-5}$ ohm^{-1} cm^{-1}. Interestingly T_σ curves follow the solidus curve (T_{mx} vs x) of the phase diagram (Fig.5.1.1).

is surprisingly similar to that of the solidus curve (T_S), not just with respect to the overall nature but also the fine details at intermediate compositions.

Both the T_σ vs x plots exhibit a pair of minima at 40 and 70 m/o NaI separated by a mixımum at ≈ 50 m/o NaI. T_{mx} vs x curve also exhibits a clear minimum at ≈ 40 m/o NaI and it almost appears to go through a maximum at ≈ 50 m/o NaI and a minimum at ≈ 70 m/o NaI. However, the T_{mx} data given in Table 5.1 do not reveal a clear double minima separated by a maximum but show only a weak maximum or a tendency to show a maximum at ≈ 50 m/o NaI. Hence for the purpose of the present discussion, the solids temperature (T_{mx}) of the mixed crystals is taken as the melting temperature. Recalling Eq. (2.33), ie., the LL model,

$$\sigma_x/\sigma_o = \exp\{-22.17\,\Delta T_{mx}/T\}$$

one can obtain the conductivity enhancement as a function of composition. Figure 5.1.8 compares the relative conductivity (σ_x/σ_o) obtained from experiments with that calculated from Eq. (2.33). It should be noted that H and h are related to the change in melting temperature (ΔT_{mx}) which is a function of the dopant concentration and is known experimentally for each composition (Table 5.1). The agreement between the experimental and the calculated results (Fig. 5.1.8) should be considered very good, particularly at lower dopant concentrations. Interestingly, it is not just the magnitudes of σ_x/σ_o which are comparable, even the fine structures observed in the experimental curve tally well with those in the calculated curves. For

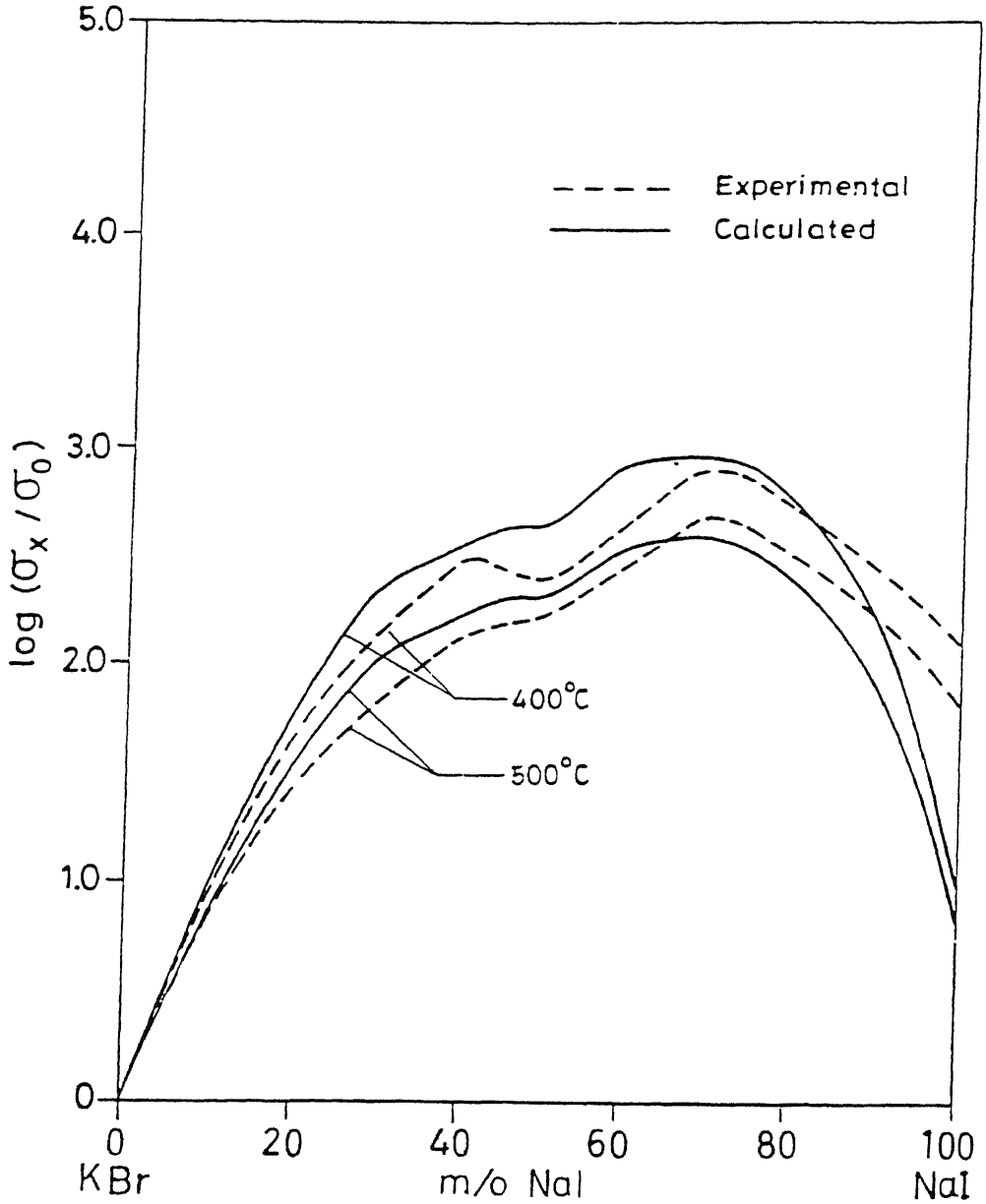

Fig.5.1.8. Relative conductivity (σ_x/σ_o) vs composition at 400 and 500°C. Solid lines corresponds to the conductivity obtained by Eq.(2.33), ie., LL model.

instance, the experimental (σ_x/σ_o) vs x curve shows a maximum at x = 70 m/o NaI which almost coincides with the minimum in the T_S-x plot (solidus temperature), and hence the maximum in the calculated σ_x/σ_o curve. The largest disagreement between the experimental and the calculated values of σ_x/σ_o in the KBr-rich region is within a factor of 2 which is well within the reproducibility limit of experimental results. The larger disagreement appearing to exist for KBr containing more than 90 m/o NaI should not be considered as a failure of the lattice loosening model; rather it should be attributed to the poor correlation between H and T_m, and between h and T_m (Eqs. 2.22 and 2.28).

Johannesen and Mckelvy (1985) have used a modified version of Eq.(2.33) in which a constant is introduced in the denominator of the exponent with the sole aim of reducing the effectiveness of the exponent so that the observed and calculated results are in better agreement. The fact that the results on KBr-NaI (Fig.5.1.8) and also on other systems (to be followed up latter in this chapter), within experimental error, are in good agreement with Eq. (2.33) would suggest that any modification of Eq. (2.33) is unnecessary.

It should, however, be pointed out that there exists a minor anomaly between the observed and calculated conductivities. Figure 5.1.8 shows that the rate of increase in the experimental relative conductivity (σ_x/σ_o) slows down considerably in the composition range 20-40 m/o NaI, and in fact σ_x/σ_o starts decreasing as x increases beyond 40 m/o NaI and goes through a

minimum at 50 m/o NaI before increasing once again. This effect is more pronounced for the 400°C-isotherm. The calculated (σ_x/σ_o) results, particularly at 400°C, do not quite agree with the observed results especially in the 35-45 m/o NaI range.

In summary, the existence of minor maxima in T_{mx}-x, σ - x, T_σ-x curves (Figs.5.1.1, 5.1.2 and 5.1.7, respectively), along with the E_a vs x curve (Fig. 5.1.5) suggests the possibility of an intermediate (new) compound which, however, could not be established. We believe that at least some preferential ordering of the host and dopant ions occurs in the solid solution range 40-70 m/o NaI. A maximum enhancement in conductivity by a factor of 500 with respect to pure KBr, and a factor of 8 with respect to pure NaI is obtained at 500°C corresponding to the composition of 70 m/o NaI. The behaviour of the σ vs x and E_a vs x plots is found consistent with the solidus curve of the phase diagram. The conductivity of solid solution $K_{0.6}Na_{0.4}Br_{0.6}I_{0.4}$ at T = 326°C (extrapolated from log σ vs 1/T plot from solid solution region) is less than 10^{-7} ohm^{-1} cm^{-1}, while that of the two-phase mixture of the same composition, ie, 60 m/o KBr + 40 m/o NaI, at the same temperature is $\approx 10^{-5}$ ohm^{-1} cm^{-1} which is two orders higher than the former.

5.2 KBr-NaBr MIXED CRYSTAL SYSTEM

5.2.1 Phase Diagram:

Figure 5.2.1 shows the temperature vs composition (T - x) phase diagram for the KBr-NaBr system. Only liquidus and solidus curves obtained on the basis of DTA results are shown in this figure. A rather well-defined minimum in the liquidus (T_L) curve appears at 616^{o}C and at a composition of 53 m/o NaBr (or x = 0.53). The solidus (T_S or T_{mx}) curve, on the other hand, shows a rather flat minimum that seems to extend from x = 0.43 to 0.72. This phase diagram appears quite similar to that of KCl-NaCl system (Coleman and Lacy 1967); both have a sort of well-defined minimum in the liquidus curve and a somewhat flat minimum in the solidus curve. In case of KCl-NaCl, the minimum in the solidus curve extends from x = 0.4 to 0.7.

Because of the small thermic effect involved during the demixing process, the shape of the demixing curve could not be ascertained from the DTA studies. The demixing process is so slow that only a very fast heating / cooling run might lead to a discernible peak in DTA. But the DTA at too fast heating/cooling rates is likely to result in an inaccurate determination of the characteristic (demixing) temperature. The XRD technique also could not be used for this purpose becuase the quenched samples do not seem to freeze the high temperature phases at which the XRD studies were supposed to be carried out. The ionic conductivity studies could also be used to construct the phase diagram (as discussed in sec.5.1.5, and also by Schrialdi et al

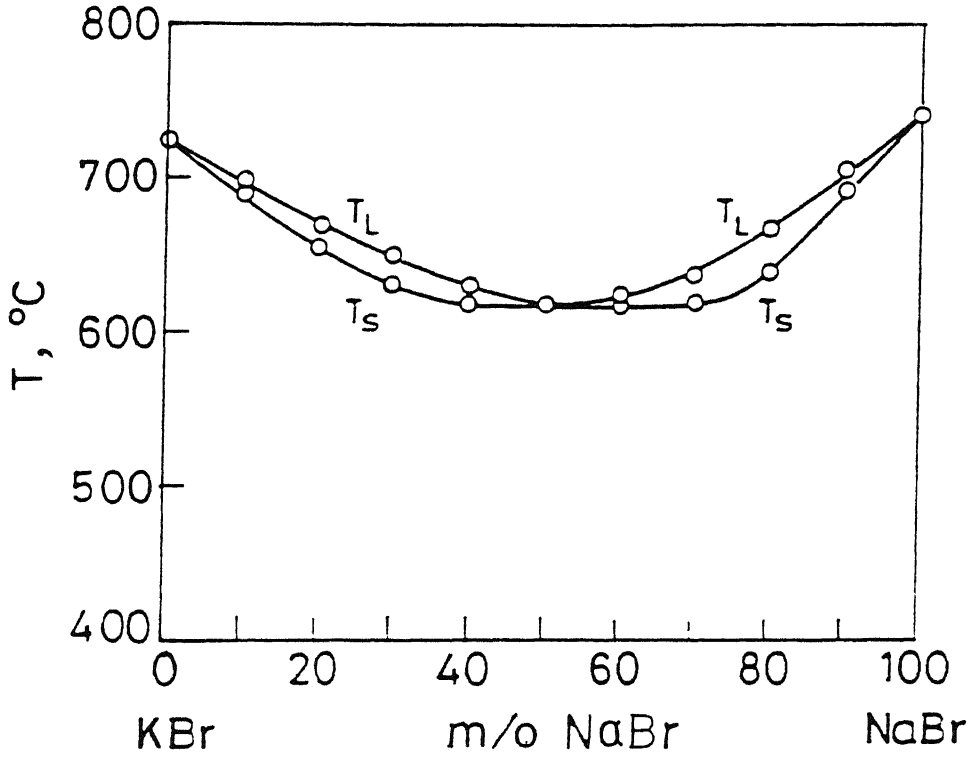

Fig.5.2.1. Phase diagram of KBr-NaBr system: Liquidus (T_L) and Solidus (T_S) temperature vs compositions (m/o NaBr in KBr).

1978 a,b), and we have found it especially useful in the determination of the demixing temperatures. The log σ - 1/T plot is generally reproducible and independent of heating/cooling rate in the solid solution region. However, below the demixing temperature, ie., in the two-phase region, the log σ - 1/T behaviour is very sensitive to the heating / cooling rate. This very feature has been used to ascertain that there exists a complete solid solubility at least above 400^{o}C in the KBr-NaBr system. The liquidus and solidus temperatures of all the compositions studied are given in Table 5.2.

5.2.2. Conductivity vs Composition:

Figure 5.2.2 shows the logarithm of conductivity (log σ), obtained from the complex impedance plots using platinum paint as electrodes, as a function of composition (m/o NaBr in KBr) at 400, 500 and 600^{o}C. Since our main interest was to investigate the conductivity enhancement due to homovalent dopants, some of the data points shown in Fig.5.2.2 are obtained by extrapolating the linear log σ vs 1/T plots in the intrinsic region to lower temperatures. It is evident that the conductivity increases as the concentration of NaBr in KBr increases, goes through a rather flat maximum that appears to extend over a wide range of composition and eventually starts decreasing. While the flat maximum extends from 40 to 70 m/o NaBr in the 600^{o}C isotherm, that in the 500^{o}C isotherm is spread from 40 to 55 m/o, and in the 400^{o}C isotherm it extends from 40 to 45 m/o NaBr. Thus, it is reasonable to suggest that the conductivity of the mixed crystals $K_{1-x}Na_xBr$ is maximum at $x = 0.42 \pm 0.02$, though it

TABLE 5.2

Melting points and the ionic transport parameters of KBr-NaBr mixed crystals

Mole fraction of NaBr	E_a intrinsic eV	E_a extrinsic eV	A intrinsic (ohm^{-1} cm^{-1})	Knee temp. (^oC)	T_L (^oC)	T_S (^oC)
0.0	1.65	0.61	3.18×10^4	612	729	729
0.1	1.61	0.81	4.55×10^4	585	700	689
0.2	1.56	0.84	6.17×10^4	516	669	655
0.3	1.53	0.80	7.57×10^4	507	647	630
0.4	1.49	0.70	7.18×10^4	502	630	620
0.5	1.47	0.86	5.19×10^4	454	616	617
0.6	1.49	0.82	6.70×10^4	452	620	618
0.7	1.55	0.86	1.59×10^4	468	635	621
0.8	1.60	0.82	6.17×10^5	490	671	644
0.9	1.66	0.83	2.85×10^5	508	702	685
1.0	1.71	0.73	4.62×10^5	565	739	739

becomes less evident as the temperature increases, ie., in the conductivity isotherms at 500 and 600°C. It should also be noted that in the NaBr-rich composition region, the conductivity falls off more rapidly in case of low temperature (400°C) isotherm.

A maximum enhancement in the conductivity with respect to KBr is by a factor of 36 at 400°C, 25 at 500°C and 19 at 600°C. These figures with respect to NaBr are 14 at 400°C, 8 at 500°C and 5 at 600°C. As for the shapes of the conductivity isotherms shown in Fig.5.2.2, it is worthwhile to point out that they have a strikingly similar shape to that of the solidus curve of the phase diagram (Fig.5.2.1).

5.2.3. Conductivity vs Temperature:

Figures 5.2.3 and 5.2.4 show the log σ vs $10^3/T$ plots for the mixed crystals of KBr containing up to 50 m/o NaBr and NaBr containing upto 50 m/o KBr respectively. These plots consist of, as usual, two linear regions, viz., intrinsic and extrinsic regions, separated by the so-called knee temperature (T_N). The ionic transport parameters such as the activation energy E_a, the pre-exponential factor A, the knee temperature T_N, etc., are also listed in Table 5.2. It is observed from Fig.5.2.3 that as the concentration of NaBr in KBr increases, not only the conductivity increases appreciably but also the overall activation energy in the intrinsic region decreases systematically (see Table 5.2). The results for NaBr containing KBr (Fig. 5.2.4) are analogous.

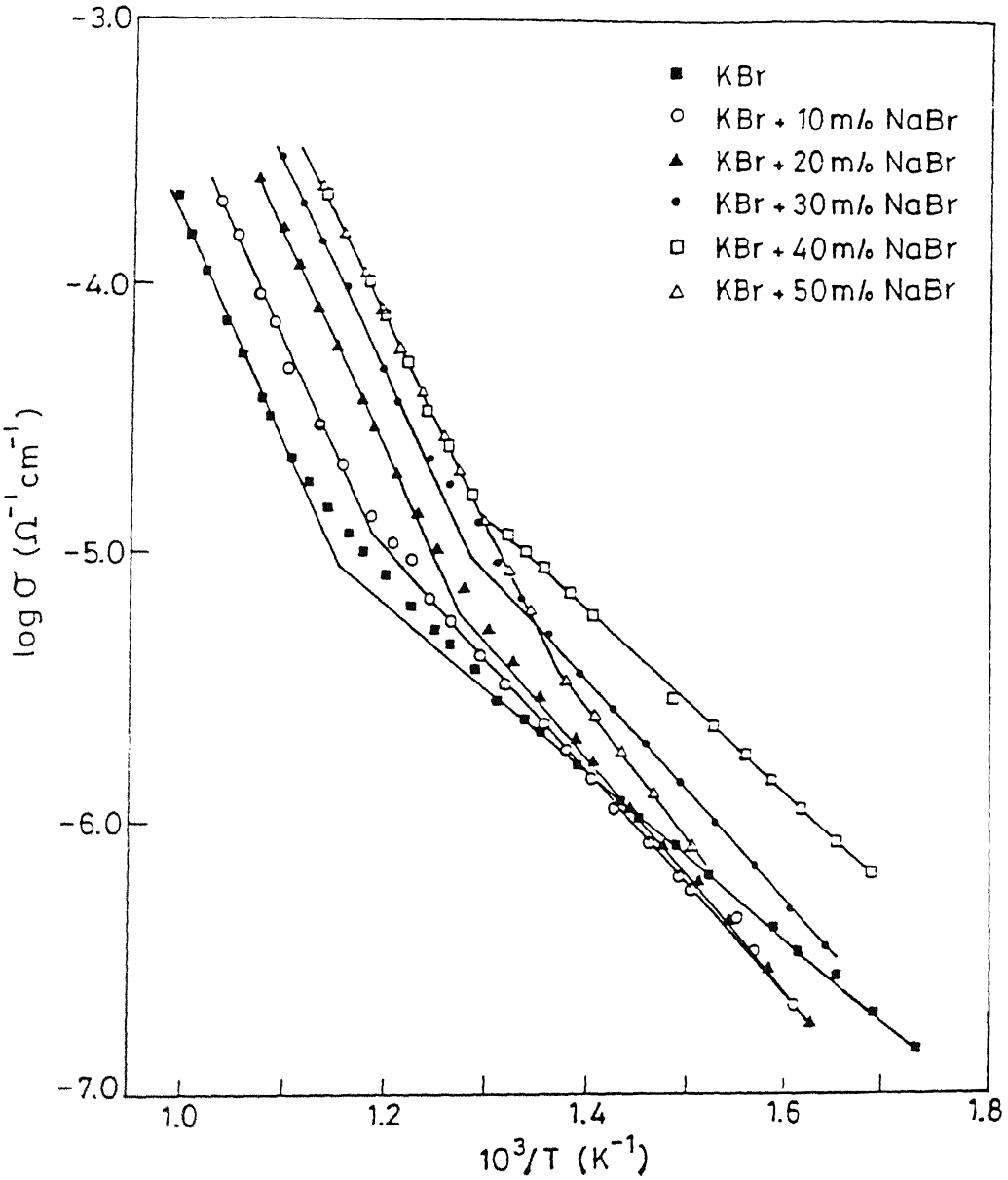

Fig.5.2.3. Logarithm of conductivity vs inverse temperature for $K_{1-x}Na_xBr$ ($0 \leq x \leq 0.5$) solid solutions.

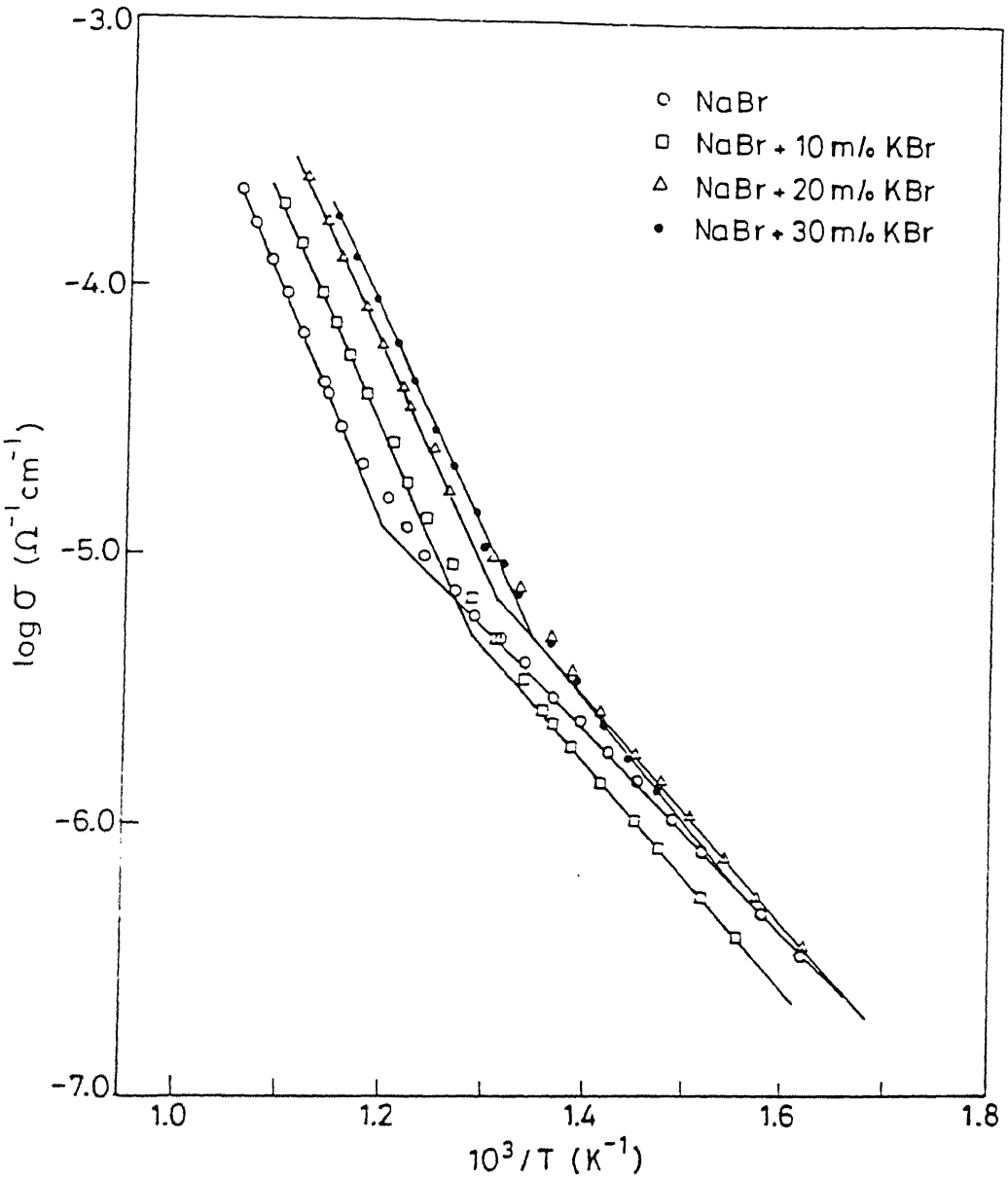

Fig.5.2.4. Logarithm of conductivity vs inverse temperature for $K_{1-x}Na_xBr$ ($0.7 \leq x \leq 1$) solid solutions.

5.2.4. Activation Energy vs Composition:

Figure 5.2.5 shows the variation of E_a (intrinsic) vs composition for KBr-NaBr system. It is evident that E_a decreases systematically as the concentration of dopants increases. The E_a vs x (m/o NaBr) plot exhibits a minimum at 52 m/o NaBr; E_a (minimum) = 1.47 eV as compared to E_a(NaBr) = 1.71 eV. Thus, E_a for $K_{0.5}Na_{0.5}Br$ mixed crystal is lowered by ≈ 12% and 14% with respect to those of KBr and NaBr respectively. While these results are, in genral, consistent with the lattice loosening concept, the E_a vs x behaviour is not exactly the same as that of T_{mx} (or T_S) vs x (see Fig. 5.2.1), the latter shows a flat minimum that extends from x = 0.4 to 0.7, while the former shows a rather well defined minimum at ≈ 50 m/o NaBr. As for the E_a in the extrinsic region, it is almost independent of composition and has more or less a fixed value in the range 0.8-0.86 eV, except for the pure salts (KBr and NaBr).

5.2.5 Discussion:

The close resemblance between the σ - x plots (Fig.5.2.2) and the T_S vs x plot (Fig.5.2.1) suggests that the conductivity enhancement in the mixed crystals follows the solidus temperature rather than the liquidus temperature. Equation (2.33) may be recalled to explain the conductivity - composition behaviour of $K_{1-x}Na_xBr$ mixed crystals on the basis of LL model. Since both KBr and NaBr exhibit Schottky defects, it is reasonable to assume that the basic defect mechanism in the $K_{1-x}Na_xBr$ mixed crystals remains the same as that in the parent crystals. Since ΔT_{mx} in Eq.(2.33) is known experimentally (Fig.5.2.1 and Table 5.2), the

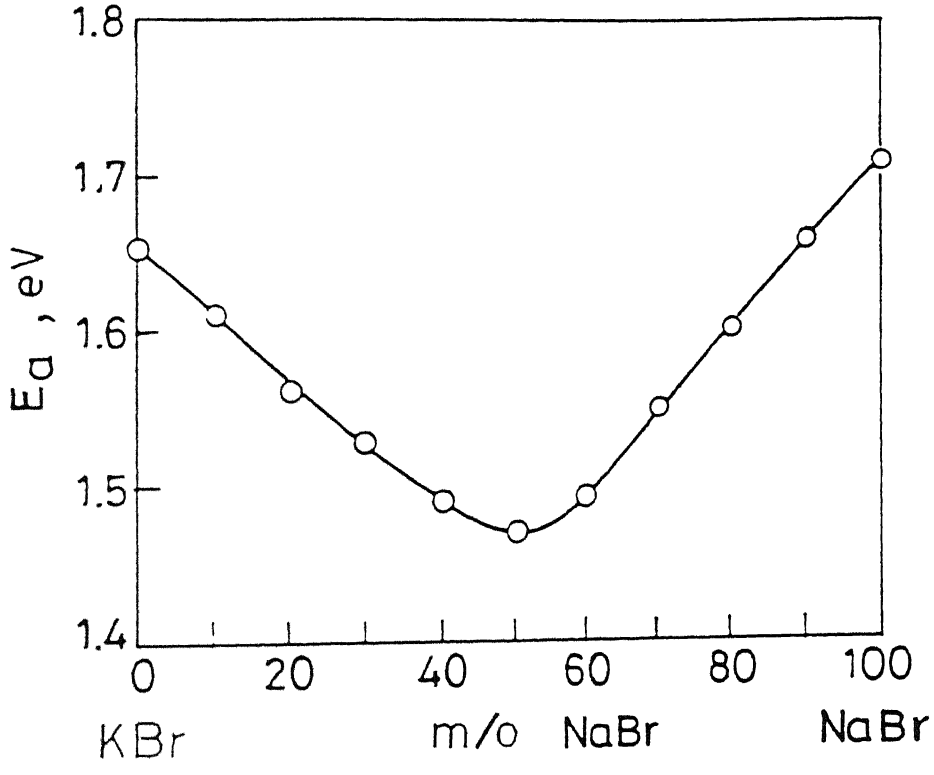

Fig.5.2.5. Activation Energy (intrinsic region) vs composition for KBr-NaBr system.

relative conductivity (σ_x/σ_o) can be calculated for various values of x. These results together with the experimental values are shown in Fig.5.2.6. The agreement between the two results is very good throughout the entire composition range, except in the NaBr-rich region. This should not be regarded as a failure of the LL model. It is rather attributable to the poor correlation between H (or h) and T_m; the data point corresponding to NaBr falls well below the H vs T_m linear plot (Barr and Lidiard 1970), implying that NaBr has a considerably lower value of H than that predicted by the correlation (Eq. 2.22) for a T_m (NaBr) = 643°C. It is interesting to note that both the calculated and the measured values of σ_x/σ_o agree with each other even with respect to fine details such as that both exhibit flat maximum extending from x = 0.4 to 0.7 (see the curve at 500°C).

Figure 5.2.7 shows the variation of T_N, the knee temperature, as a function of composition. Since T_N is the temperature at which the concentration of thermally generated defects equals that due to aliovalent impurities, it is expected that a mixed crystal having a lower formation enthalpy (than that of pure salt) will generate a certain concentration of defects at a lower temperature, and hence will have a lower T_N. Thus, T_N vs x behaviour found for KBr-NaBr system (Fig.5.2.7) is also consistent with the LL model.

Figure 5.2.8 shows the variation of solidus temperature (T_S), taken to be the melting temperature (T_{mx}), as a function of composition (m/o NaBr in KBr). The temperatures, ie., T_σ, at which the mixed crystals atttain the fixed conductivities of σ_1 =

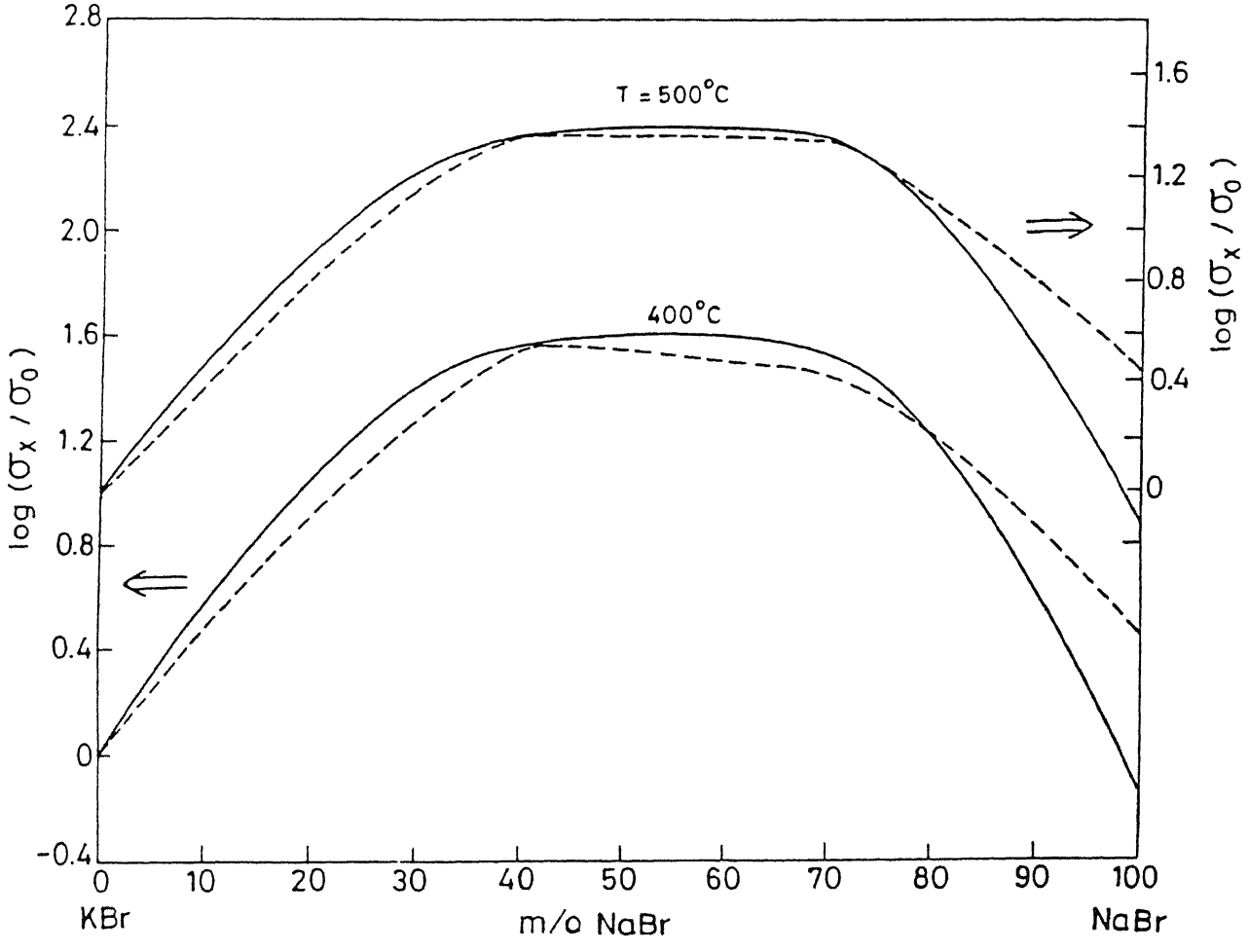

Fig.5.2.6. Relative conductivity (σ_x/σ_0) vs composition at 400 and 500°C. The solid and broken lines respectively represent the calculated and experimental values of σ_x/σ_0.

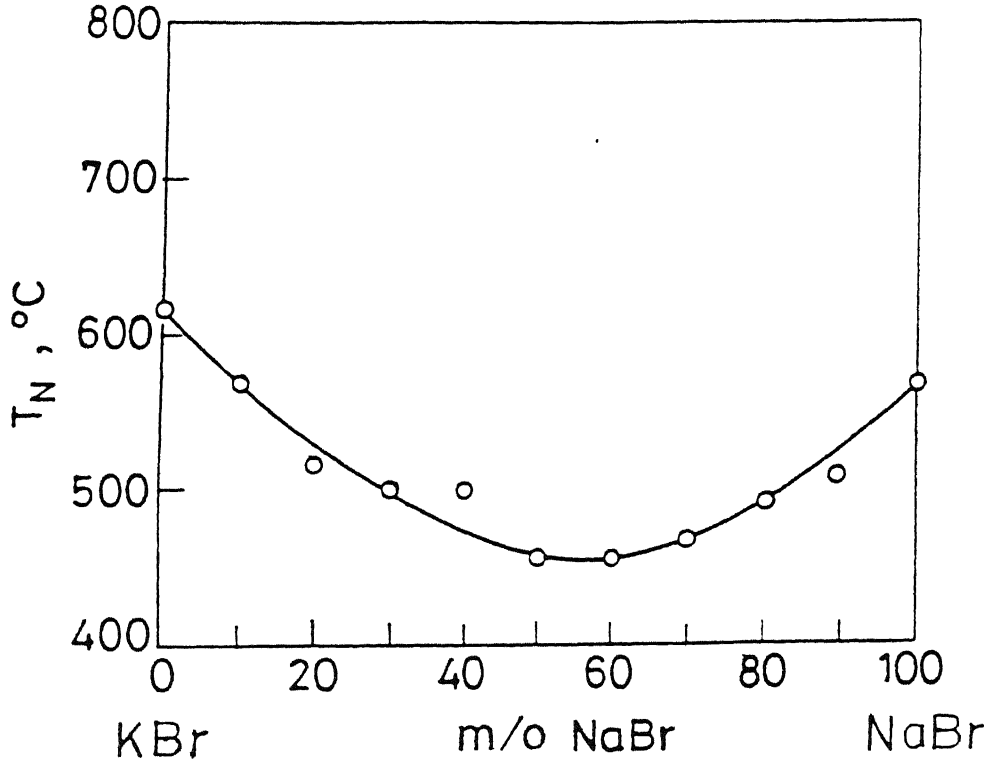

Fig.5.2.7. Knee temperature vs composition for KBr-NaBr system.

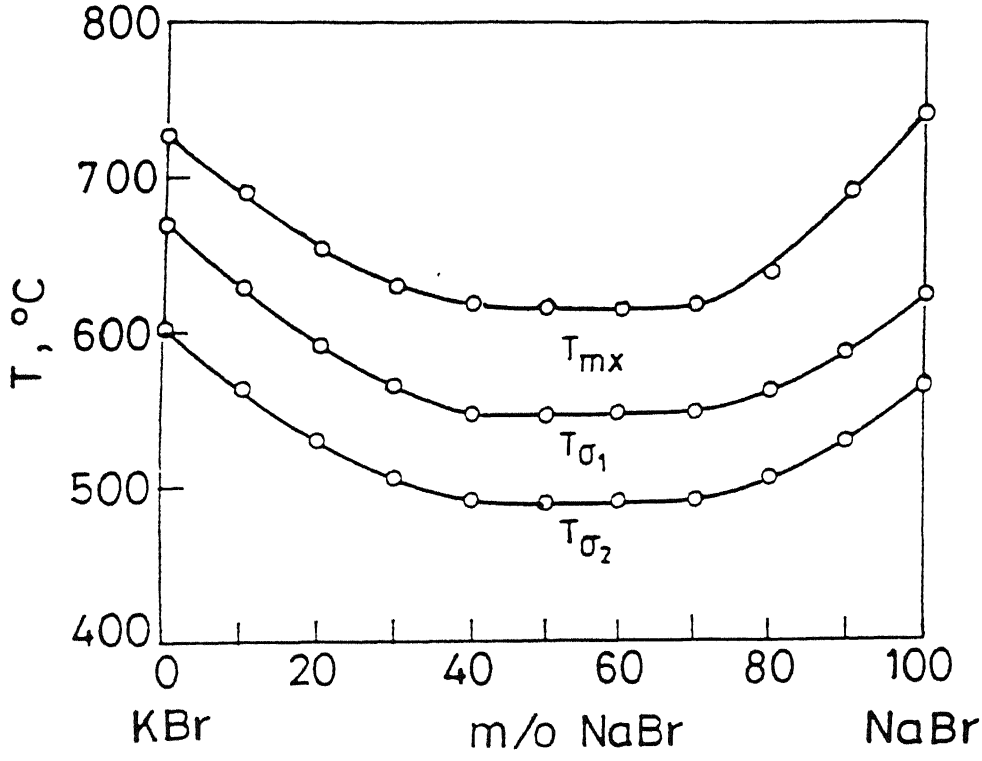

Fig.5.2.8. T_σ as a function of composition for KBr-NaBr system. $\sigma_1 = 5 \times 10^{-5}$ and $\sigma_2 = 10^{-5}$ ohm^{-1} cm^{-1}. T_{mx} curve is the melting (solidus) curve of the phase diagram (Fig.5.2.1).

5×10^{-5} and $\sigma_2 = 10^{-5}$ ohm^{-1} cm^{-1} respectively are also shown as a function of composition in Fig.5.2.8. The σ data for these plots are taken from the log σ vs $10^3/T$ plots shown in Figs. 5.2.3 and 5.2.4. Both the T_σ vs composition plots exhibit flat minima in the same composition range where the solidus curve does.

According to the CBΩ model (see Sec. 2.3.2) the composition (x_m) corresponding to the maximum conductivity is given by (Eq. 2.43)

$$x_m = \frac{(k_d/k_o)-2}{\lambda\ (k_d/k_o)}$$

Substituting the values of λ and (k_d/k_o) which were calculated from the data given by Smith and Cain (1975) and Roberts and Smith (1970) (see Appendix A) in the above equation, we get

$$x_m = 0.37$$

Thus, according to the CBΩ model, KBr containing 37 m/o NaBr should exhibit the maximum conductivity which is not too far from the value (≈ 42 m/o NaBr) inferred from the experiments (Fig. 5.2.2).

Alternatively, if we consider KBr as the dopant in NaBr for which case $k_d/k_o = 2.222$, we get

$$x_m = 0.29$$

ie., NaBr containing ≈ 29 m/o KBr should have the maximum

conductivity which is in good agreement with the observed value (≈ 30 m/o KBr).

In summary, there is appreciale enhancement in the conductivity of $K_{1-x}Na_xBr$ mixed crystals, and that the enhancement in the conductivity is consistent with the phase diagram. The close agreement between the observed and the calculaed (σ_x/σ_o), Fig. 5.2.6, and the close resemblance between T_σ vs composition (Fig. 5.2.8), T_N vs composition (Fig. 5.2.7) and the melting temperature vs composition (Fig. 5.2.7) provides strong support to the LL model. The CBα model is found to correctly predict the composition corresponding to the maximum conductivity in this system.

5.3 NaBr-NaI MIXED CRYSTAL SYSTEM

5.3.1 Phase Diagram:

The liquidus and the solidus curves of the phase diagram of NaBr-NaI system, as inferred from the DTA studies are shwon in Fig.5.3.1. The literature values (International Critical Tables, ICT, 1928) corresponding to the liquidus curve are also shown for comparison. There is a good agreement between the two results as far as the nature of the liquidus curve is concerned. However, the ICT (1928) values of the melting point of pure as well as mixed crystals, and also the melting points of the pure salts quoted in CRC Handbook (Weast 1980) are consistently higher (by 8 - 10^{o}C) than the present values. We, however, rely on the present set of data because (i) the melting points were determined from DTA using precalibrated thermocouples, (ii) the same set up yielded more reasonable values for other salts used in this work, and (iii) the comparative study and analysis of the subsequent data may then be more meaningful. In any case, the above discrepancy may be attributed to the errors in the experimental determination of melting point from DTA, as well as to varying degree of the purity of the salts.

Both the liquidus and the solidus curves (Fig.5.3.1) exhibit a minimum at ≈ 70 m/o NaI; the lowest melting point observed is ≈ 630^{o}C which is about 107 and 21^{o}C lower than those of pure NaBr and NaI respectively. The liquidus and the solidus temperatures of all compositions studied are listed in Table 5.3. The solid solution / two-phase boundary (demixing curve) could

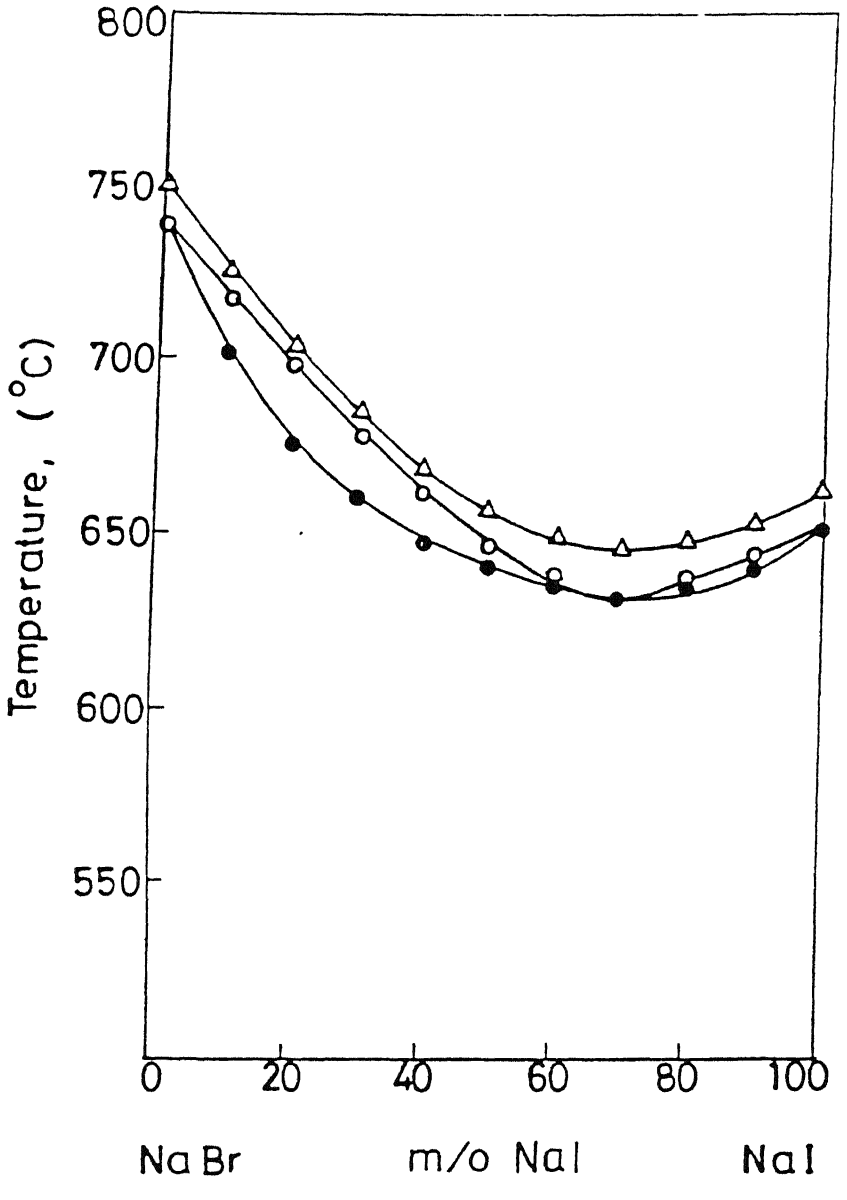

Fig.5.3.1. Phase diagram of NaBr-NaI system: Liquidus (T_L) and Solidus (T_S) temperature vs compositions (m/o NaI in NaBr). Δ - Melting points (Liquidus) according to ICT (1928).

TABLE 5.3

Melting points and the ionic transport parameters of NaBr-NaI mixed crystal system

Mole fraction of NaI	E_a intrinsic eV	E_a extrinsic eV	A intrinsic (ohm^{-1} cm^{-1})	Knee temp. (^oC)	T_L (^oC)	T_S (^oC)
0.0	1.71	0.88	2.53×10^5	531	737	737
0.1	1.68	1.11	3.51×10^5	490	717	705
0.2	1.64	1.02	5.32×10^5	472	796	675
0.3	1.60	1.12	3.01×10^5	466	677	660
0.4	1.57	1.00	3.87×10^5	434	661	646
0.5	1.55	1.04	4.34×10^5	415	646	641
0.6	1.48	1.12	2.43×10^5	410	638	633
0.7	1.44	0.97	1.38×10^5	426	630	629
0.8	1.48	1.05	2.05×10^5	413	638	634
0.9	1.52	0.95	4.36×10^5	424	644	639
1.0	1.57	0.88	5.57×10^5	439	651	651

not be studied using DTA because of the small thermic effect associated with that process. The conductivity studies which extend down to 350°C, in a normal Arrhenius manner, suggest that the NaBr-NaI system forms a complete solid solution, at least above 350°C.

5.3.2. Conductivity vs Composition:

Complex impedance analysis (CIA) was used to obtain the dc conductivity of each sample at various temperatures. Figure 5.3.2 shows the (dc) conductivity obtained from the CIA as a function of composition at three different temperatures. Since our primary aim was to investigate the conductivity enhancement due to the substitution of homovalent dopants, only the intrinsic condctivity and the extrapolated intrinsic conductivity at lower temperatures were considered while drawing the conductivity isotherms (Fig.5.3.2). It is observed that as the concentration of NaI increases, the ionic conductivity of the mixed crystal also increases, goes through a maximum at the composition of ≈ 70 m/o NaI and starts decreasing subsequently. It is also evident that the enhancement in conductivity is more prominent at lower temperatures. A maximum enhancement by a factor of 46 with respect to pure NaBr, and 2 with respect to pure NaI, is observed at 400°C and at a composition of 70 m/o NaI.

5.3.3. Conductivity vs Temperature:

Figures 5.3.3 and 5.3.4 show the log σ vs 1/T plots for solid solutions $NaBr_{1-x}I_x$ in the range $0 \leq x \leq 0.7$ and $0.7 \leq x \leq 1$ respectively. The conductivity-temperature plots follow the usual Arrhenius equation, and consist of two linear regions,

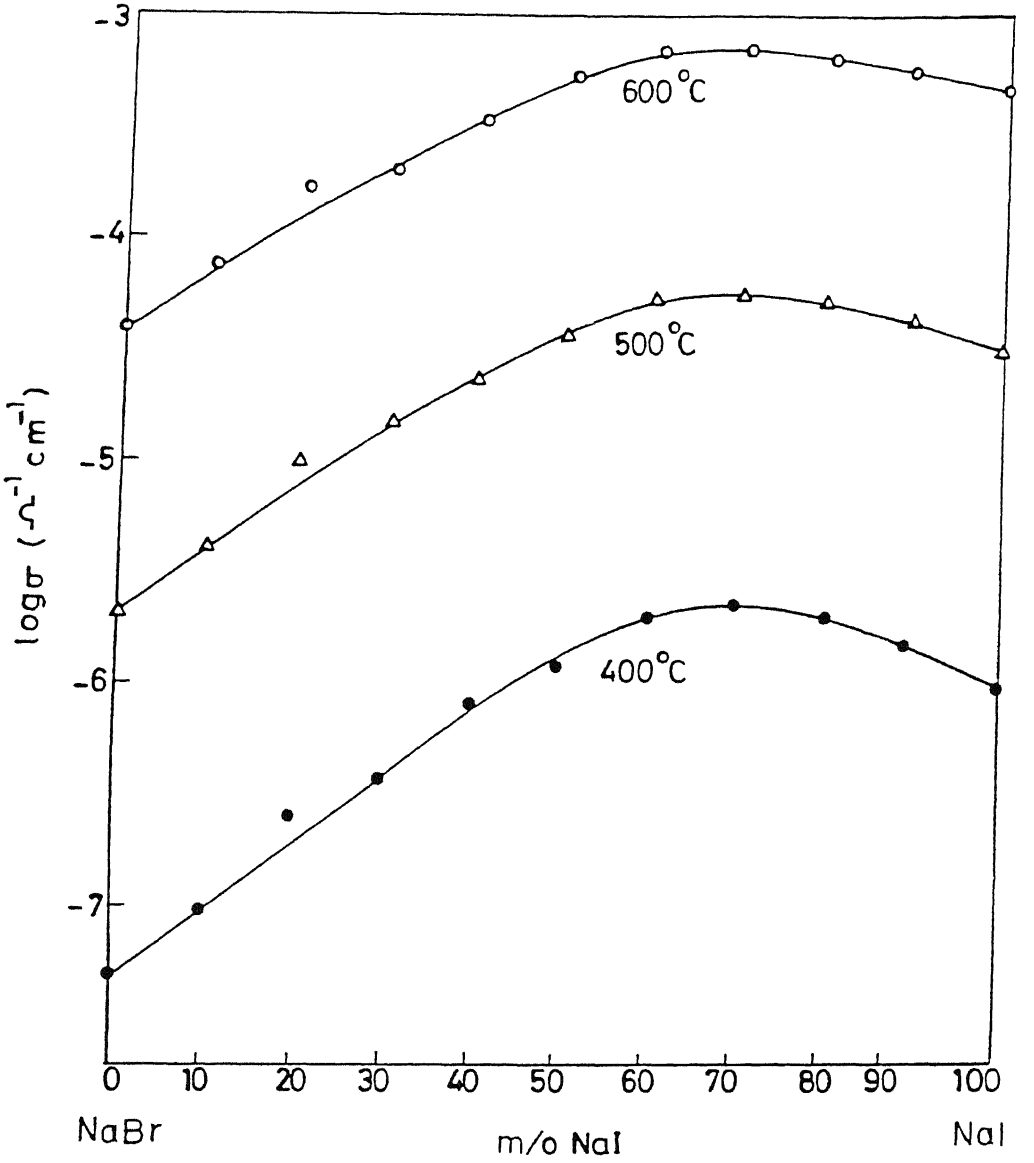

Fig.5.3.2. Logarithm of conductivity vs composition (m/o NaI in NaBr) at 400, 500 and 600°C. The curve corresponding to T = 400°C is based on conductivity data obtained by extrapolating the linear log σ vs 1/T plot (intrinsic region) to 400°C.

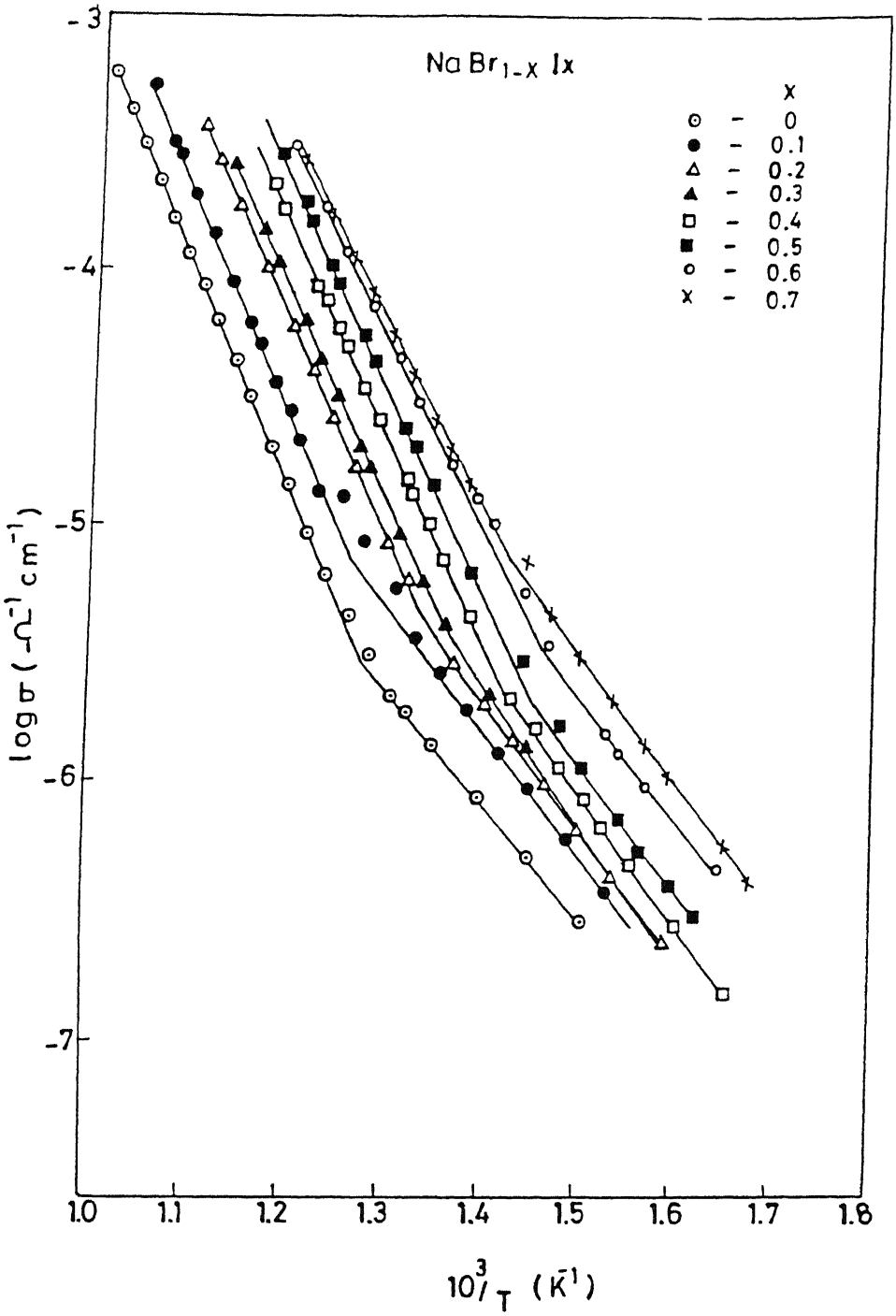

Fig.5.3.3. Logarithm of conductivity vs inverse temperature for $NaBr_{1-x}I_x$ ($0 \leq x \leq 0.7$) solid solutions.

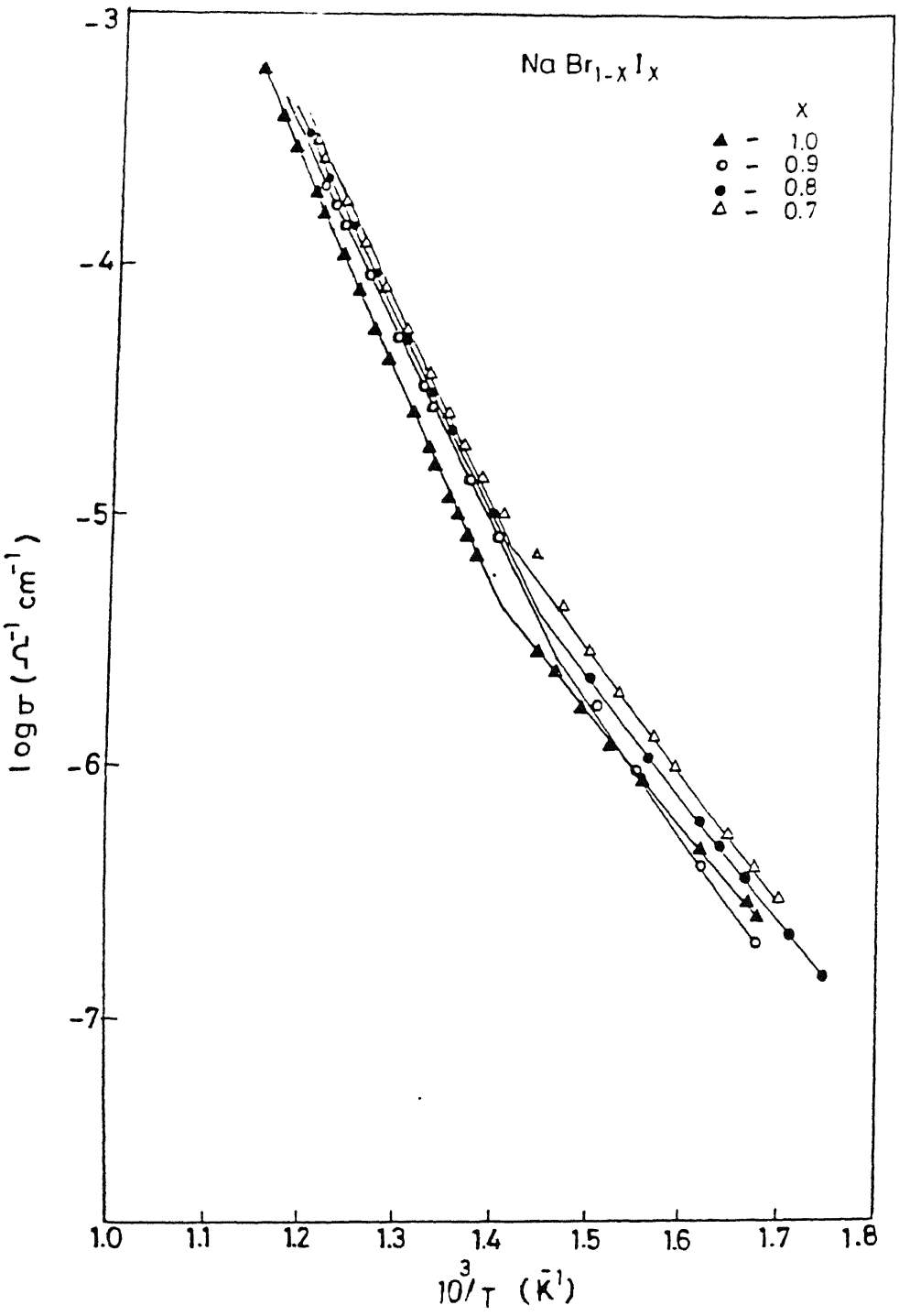

Fig.5.3.4. Logarithm of conductivity vs inverse temperature for $NaBr_{1-x}I_x$ ($0.7 \leq x \leq 1$) solid solutions.

viz., intrinsic and the extrinsic regions, separated by a knee point (T_N). The pre-exponential factor,A, the activation energy,E_a (both intrinsic and extrinsic) and the knee point for various compositions for the present mixed crystal system are given in Table 5.3.

The variations of activation energy (E_a) and the knee temperature as a function of composition are shown in Figs. 5.3.5 and 5.3.6 respectively. While the conductivity increases due to the substitution of homovalent dopants, both the intrinsic E_a and T_N decrease. As expected, the E_a vs x and T_N vs x plots exhibit a minimum at around the same composition (70 m/o NaI) at which the σ vs x plot exhibits a maximum. These results are qualitatively in agreement with the LL model.

5.3.4. Discussion:

Figure 5.3.7 shows the experimental and calculated (Eq.2.33) relative conductivities (σ_x/σ_o) vs composition at three different temperatures (400, 500 and 600^oC) for NaBr-NaI mixed crystals. Eq.(2.33), ie., the LL model, predicts σ enhancements by factors of 35, 22 and 14 with respect to pure NaBr at 400, 500 and 600^oC respectively, for the $NaBr_{0.3}I_{0.7}$ solid solution, while the corresponding experimental values are 46, 26 and 15. Despite various approximations used to derive Eq.(2.33), the agreement between the observed and calculated values is fairely good, particularly at higher temperatures where the impurities and thermal history of the samples have minimal effect. Thus the LL model appears to be quite satisfactory for NaBr-NaI mixed crystals.

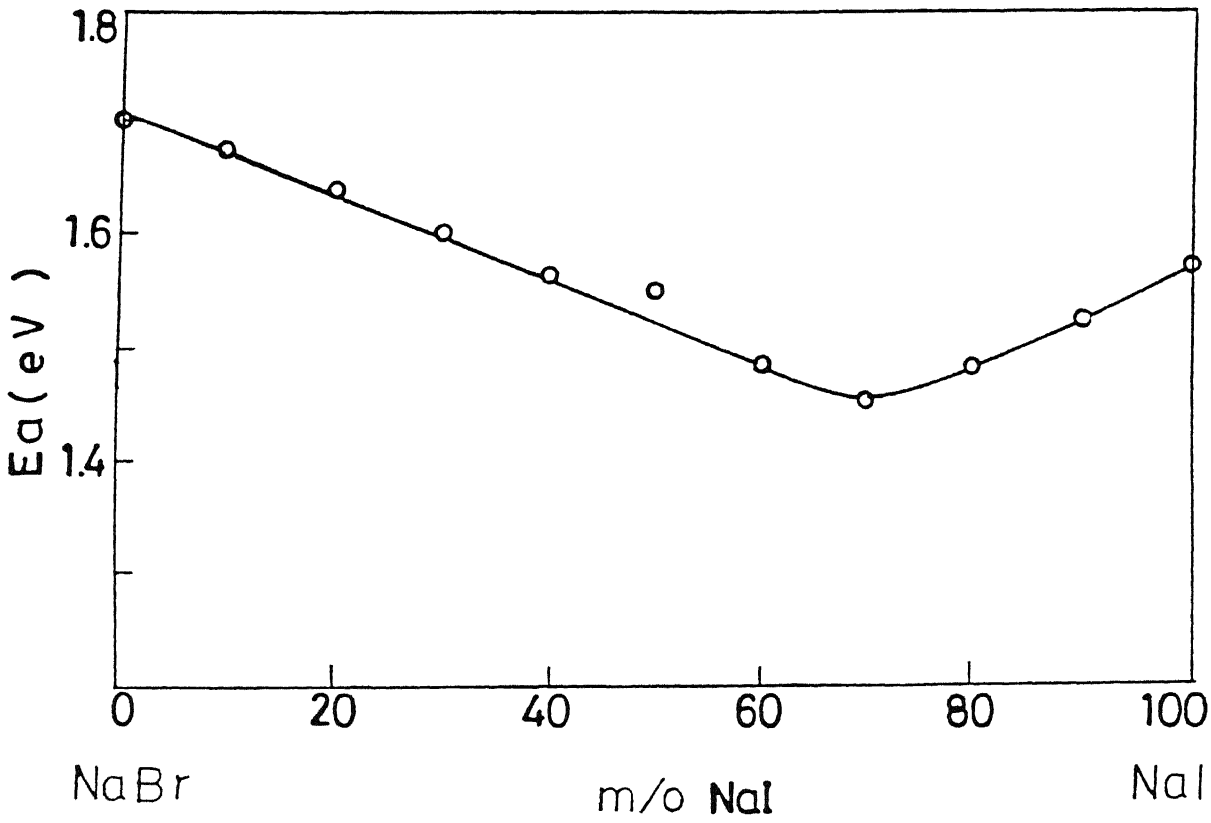

Fig.5.3.5. Activation Energy (intrinsic region) vs composition for NaBr-NaI system.

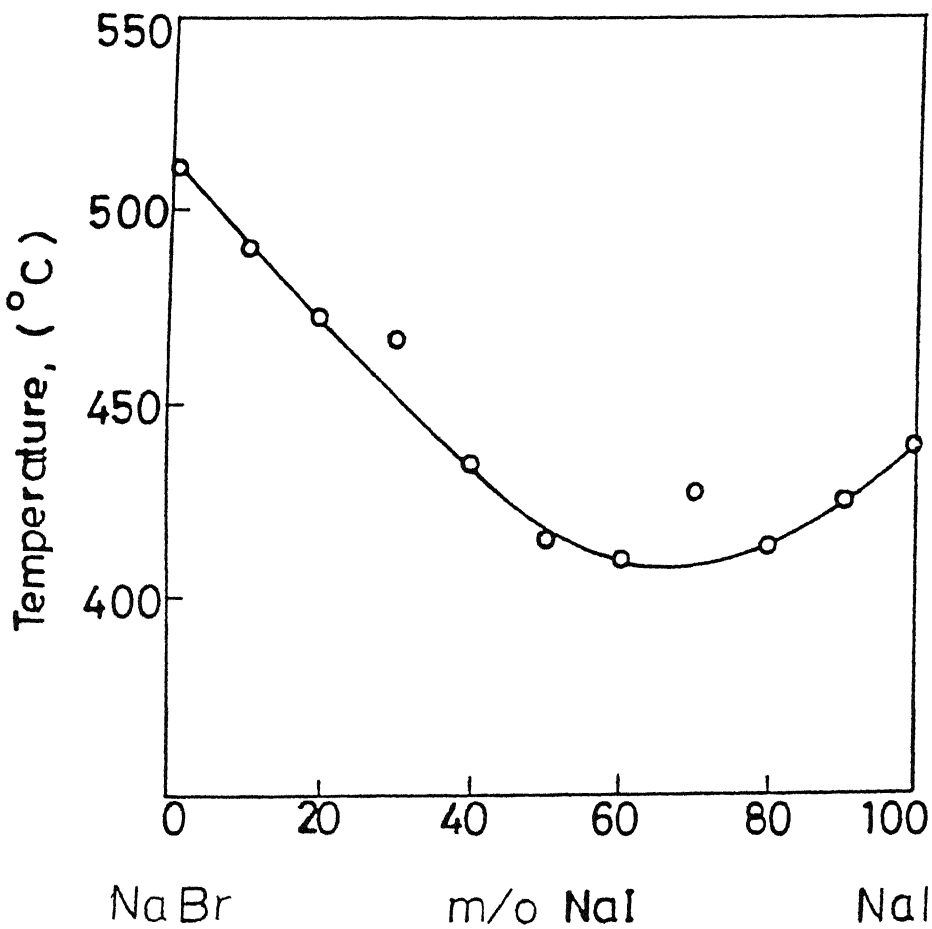

Fig.5.3.6. Knee temperature vs composition for NaBr-NaI system.

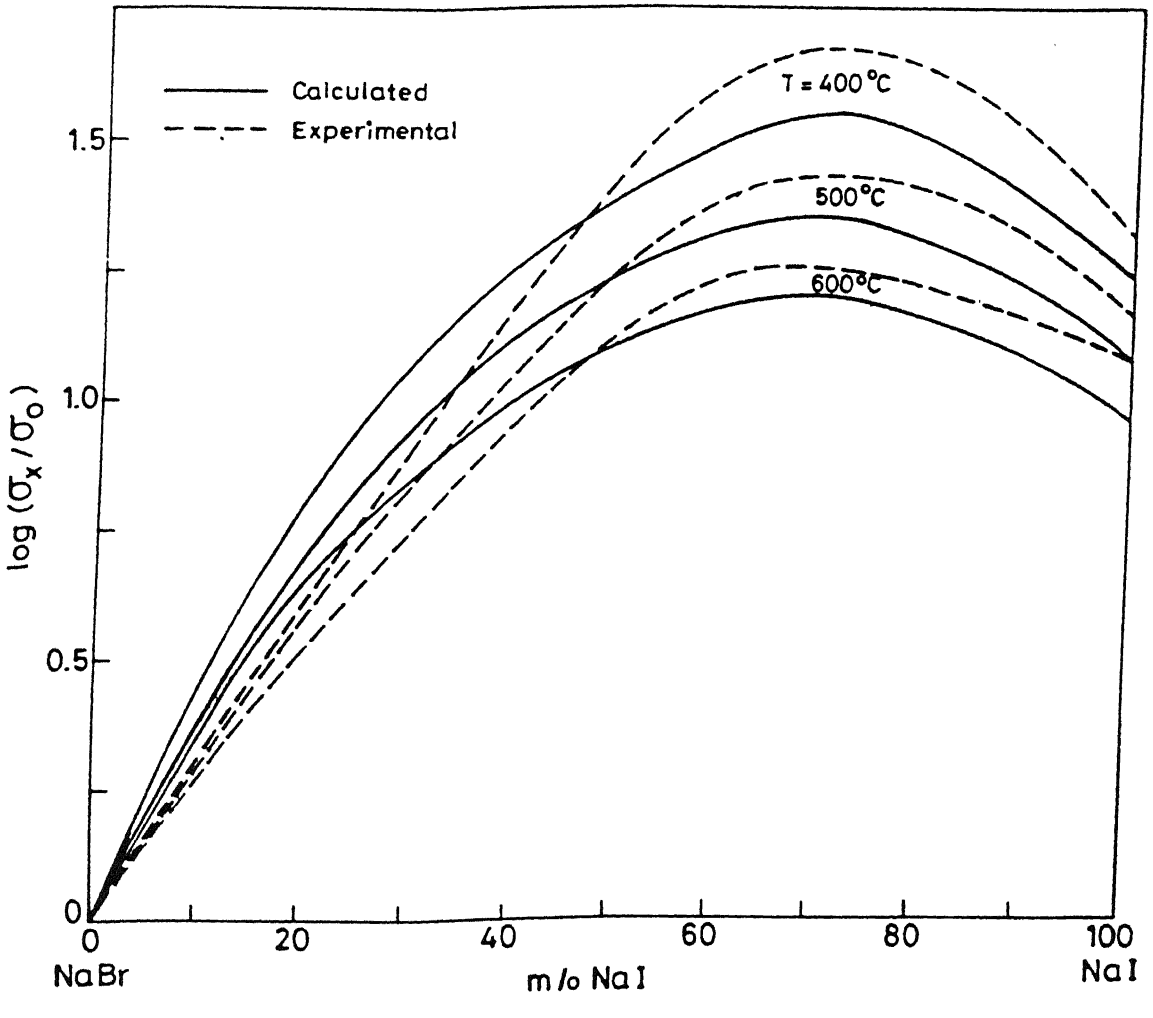

Fig.5.3.7. Relative conductivity (σ_x/σ_o) vs composition at 40(and 500°C. The solid and broken lines respectively represent the calculated and experimental values of σ_x/σ_o.

The temperature (T_σ) at which the mixed crystal attains a certain (fixed) value of conductivity (σ) is shown as a function of composition in Fig.5.3.8. The $T_{\sigma 1}$ and $T_{\sigma 2}$ curves corresponding to $\sigma 1 = 5 \times 10^{-5}$ and $\sigma_2 = 10^{-5}$ ohm^{-1} cm^{-1} respectively are constructed from the data shown in Figs.5.3.3 and 5.3.4 (with the intrinsic region extrapolated to appropriate temperatures). The solidus curve (T_{mx}) of the phase diagram (Fig.5.3.1) is also shown in Fig.5.3.8. The resemblance between the T_{mx} vs x and T_σ vs x curves alongwith the results shown in Figs.5.3.5 and 5.3.6 provide strong support to the LL model.

By considering NaBr as the pure component and NaI as the second component (dopant) and substituting the corresponding values of n, dB/dP and λ (Appendix A) in Eq. (2.43), ie., the CBa model, we find that the maximum conductivity enhancement should occur at

$$x_m = 0.37$$

ie., the NaBr-NaI mixed crystal system should exhibit maximum conductivity at $\approx$ 37 m/o NaI.

However, if we consider NaI as the pure component and NaBr as the dopant, we get

$$x_m = 0.40$$

ie., the σ in the NaBr-NaI system should be a maximum at $\approx$ 40 m/o NaBr (or 60 m/o NaI). Thus the CBa model, with the given set of input parameters(n, dB/dP, etc.), predicts the existence of a

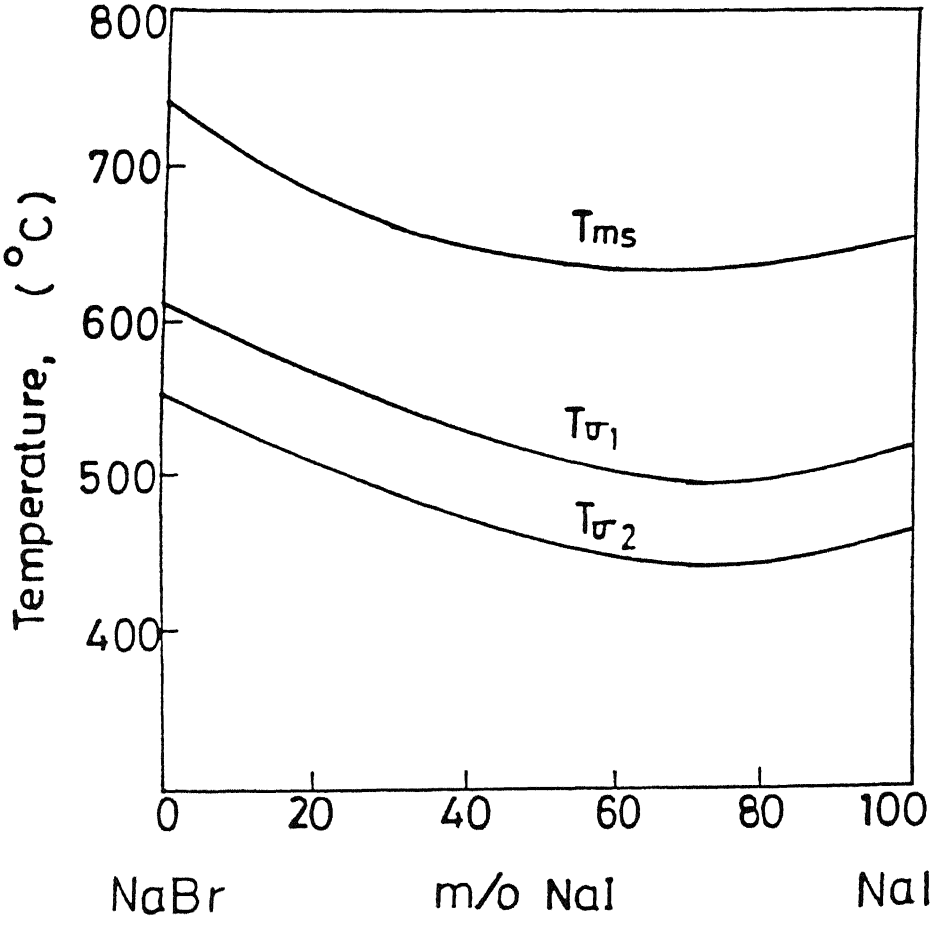

Fig.5.3.8. T_σ as a function of composition for NaBr-NaI system. $\sigma_1 = 5 \times 10^{-5}$ and $\sigma_2 = 10^{-5}$ ohm^{-1} cm^{-1}. T_{ms} curve is the melting (solidus) curve of the phase diagram (Fig.5.3.1).

maximum in the conductivity vs composition curve in the composition range $0.37 \leq x_m$ (mole fraction NaI) ≤ 0.60, while the experimental value of x_m is 70 m/o NaI. The disagreement between the calculated and the observed values of x_m is rather surprising especially because the conditions of the CBΩ model (Varotsos and Alexopolous 1986), viz;

$$k_d/k_o \geq 2 \quad \text{and} \quad 1 - \frac{2}{(k_d/k_o)} \leq \lambda$$

are well satisfied by the present NaBr-NaI system. Thus, it would appear that the above model needs suitable modifications to widen its generality (see Chapter-6).

In summary, there is appreciable enhancement in the conductivity due to the substitution of homovalent I^- ions in NaBr, whereas the conductivity enhancement in NaI due to Br^- ions substitution is relatively small. The maximum ehancement in the conductivity is observed for $NaBr_{0.3}I_{0.7}$ solid solution which also has the minimum melting point (630^oC) and the lowest activation energy (1.44 eV). These results are consistent with the LL model. The conductivity studies suggest that a complete solid solubility exists in NaBr-NaI mixed crystal system at least above 350^oC.

5.4 NaBr-LiBr MIXED CRYSTAL SYSTEM

5.4.1 Phase Diagram:

The phase diagram of NaBr-LiBr system is shown in Fig. 5.4.1. The liquidus and the solidus curves are drawn as usual on the basis of DTA results. Also shown in the above figure are the liquidus and solidus curves as reported in the International Critical Tables (ITC, 1928) which are in good agreement with the present results. The liquidus curve exhibits a minimum at 530^{o}C at a composition of 80 m/o LiBr. The minimum in the solidus curve occurs at about the same temperature (528^{o}C, to be precise) in the composition range 70 - 80 m/o LiBr. Thus a maximum decrease in the melting point of 211^{o}C (27^{o}C) with respect to pure NaBr (LiBr) is obtained. These results suggest that the substitution of smaller Li^{+} ions introduces more lattice strain in the NaBr lattice than does the substitution of larger Na^{+} ions in LiBr lattice. As a result, there is a sharp decrease in the melting point of NaBr doped with LiBr. The difference between the liquidus and the solidus temperatures is generally higher for NaBr-rich compositions. For instance, it is 45^{o}C for NaBr + 40 m/o LiBr as compared to 5^{o}C for the LiBr-rich ($\geq$ 70 m/o) compositions. The liquidus and solidus temperatures corresponding to all the compositions studied as well as the literature values are listed in Table 5.4.

The single-phase/two-phase demixing curve could not be obtained from the DTA studies. However, the demixing temperatures obtained from the conductivity vs temperature studies are ploted

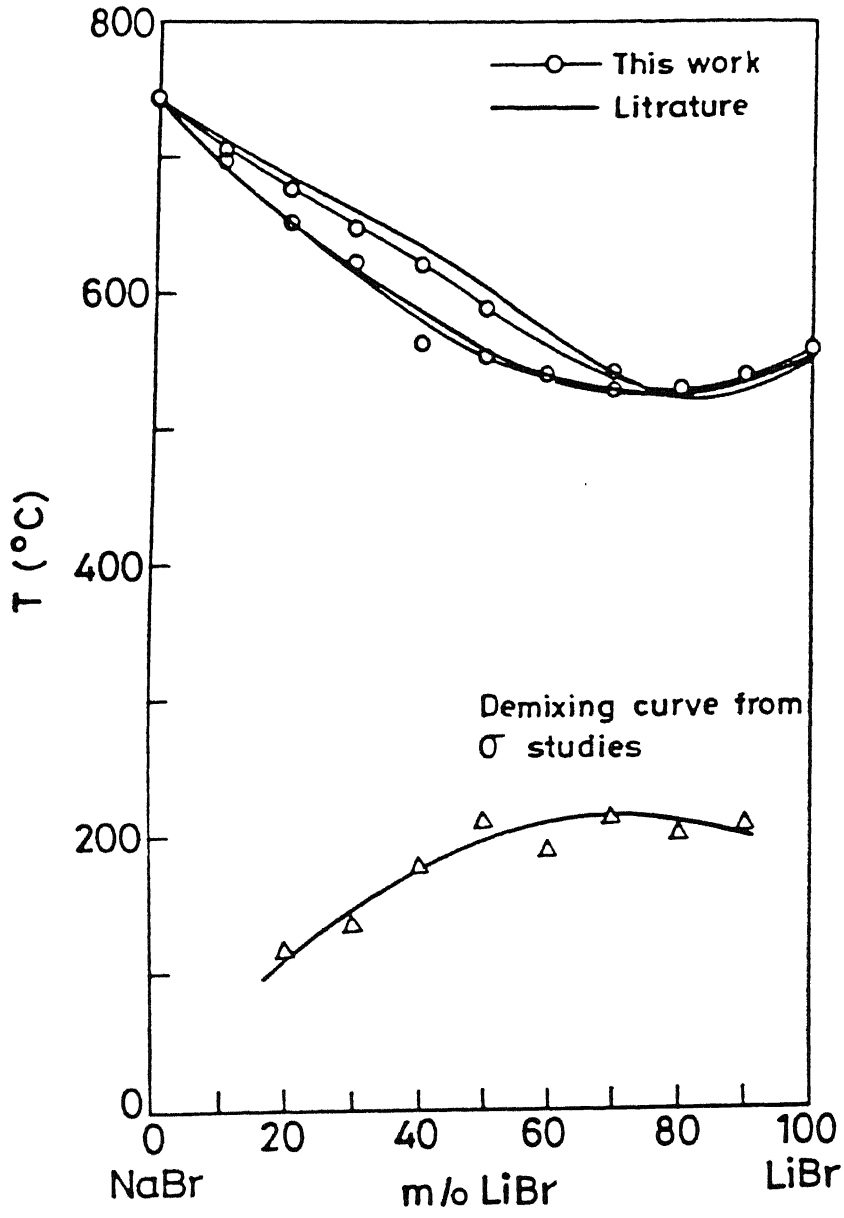

Fig.5.4.1. Phase diagram of NaBr-LiBr system: (T_L) and (T_S) are the liquidus and the solidus curves as interpreted from the DTA studies. Also shown are the curves according to ICT (1928). Δ -Single phase / two phase demixing boundary.

TABLE 5.4

Melting and the demixing temperatures for NaBr-LiBr mixed cryste system.

Mole fraction of LiBr in NaBr	T_L Present study (^oC)	T_L Literature* (^oC)	T_S Present study (^oC)	T_S Literature* (^oC)	Demixing temperature (^oC)
0	739	740	739	740	——
0.1	705	714	697	692	X
0.2	675	686	652	653	118
0.3	646	660	614	614	166
0.4	620	685	575	633	174
0.5	588	602	550	557	210
0.6	557	569	537	537	190
0.7	535	538	528	526	214
0.8	530	520	530	520	200
0.9	535	525	532	533	210
1.0	555	550	555	550	——

*International Critical Tables (1928).

TABLE 5.5

Mixed crystal system	KCl-NaCl	KI-NaI	NaCl-NaBr	KBr-NaI	NaBr-LiBr
Lattice constant, (A)	6.278 - 5.627	7.052 - 6.462	5.627 - 5.95	6.58 - 6.462	5.95 - 5.49
composition corresponding to the peak in the demixing curve	65 m/o NaCl	63 m/o NaI	45 m/o NaBr	50 m/o NaI	70 m/o LiBr

in Fig.5.4.1. In the conductivity measurements during cooling cycle, the demixing temperatures were characterized by an abnormal fall in the conductivity values as soon as the demixing temperature was attained (see Fig.5.4.2). Unlike the conductivity behaviour of KBr-NaI system (sec. 5.1.5) where the demixing process was very slow and dependent on the cooling rate, the present NaBr-LiBr system shows almost no dependence on the cooling rate. A peak in the demixing curve occurs at the composition of ≈ 70 m/o LiBr which is the same as the composition at which the solidus/liquidus curve exhibits a minimum. Thus, the NaBr-LiBr system forms a complete solid solution only at temperatures above ≈ 215. The demixing curve (Fig.5.4.1) has a parabolic shape that is somewhat asymmetrical, and its peak is tilted towards the LiBr-rich region. These results compare well with those of KI-NaI, KCl-NaCl and NaBr-NaCl systems (see, Sec. 5.1.1). As pointed out earlier, the extent of the asymmetrical tilt depends on the mismatch between the lattice constants of the components and occurs close to that component whose lattice constant is lower. This is again consistent with the fact that a solid having a larger lattice constant is soluble to a smaller extent in a solid having a smaller lattice constant at any given temperature. The demixing temperatures corresponding to all the compositions studied are listed in Table 5.4. Table 5.5 gives the lattice constant and the composition for which the peak in the demixing curve is obtained for similar binary system of alkali halides.

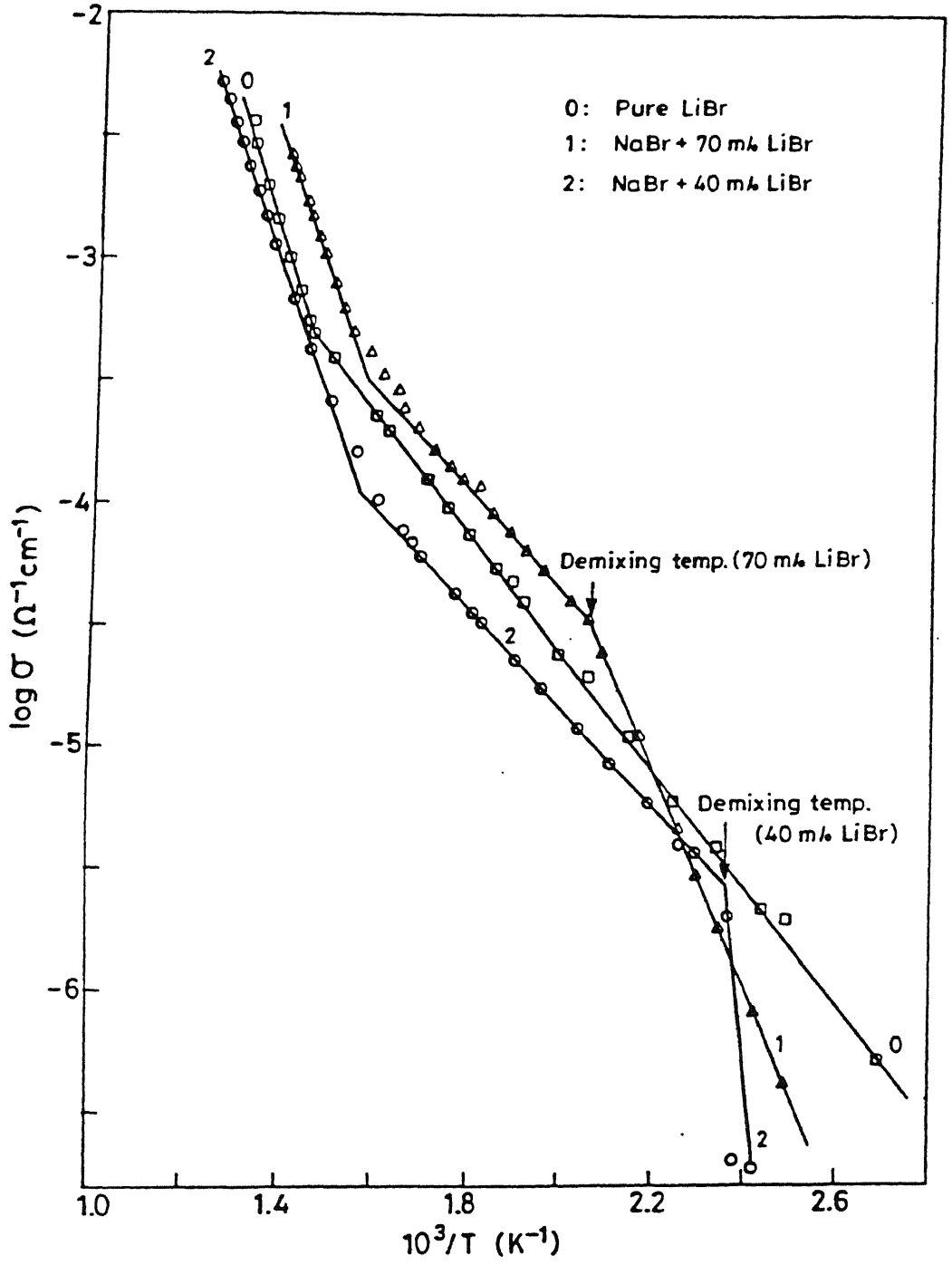

Fig.5.4.2. Logarithm of conductivity vs inverse temperature showing the demixing process. ▫ - Pure LiBr, Δ - NaBr + 70 m/o LiBr and o - NaBr + 40 m/o LiBr.

5.4.2. Conductivity vs Composition:

The dc conductivity values were obtained, as usual, from complex impedance analysis (see, Chapter-4) using platinum paint electrodes. Figure 5.4.3 shows the conductivity - composition isotherms at 400 and 500°C. An enhancement in the conductivity by a factor of 2.3×10^4 (5.1×10^3) is obtained with respect to pure NaBr at 400 (500°C) at the composition of 70 m/o LiBr, ie., for $Na_{0.3}Li_{0.7}Br$ solid solution. Similarly the conductivity enhancement with respect to LiBr is by factors of 2.8 and 2.1 at 400 and 500°C respectively for the same composition. Even though the conductivity enhancement of 4 orders of magnitude is observed in the present mixed crystal system at 400°C, it is not very surprising because of the fact that the conductivity of pure LiBr itself is more than 3 orders of magnitude larger than that of pure NaBr.

5.4.3 Conductivity vs Temperature:

Figures 5.4.4 and 5.4.5 show the log σ vs 10^3 / T plots for $Na_{1-x}Li_xBr$ mixed crystal systems for $0 \leq x \leq 0.7$ and $0.7 \leq x \leq 1.0$ respectively. These plots display the usual intrinsic and the extrinsic regions, separated by the knee points. The pre-exponential factor and the activation energy (both in the intrinsic and the extrinsic regions) for each composition studied are listed in Table 5.6.

The activation energy (both intrinsic and extrinsic) vs composition plots are shown in Fig.5.4.6. The defect formation (H) and migration (h) energies for pure NaBr are found to be 1.94 and 0.74 eV respectively. The respective values reported in the

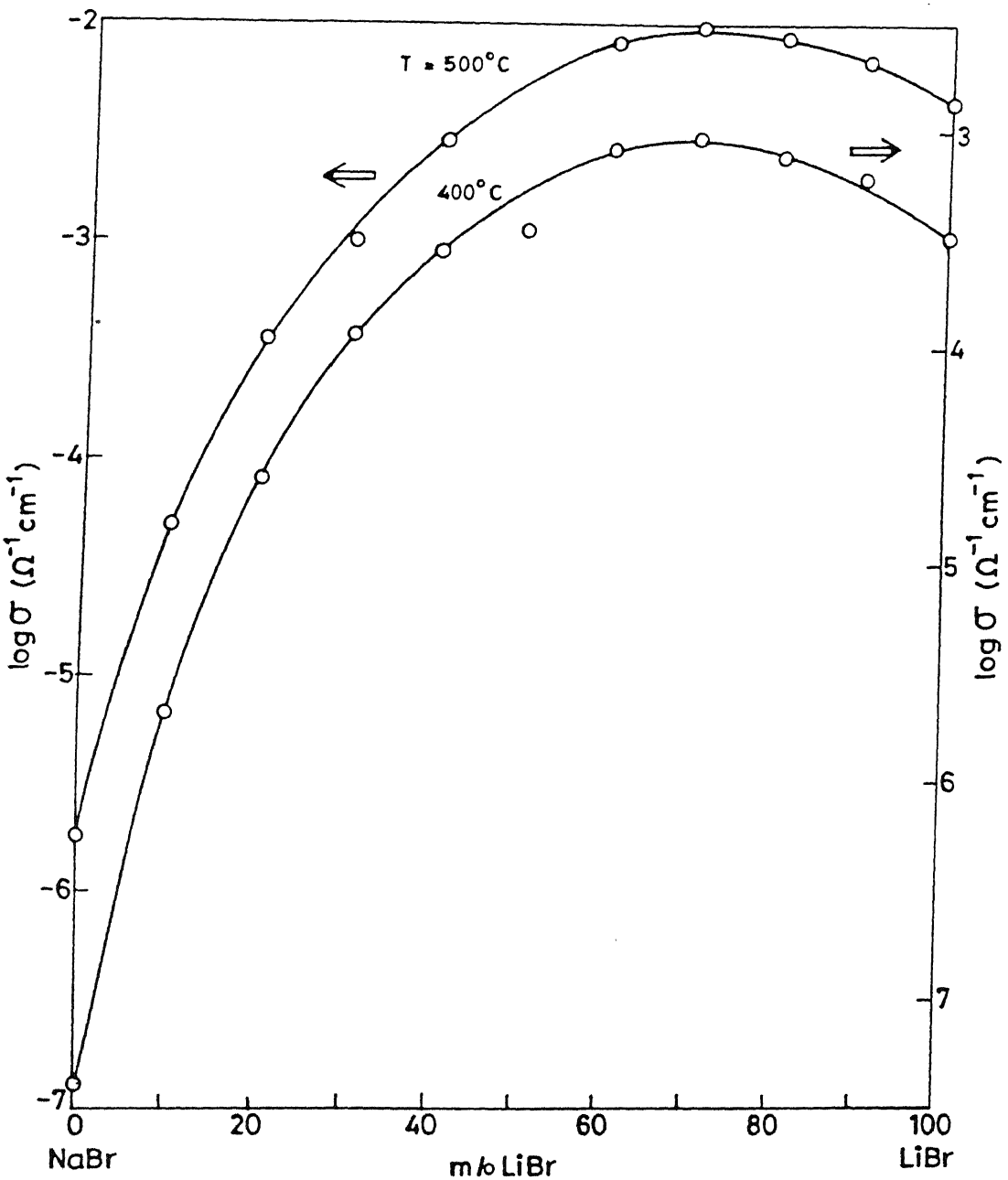

Fig.5.4.3. Logarithm of conductivity vs composition (m/o LiBr in NaBr) at 400 and 500°C.

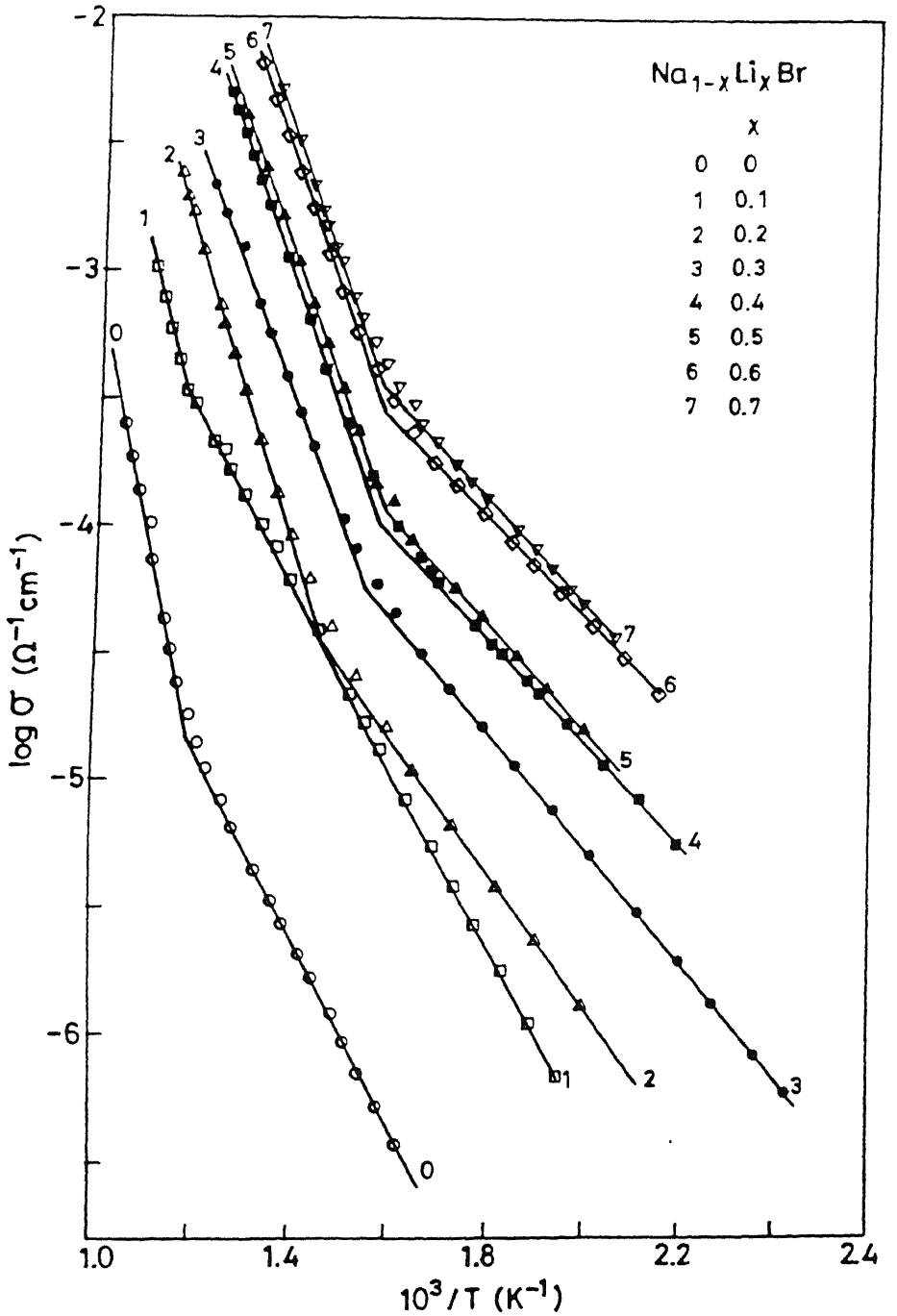

Fig.5.4.4. Logarithm of conductivity vs inverse temperature for $Na_{1-x}Li_xBr$ ($0 \leq x \leq 0.7$) solid solutions.

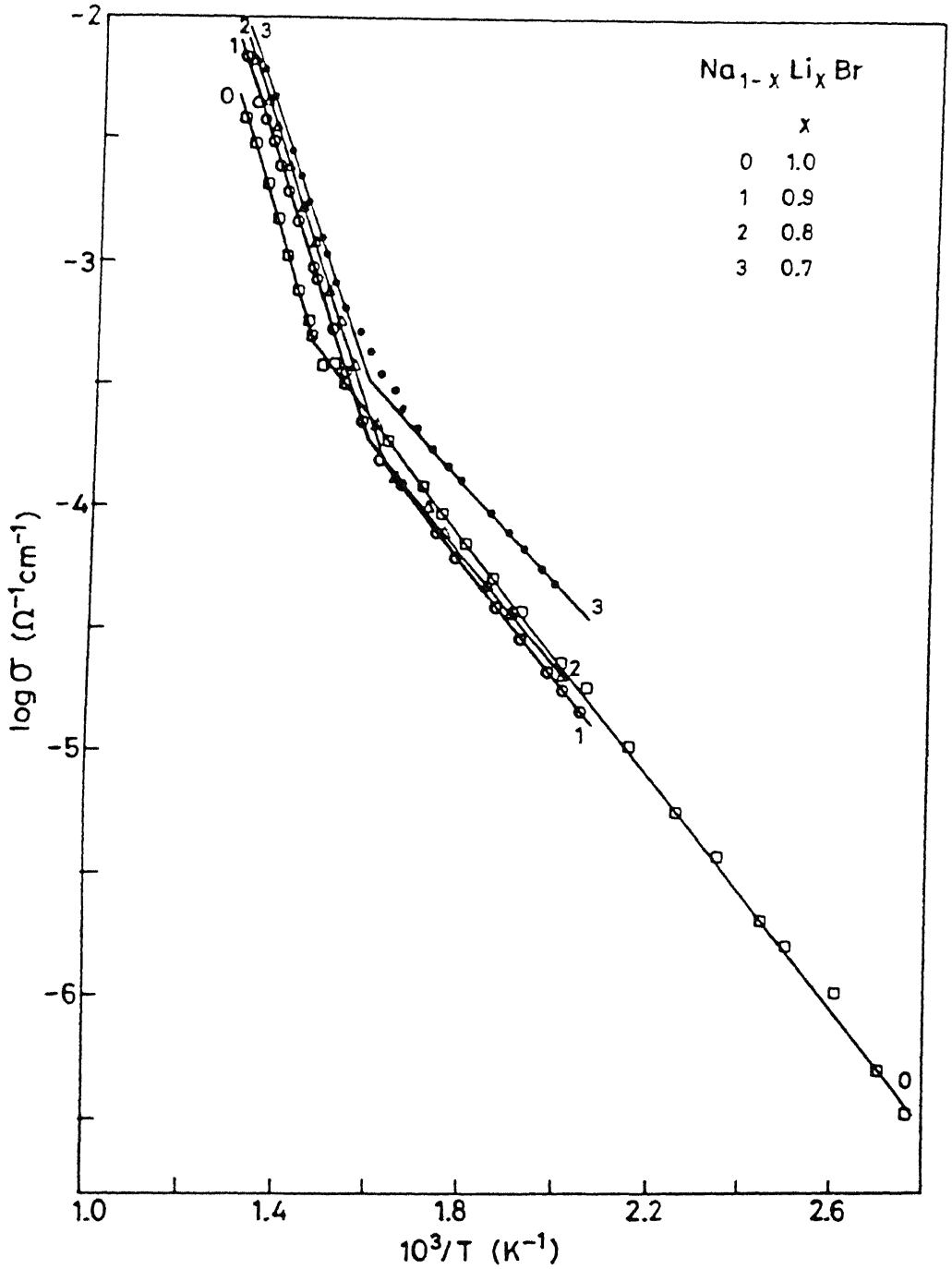

Fig.5.4.5. Logarithm of conductivity vs inverse temperature for $Na_{1-x}Li_xBr$ ($0.7 \leq x \leq 1$) solid solutions.

TABLE 5.6

Ionic transport parameters for NaBr-LiBr mixed crystal system

molar fraction of LiBr in NaBr	E_a intrinsic (eV)	E_a extrinsic (eV)	A intrinsic ($ohm^{-1} cm^{-1}$)	T_N (^oC)
0	1.71	0.74	2.5×10^5	561
0.1	1.43	0.72	1.0×10^5	533
0.2	1.19	0.53	2.1×10^4	412
0.3	0.97	0.45	2.1×10^3	372
0.4	1.05	0.40	2.1×10^4	326
0.5	1.07	0.41	4.5×10^4	352
0.6	1.04	0.38	6.0×10^4	360
0.7	1.04	0.39	6.3×10^4	360
0.8	1.07	0.43	7.0×10^4	345
0.9	1.09	0.47	8.9×10^4	360
1.0	1.17	0.47	1.9×10^5	417

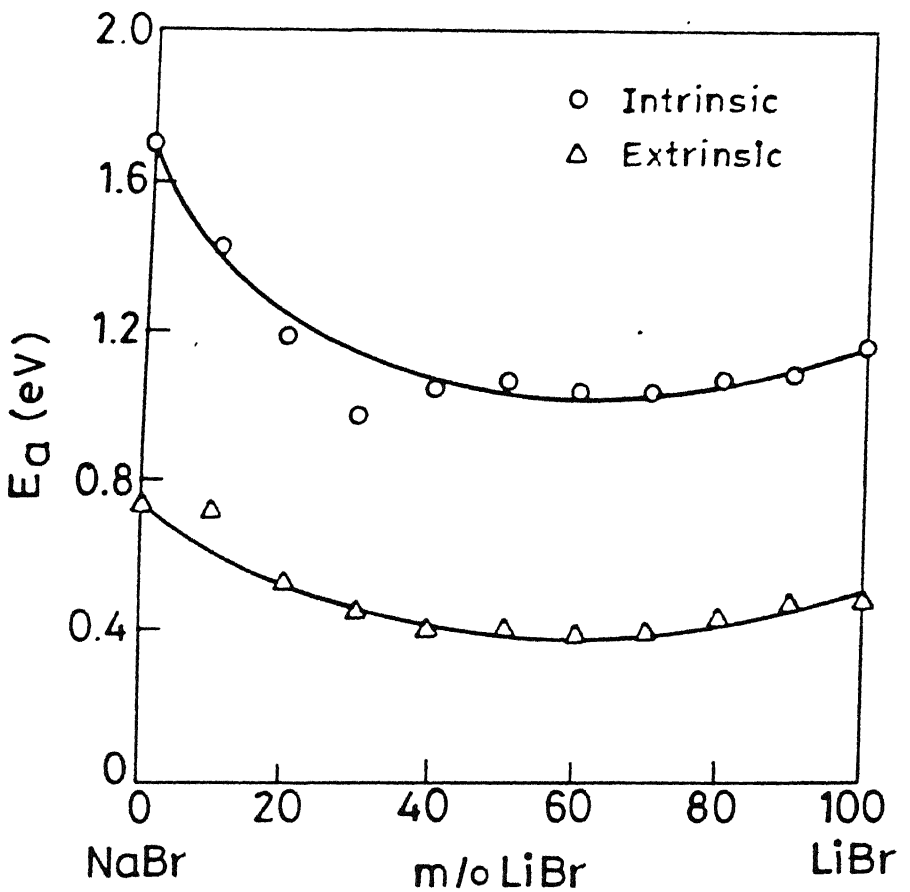

Fig.5.4.6. Activation Energy vs composition for NaBr-LiBr system. o- intrinsic region, Δ- extrinsic region.

literature are 1.68 and 0.8 eV (Schamp and Katz 1954); 1.72 and 0.8 eV (Hoshino and Shimoji 1967); 1.68 and 0.84 eV (Mapother et al 1950). The corresponding values of H and h for pure LiBr are: 1.4 and 0.47 eV (present study); 1.8 and 0.39 eV (Haven 1950); 1.32 and 0.56 eV (Ginnings and Phipps 1930). Figure 5.4.6 also shows that as the concentration of LiBr in NaBr increases, the activation energy decreases and goes through a minimum at ≈ 60-70 m/o LiBr, and starts increasing thereafter. However, the change in the activation energy is very small for compositions > 30 m/o LiBr. The knee temperature (T_N) vs composition (m/o LiBr) is shown in Fig.5.4.7.

5.4.5. Discussions:

Figure 5.4.8 shows the temperature (T_σ) at which the $Na_{1-x}Li_xBr$ mixed crystals attain a fixed conductivity ($\sigma_1 = 5 \times 10^{-5}$ or $\sigma_2 = 10^{-5}$ ohm^{-1} cm^{-1}), as a function of composition. Also shown in the figure is the melting (solidus) curve, T_{mx}, which resembles the T_σ curves rather well. The calculated σ_x/σ_o values are compared with the experimentally observed values in Fig.5.4.9. Both the experimentally observed and the calculated curves (Fig.5.4.9) exhibit a maximum at around the same composition (≈ 70 m/o LiBr). However, the calculated and the observed (relative) conductivity values are not in good agreement; The former being (approximately) an order of magnitude smaller than the latter ones. According to the LL model, the addition of 30 m/o NaBr in LiBr enhances the conductivity by a factor of 2.5 at 400^oC which agrees well with the experimental value (2.8). The observed conductivity of pure LiBr is higher

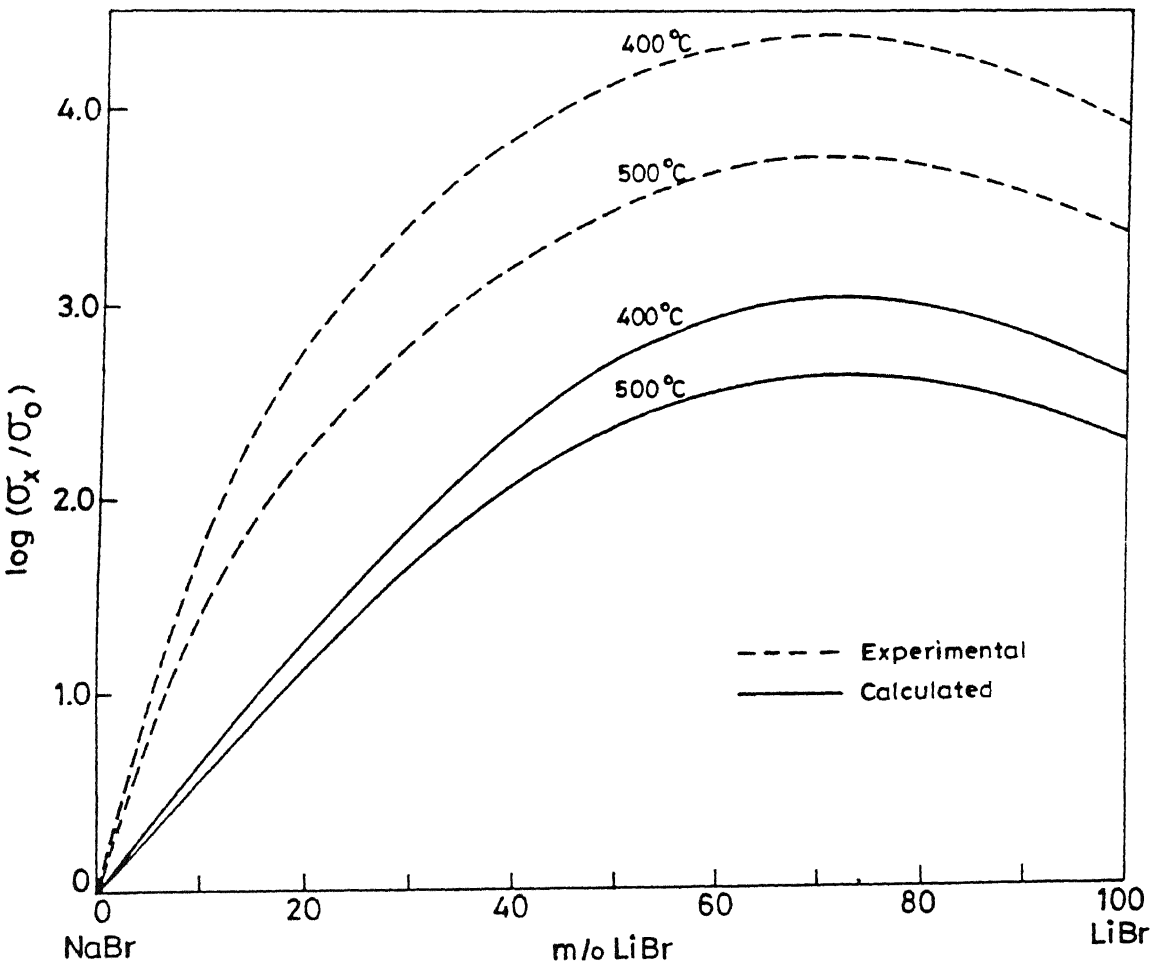

Fig.5.4.9. Relative conductivity (σ_x/σ_o) vs composition at 400 and 500°C. The solid and broken lines respectively represent the calculated and experimental values of σ_x/σ_o.

than that of pure NaBr by a factor of 8×10^3 at 400°C, but the LL model predicts this figure to be 4.2×10^2 (Fig.5.4.9 using eq. 2.33.). That is, at T = 400°C,

$$\frac{\sigma_{LiBr}}{\sigma_{NaBr}} \quad \text{(observed)} \quad = \quad 8 \times 10^3$$

$$\frac{\sigma_{LiBr}}{\sigma_{NaBr}} \quad \text{(calculated)} \quad = \quad 4 \times 10^2$$

(or)
$$\frac{\sigma_{LiBr}/\sigma_{NaBr} \text{ (observed)}}{\sigma_{LiBr}/\sigma_{NaBr} \text{ (calculated)}} \approx 20 \qquad (5.1)$$

Similarly,

$$\frac{\sigma_{Na_{0.3}Li_{0.7}Br} / \sigma_{NaBr} \text{ (observed)}}{\sigma_{Na_{0.3}Li_{0.7}Br} / \sigma_{NaBr} \text{ (calculated)}} \approx 23 \qquad (5.2)$$

Eqs.(5.1) and (5.2) suggest that the discrepancy between the observed and the calculated values of the relative conductivity exists almost uniformely for all the mixed crystals in the LiBr-rich region and is attributable to the inconsistent parameters (eg., H, h, T_m, etc.) of the pure salts used in the calculation of relative conductivity.

By considering NaBr as the pure component and LiBr as the dopant, and substituting the relevant parameters (see Appendix A) in eq.(2.43), ie., the CBα model, we get

$$x_m = 0.35$$

ie., the maximum conductivity should occur at the composition of 35 m/o LiBr in NaBr. On the other hand, if we consider LiBr as the pure component and NaBr as the dopant, one obtains

$$x_m = 0.14$$

ie., the maximum conductivity should occur at the composition of 14 m/o NaBr (or 86 m/o LiBr). The above results may be interpreted to mean that the eq.(2.43) predicts a maximum in the composition range $35 \leq$ (m/o) LiBr ≤ 86, while the experimental results (Figs.5.4.3 and 5.4.9) exhibit a rather well defined maximum at $\approx$ 70 m/o LiBr. Thus it appears once again that the prediction of the CBα model is critically dependent upon the input parameters such as dB/dP, n etc.

In summary, the NaBr-LiBr forms a complete solid solution above 215 ($\pm$ 20)^{o}C. The asymmetrical tilt of the demixing curve of the phase diagram towards the LiBr-rich region suggests that a solid having a larger lattice constant is soluble to a smaller extent in a solid having a smaller latttice constant than the reverse, at any given temperature. A substantial enhancement in conductivity (by more than three orders of magnitude at 400^{o}C) is observed in NaBr due to the substitution of $\approx$ 70 m/o LiBr. However, the conductivity enhancement in LiBr due to the substitution of NaBr is relatively insignificant, by a factor of 3 only at 400^{o}C.

5.5 NaCl-NaBr MIXED CRYSTAL SYSTEM

5.5.1 Phase Diagram:

Figure 5.5.1 shows the melting point as a function of composition for the NaCl-NaBr mixed crystal system. The liquidus and the solidus temperatures in the present binary system are so close to each other that all the DTA curves for this system were charecterized by a single peak only, and hence the solidus and liquidus temperatures could not be resolved. The melting point vs composition curve exhibits a minimum at ≈ 65-70 m/o NaBr. The melting points corresponding to all the 11 compositions studied are listed in Table 5.7. The single-phase/two-phase demixing curve could not be established either. However, the conductivity measurements carried out down to 350°C suggest that a complete solid solubility exists at least above 350°C. This result is in agreement with Fineman and Wallace (1948) in which the peak in the dome-shaped demixing curve occurs at 330°C and at a composition of 45 m/o NaBr.

5.5.2 Conductivity vs Composition:

The conductivity isotherms for the NaCl-NaBr mixed crystal system are shown in Fig. 5.5.2. The conductivity of NaCl increases with the addition of NaBr, goes through a maximum at 60 m/o NaBr and eventually starts decreasing on further addition. This behaviour is consistent with those of the other systems discussed in previous sections. The maximum conductivity enhancement by a factor of 4.9 with respect to pure NaCl, and 1.3

TABLE 5.7

Melting temperature and ionic transport parameters of NaCl-NaBr mixed crystal system.

Mole fraction of NaBr in NaCl	T_m (^oC)	E_a intrinsic (eV)	E_a extrinsic (eV)	A intrinsic (ohm^{-1} cm^{-1})	T_N (^oC)
0	796	1.89	0.83	6.76×10^5	593
0.1	782	1.84	0.84	4.45×10^5	589
0.2	774	1.77	0.8	2.83×10^5	545
0.3	755	1.69	0.86	1.68×10^5	540
0.4	748	1.67	0.81	1.49×10^5	562
0.5	741	1.63	0.77	1.07×10^5	547
0.6	732	1.6	0.9	7.5×10^4	553
0.7	733	1.63	0.83	1.13×10^5	518
0.8	735	1.65	0.78	1.26×10^5	537
0.9	737	1.68	0.85	1.96×10^5	530
1.0	741	1.71	0.78	2.48×10^5	533

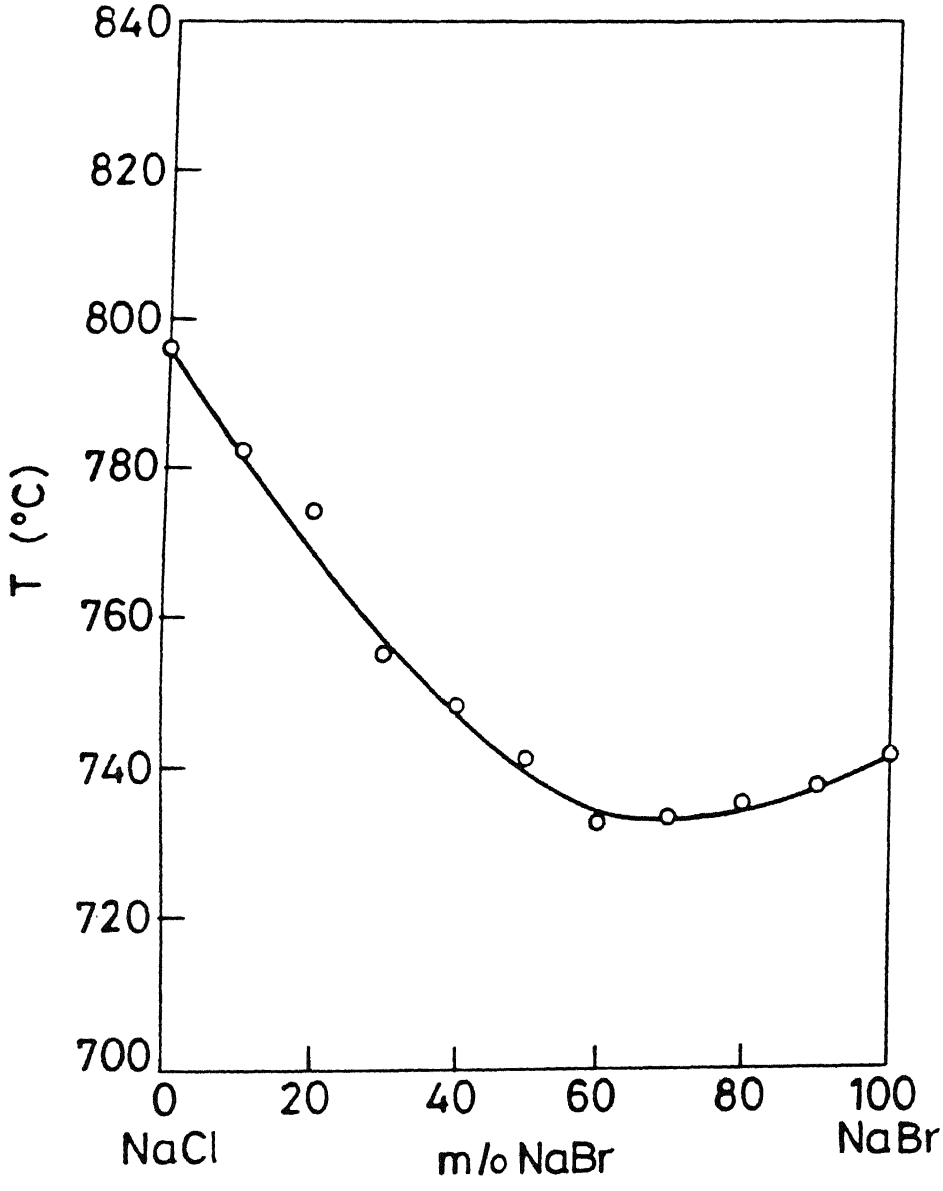

Fig.5.5.1. Melting point vs composition for NaCl-NaBr system.

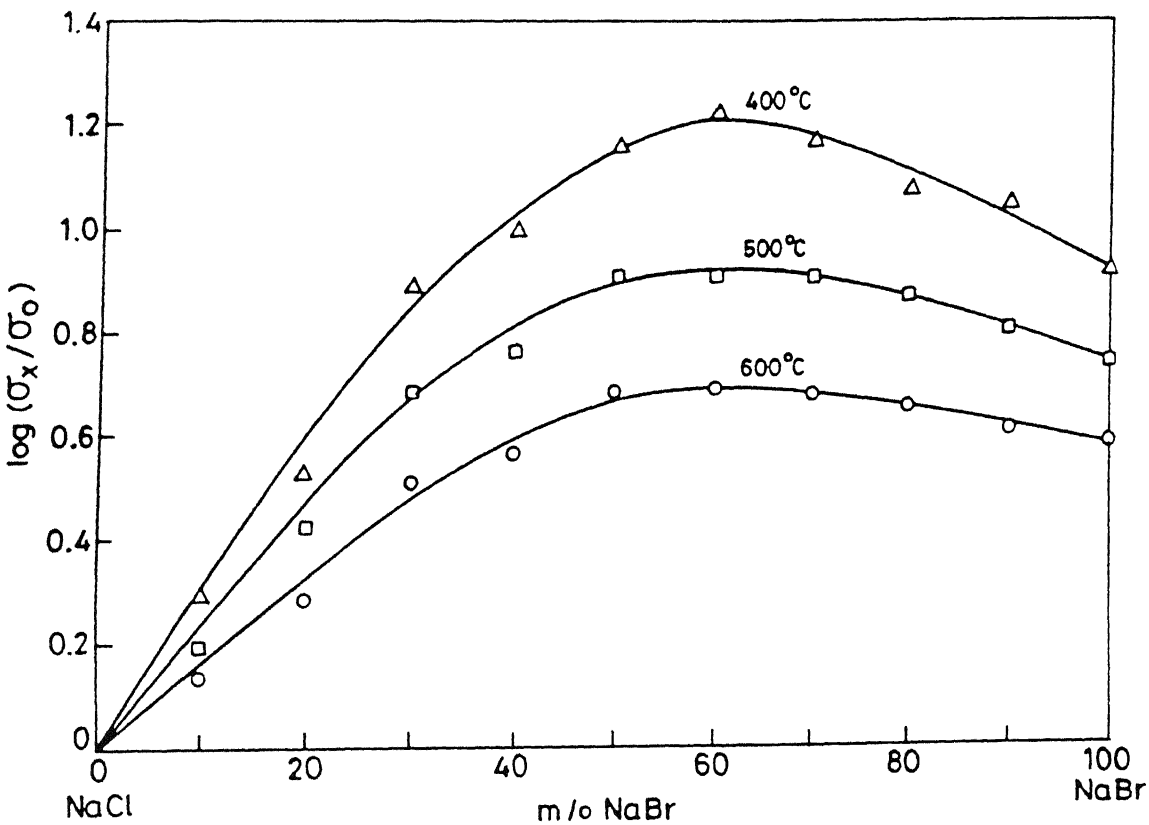

Fig.5.5.2. Logarithm of conductivity vs composition (m/o NaBr in NaCl) at 400, 500 and 600°C. The curves corresponding to 400 and 500°C are based on conductivity data obtained by extrapolating the linear log σ vs 1/T plot (intrinsic region) to appropriate temperatures.

with respect to pure NaBr, has been obtained at 600°C for $NaCl_{0.4}Br_{0.6}$ solid solution.

5.5.3 Conductivity vs Temperature:

The Arrhenius plots for the $NaCl_{1-x}Br_x$ mixed crystals are shown in Fig.5.5.3 for $0 \leq x \leq 0.6$ and in Fig.5.5.4 for $0.6 \leq x \leq 1.0$. These plots, as usual, consist of two linear regions, viz., intrinsic and extrinsic, separated by the knee temperature. Figure 5.5.5 displays the activation energy vs composition curve. This curve exhibits a minimum at ≈ 60 m/o NaBr which is the same composition at which the conductivity is maximum. The activation energies (both intrinsic and extrinsic) and the pre-exponential factors for all the compositions studied are listed in Table 5.7.

5.5.4 Discussion:

A maximum conductivity enhancement by a factor of 10 was observed by BimaSankaram and Bansigir (1978) at 393°C for ≈ 50 m/o NaBr in NaCl. However, this figure does not seem suitable for comparison because their reported activation energy of 0.6 eV suggests that this region is extrinsic rather than intrinsic. Since the aim of the present study was to investigate the effect of homovalent dopants, and hence only the conductivity values in the intrinsic region, or if the intrinsic region was at higher temperatures, the extrapolated conductivity values to appropriate temperatures were considered for comparison.

Figure 5.5.6 compares the melting curve with the T_σ vs x curves corresponding to fixed conductivities of $\sigma_1 = 5 \times 10^{-5}$ and $\times 10^{-5}$ ohm^{-1} cm^{-1}. It is noticed that $T_{\sigma 1}$ and $T_{\sigma 2}$ curves

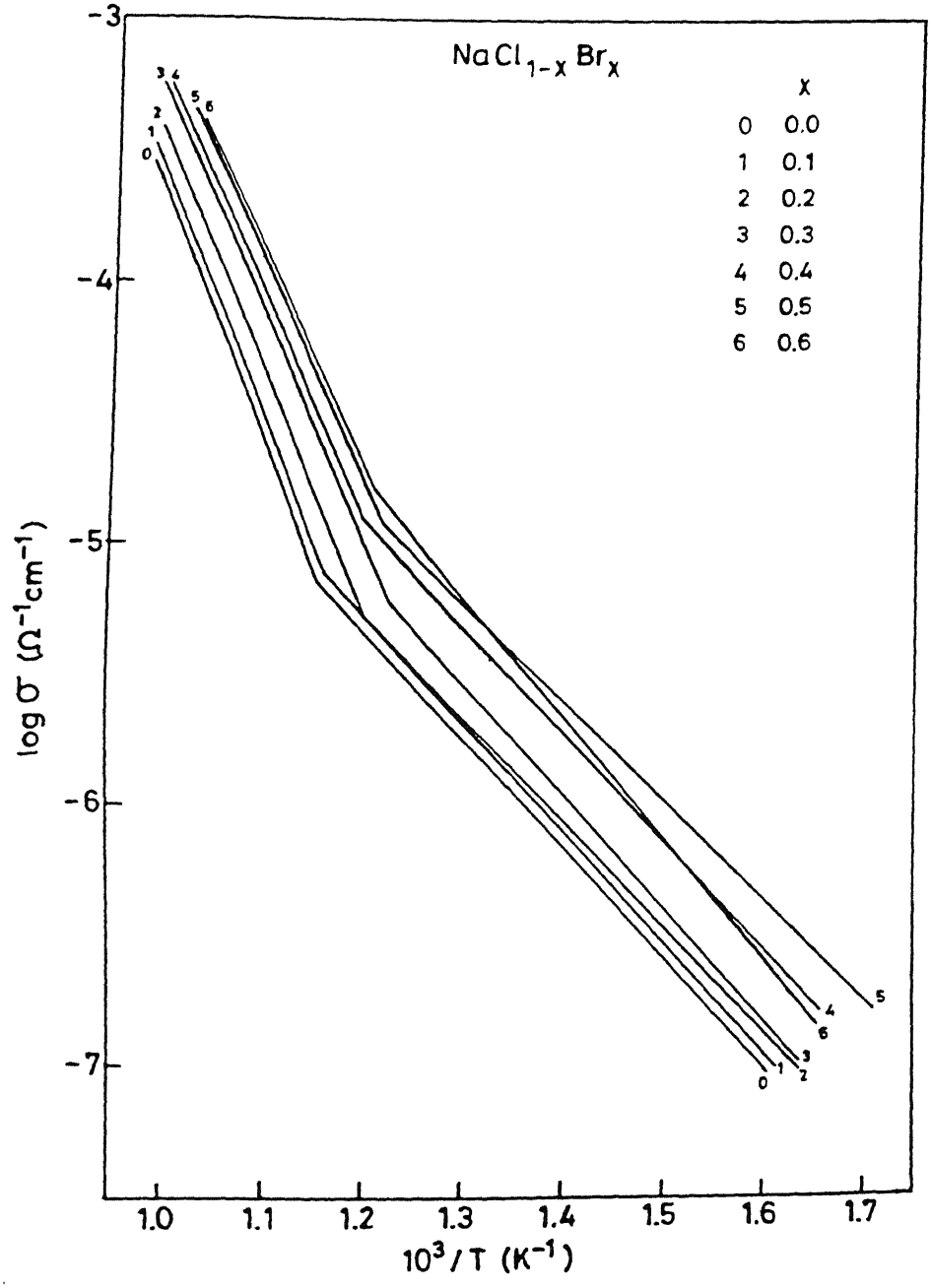

Fig.5.5.3. Logarithm of conductivity vs inverse temperature for $NaCl_{1-x}Br_x$ ($0 \leq x \leq 0.6$) solid solutions.

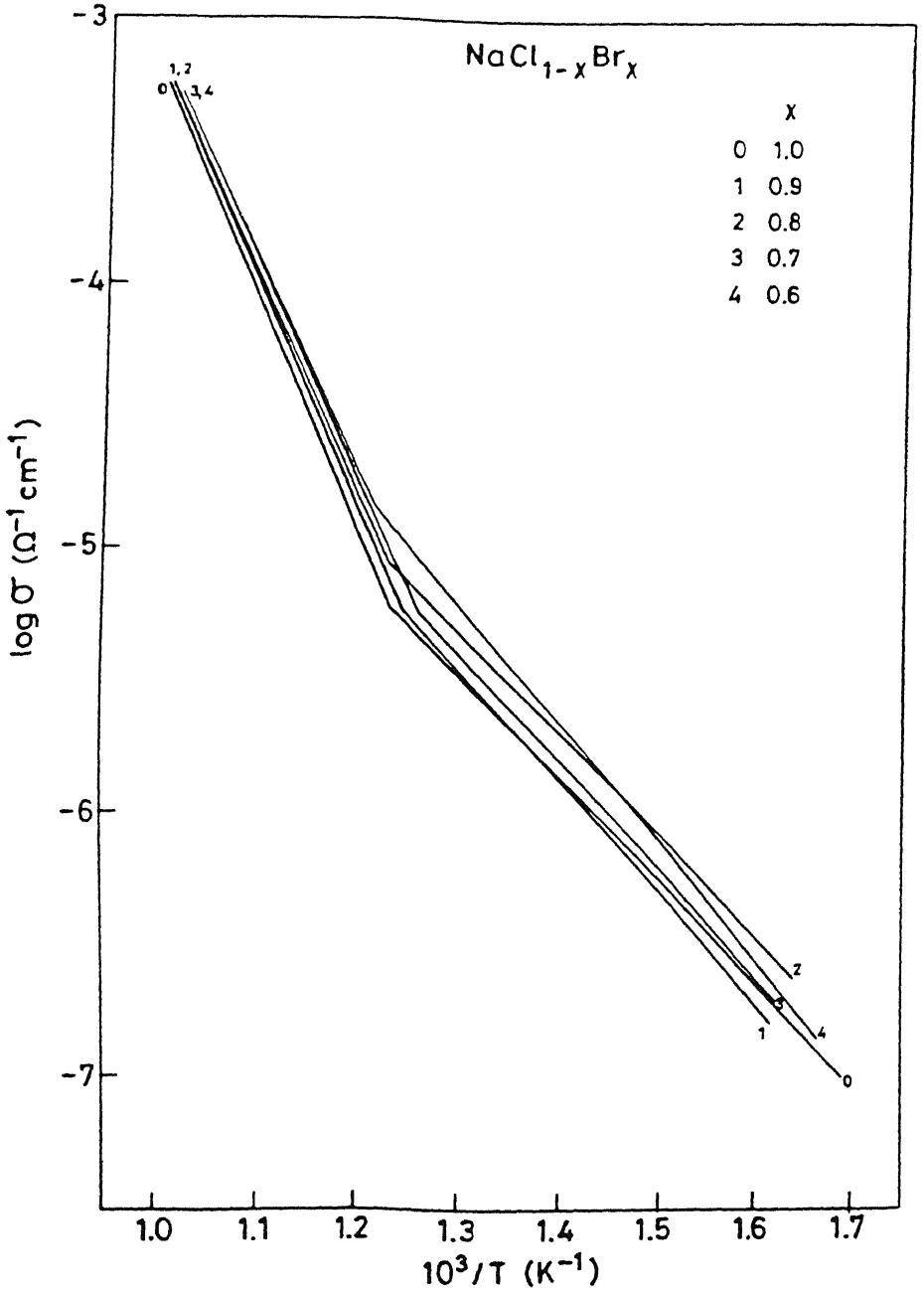

Fig.5.5.4. Logarithm of conductivity vs inverse temperature for $NaCl_{1-x}Br_x$ ($0.6 \leq x \leq 1$) solid solutions.

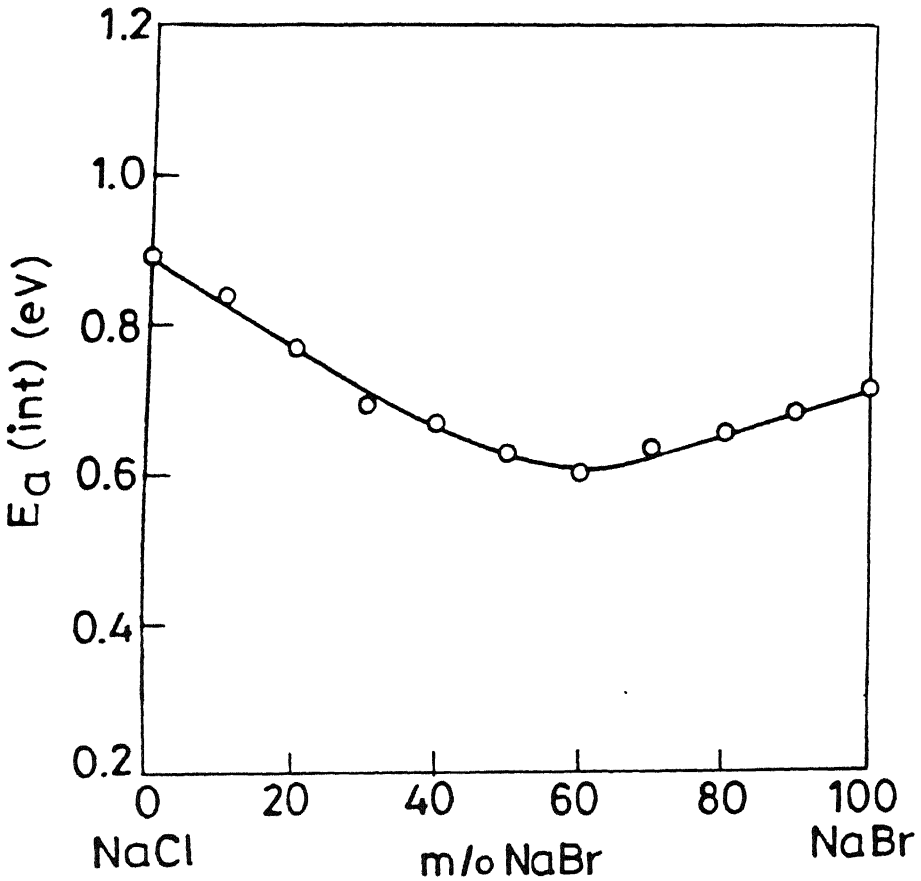

Fig.5.5.5. Activation Energy (intrinsic region) vs composition for NaCl-NaBr system.

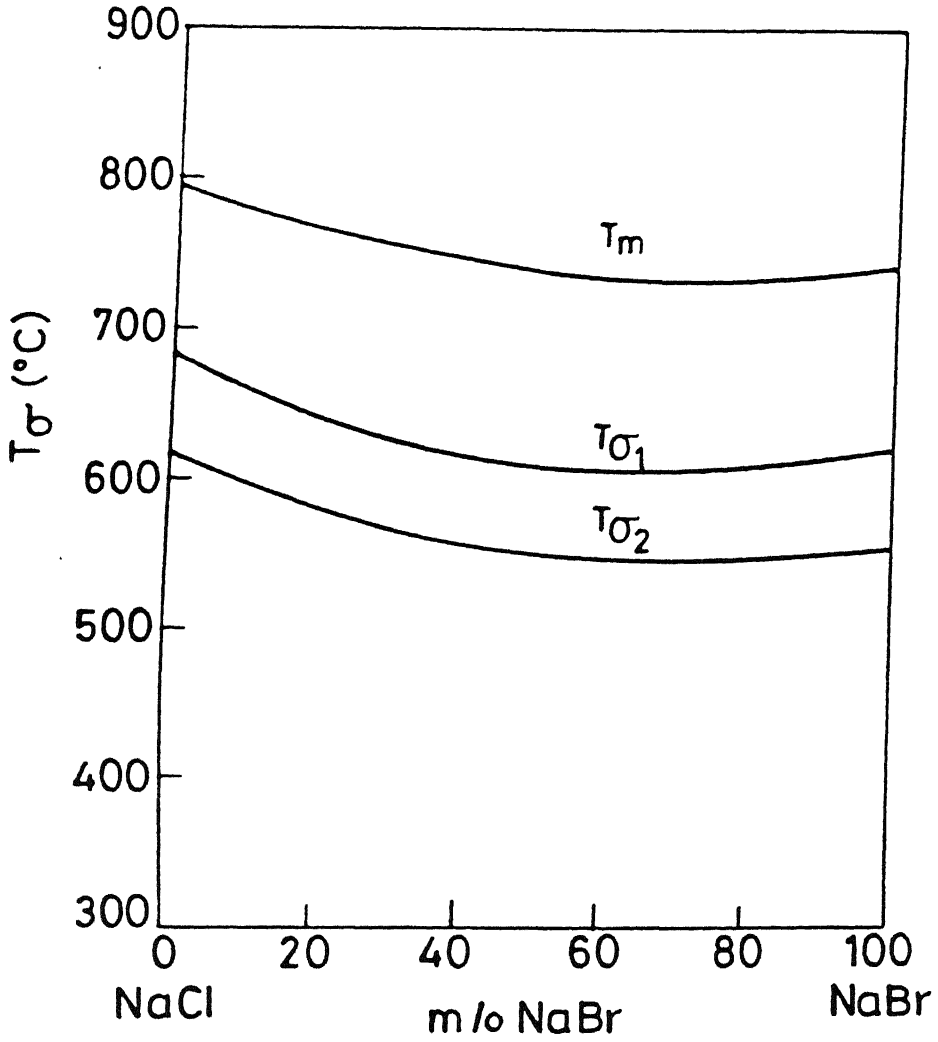

Fig.5.5.6. T_σ as a function of composition for NaCl-NaBr system. $\sigma_1 = 5 \times 10^{-5}$ and $\sigma_2 = 10^{-5}$ ohm^{-1} cm^{-1}. T_m is the melting curve of $NaCl_{1-x}Br_x$ mixed crystals.

ollow the melting curves qualitatively. The LL model (Eq. 2.33) as used to calculate the σ enhancement in the present system and he results are shown in Fig.5.5.7 (solid lines). The xperimental results are also shown in Fig. 5.5.7 for comparison. here is a fair agreement between the calculated and experimental esults at 600°C. However, at 400 and 500°C, the calculated alues of are somewhat lower than the experimental values the elative conductivity (σ_x/σ_0). In addition, the calculated curves xhibit a maximum at ≈ 65-75 m/o NaBr, while the experimental urves exhibit a maximum at a somewhat lower composition (≈ 60 /o NaBr). This discrepancy may be attributed largely to the xperimental error, typically ± 5°C, in the determination of the elting point of the mixed crystals using DTA. It may be pointed it that an error of ± 5°C in the melting point is not insignificant particularly for a system like NaCl-NaBr in which he total change (decrease) in the melting point itself is ≈ 60°C.

The composition corresponding to maximum conductivity can e calculated using the CBΩ model (Eq.2.43). Considering NaCl as he pure component and NaBr as the dopant, and by substituting he relevant parameters such as dB/dP, n etc., (see Appendix A) n Eq.(2.43), we get $x_m = 0.46$. If, on the other hand, one onsiders NaBr as the pure component and NaCl as the dopant and epeats the above calculation, $x_m = 0.52$ is obtained. Thus the BΩ model, Eq.(2.43), predicts a conductivity maximum at ≈ 46-48 /o NaBr which is lower than the observed value (60 m/o NaBr).

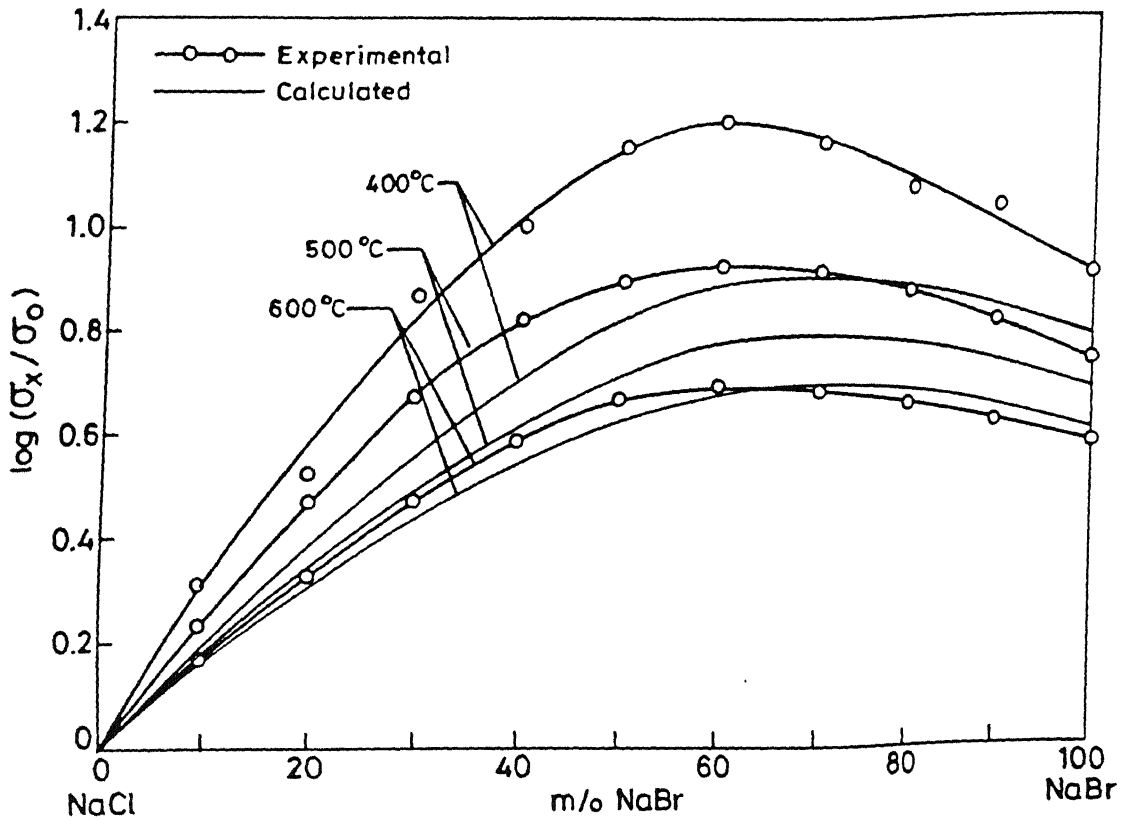

Fig.5.5.7. Relative conductivity (σ_x/σ_o) vs composition at 400, 500 and 600°C.

In summary, the NaCl-NaBr system exhibits a complete solid solubility at least above 350°C. A maximum enhancement in σ by a factor of 4.9 is obtained at $\approx$ 60 m/o NaBr, ie., for $NaCl_{0.4}Br_{0.6}$ solid solution at 600°C. The composition corresponding to maximum conductivity in NaCl-NaBr system, according to the LL model, is 65-75 m/o NaBr and according to the CBΩ model (Eq. 2.43) is 46-48 m/o NaBr. The behaviours of E_a vs x and T_σ vs x are consistent with that of T_{mx} vs x and hence the σ-isotherms.

CHAPTER-6

SUMMARY DISCUSSION

6.1 Conductivity Enhancement:

The substitution of wrong size homovalent ions enhances the ionic conductivity appreciably. The magnitude of conductivity enhancement depends on the extent of mismatch between the sizes of the host and the dopant ions. For example, the substitution of 50 m/o Cl^--ion in NaBr leads to a conductivity enhancement by a factor of just 2 at 400°C, whereas the substitution of the same amount (50 m/o) of K^+-ions in the same salt (NaBr) enhances the conductivity by a factor of 12, I^--ion by a factor of 27 and Li^+-ion by a factor of 1.3×10^4 at the same temperature (400°C). The large conductivity enhancement observed in case of NaBr-LiBr system should be viewed rather differently; Apart from the larger lattice strain which leads to a larger enhancement in the concentration of the Schottky defects, the high mobility of Li^+ -ions also plays a vital role. Hence, an unusually larger enhancement in σ is observed in NaBr-LiBr mixed crystals with respect to pure NaBr.

Similarly, the substitution of 50 m/o Cl^--ion in the KBr lattice leads to a conductivity enhancement by a factor of just 2, whereas the substitution of 50 m/o of Na^+-ion leads to an enhancement by a factor of 35 at 400°C. Shahi and Wagner (1983) have reported a maximum σ enhancement in KBr-KI by a factor of 63 at 400°C for $KBr_{0.5}I_{0.5}$. We have recalculated the σ enhancement by extrapolating their data to intrinsic region and found that

the maximum enhancement is by a factor of 180 rather than 63 at the same temperature (400°C). The conductivity enhancement in KBr due to the substitution of 50 m/o NaI is by a factor of 250 at 400°C which is larger than those in KBr-KI and KBr-NaBr systems (factors of 180 and 36 respectively). Table 6.1 compares the conductivity enhancement observed in KBr-KI (Shahi and Wagner 1983) with that of KBr-NaI (present study). The results are understandable qualitatively in view of the LL model as in KBr-NaI system, both cations and anions are substituted simultaneously leading to a larger strain in the lattice than that in KBr-KI system.

6.2 The Lattice Loosening Model:

The LL model which is discussed in Chapter-2, not only explains the conductivity enhancement in mixed crystals, but also explains a few other related properties.

6.2.1 T_σ vs Composition:

The validity of the LL model can be tested in another way, viz., by noting that the conductivity of a mixed crystal of a certain composition (x) can be written as (eq.2.20)

$$\sigma_x = A_x \exp \{ - (½ H_x + h_x) / kT \}$$

Using the correlations given by eqs.(2.22) and (2.28), we have

$$\frac{\sigma_x}{A_x} = \exp \left[- \frac{(\alpha/2 + \beta) T_{mx}}{kT} + \frac{r}{kT} \right] \qquad (6.1)$$

Assuming, as before (Sec.2.3.1), that the dopants do not affect

TABLE 6.1

Comparison of σ enhancements in KBr-KI and KBr-NaBr with that of KBr-NaI system at T = 400^{o}C.

Mole fraction of dopant in KBr	$^{*}\sigma_x/\sigma_o$ KBr-KI	σ_x/σ_o KBr-NaBr	σ_x/σ_o KBr-NaI
0	1	1	1
0.1	4	3	10
0.2	29	8	49
0.3	63	19	132
0.4	113	36	301
0.5	180	35	250

* Data points recalculated from Shahi and Wagner (1983).

the pre-exponential factor A_x, ie., $A_x = A$, a constant, eq.(6.1) may be written as

$$T_\sigma = \left[- \frac{(\alpha/2 + \beta)}{k \ln(\sigma/A)} \right] T_{mx} + \left[\frac{r}{k \ln(\sigma/A)} \right] \qquad (6.2)$$

Since α, β, r and k are constants, the quantities in the square brackets will be constant (independent of the composition) if the conductivity, σ, is constant. Thus eq.(6.2) states that the temperature at which the mixed crystals attain a fixed conductivity, ie., T_σ, varies linearly with the melting point (solidus temperature, T_{mx}) of the mixed crystals. Thus, T_σ and T_{mx} should have a similar dependence on the composition x. Figures (5.1.7), (5.2.8), (5.3.8), (5.4.8) and (5.5.6) show the T_σ vs composition behaviour observed for KBr-NaI, KBr-NaBr, NaBr-NaI, NaBr-LiBr and NaCl-NaBr systems respectively for two different fixed values of the conductivity. The fact that the behaviour of T_σ vs composition curves is indeed very similar to that of T_{mx} (or T_{ms}, ie., the solidus curve of the phase diagram) for all the five systems examined in this work, adds further credence to the LL model.

6.2.2 Prediction of the Phase Diagram Solidus Curve

The good resemblance between the solidus curve of the phase diagram (T-x) and the conductivity vs composition (σ-x) plot can be used to predict the melting curve, ie., the solidus curve of the phase diagram, from the observed conductivity data. Recalling eq.(2.32),

$$\sigma_x/\sigma_o \approx \exp\{- (\alpha/2 + \beta) \Delta T_{mx} /kT\}$$

or $$\Delta T_{mx} (= T_{mx} - T_{mo}) = \frac{- kT}{(\alpha/2 + \beta)} \ln (\sigma_x/\sigma_o)$$

or $$\Delta T_{mx} \approx - 4.5 \times 10^{-2} T \ln (\sigma_x/\sigma_o) \qquad (6.3)$$

gives the change in the melting point of a mixed crystal if the relative conductivity (σ_x/σ_o) is known at some temperature T. Since σ_x is generally greater than σ_o or $\sigma_x/\sigma_o \geq 1$, eq.(6.3) correctly suggests that the ΔT_{mx} is negative; ie., the melting point of the crystal generally decreases as a result of doping. Figures 6.1 - 6.5 compare the melting curves obtained from DTA studies with those obtained from eq.(6.3). It should be emphasized that the calculated curves shown in the above figures are based on two sets of data points obtained corresponding to the conductivity isotherms at two different temperatures. In case the conductivity falls in the extrinsic region for the temperature considered, only the intrinsic values of σ obtained by extrapolating the linear log σ vs 1/T plots to that temperature should be taken for calculations since the LL model implies that the homovalent dopants change the transport properties intrinsically.

The agreement between the calculated and the experimental melting curves is satisfactory in case of NaBr-NaI and NaBr-NaCl systems (Figs.6.3 and 6.5). The maximum disagreement is by about $10^{o}C$ for NaBr-NaI system which is of the order of experimental error in the determination of ΔT_m $(= T_{mx}-T_{mo})$ while it is $15^{o}C$ for NaCl-NaBr system. However, the maximum disagreement between the calculated and experimental results in KBr-NaI (Fig.6.1),

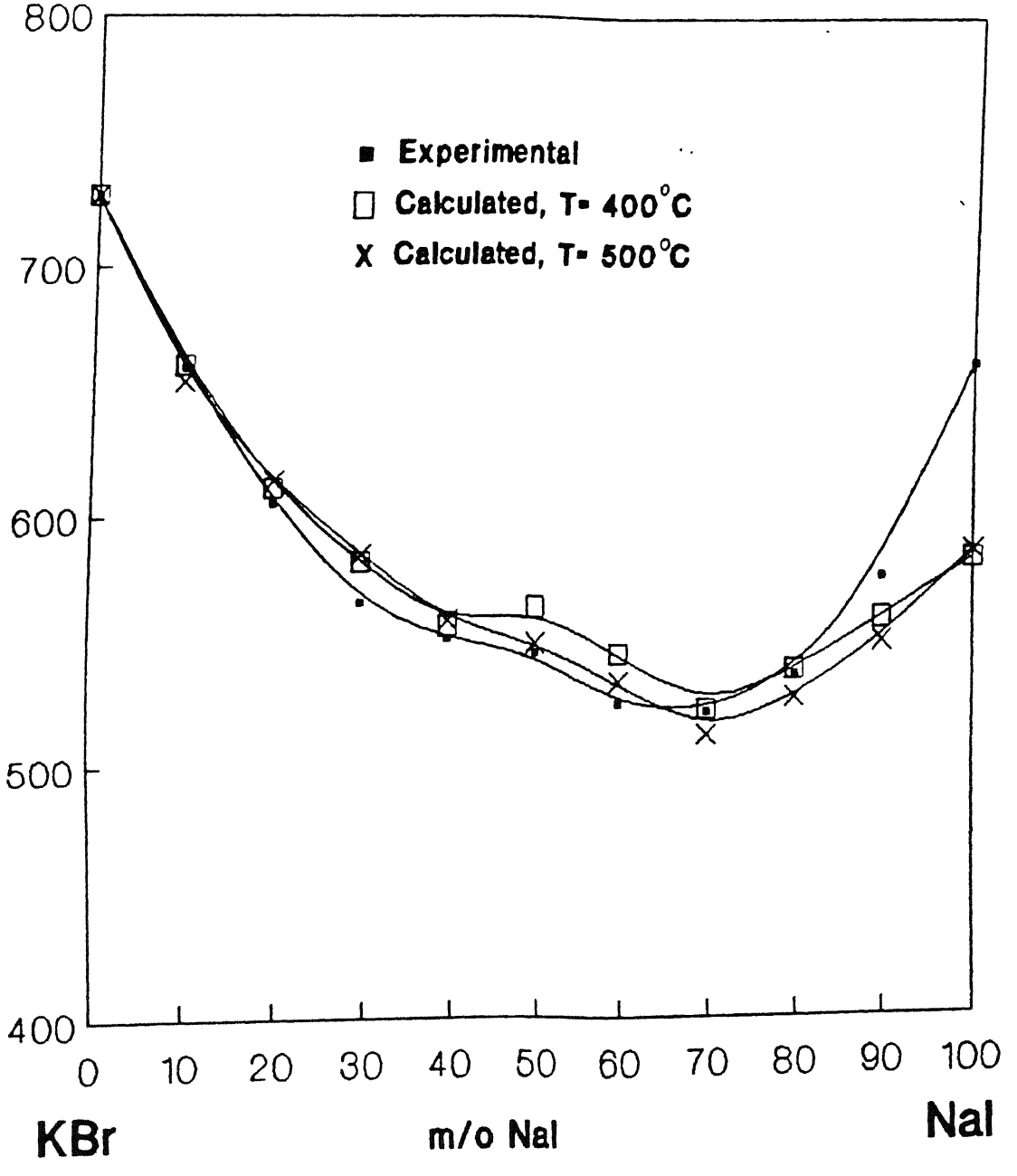

Fig.6.1 Calculated T_m (solidus curve) using LL model, Eq.(2.33) for KBr-NaI system.

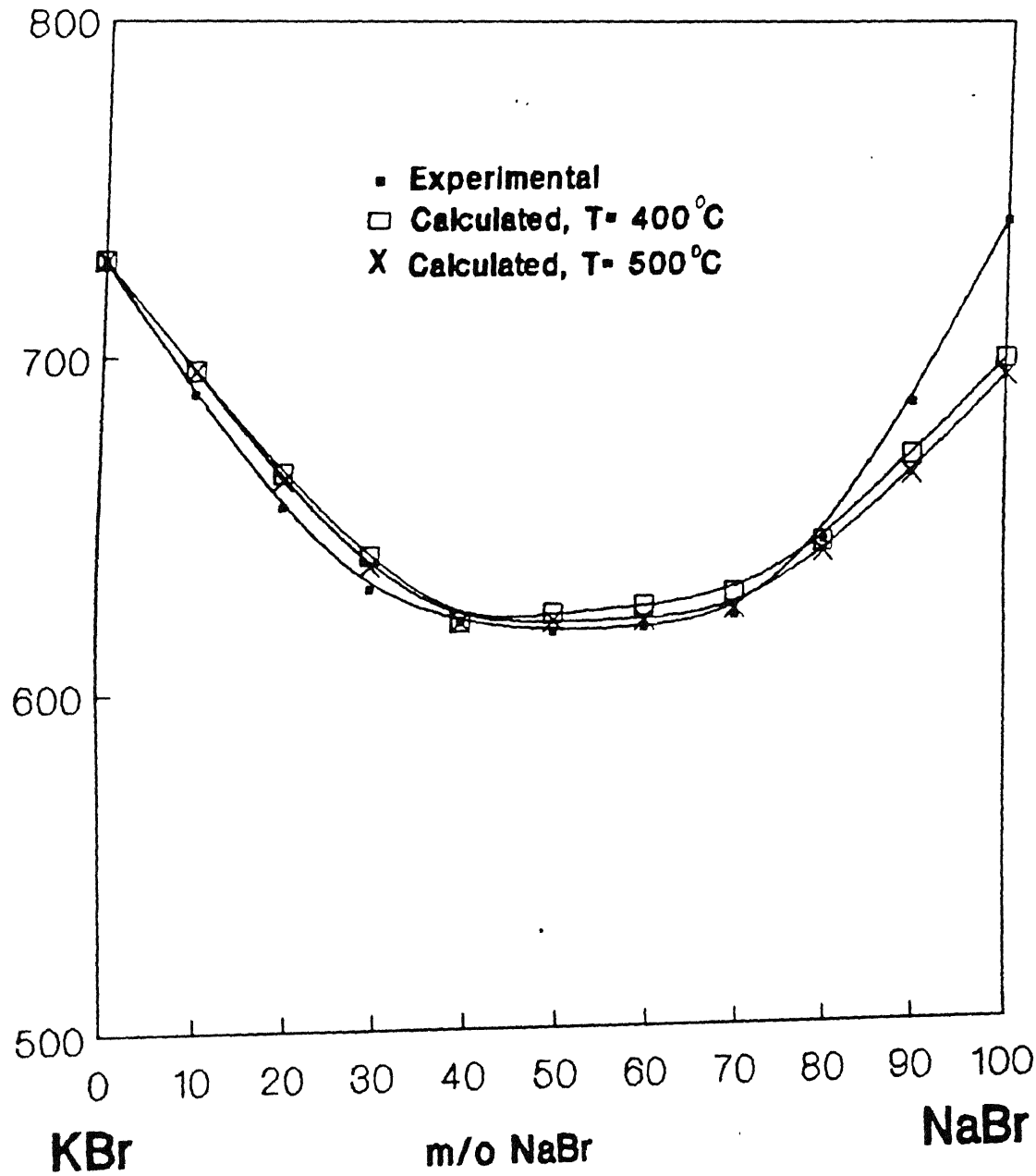

Fig.6.2 Calculated T_m (solidus curve) using LL model, Eq.(2.33) for KBr-NaBr system.

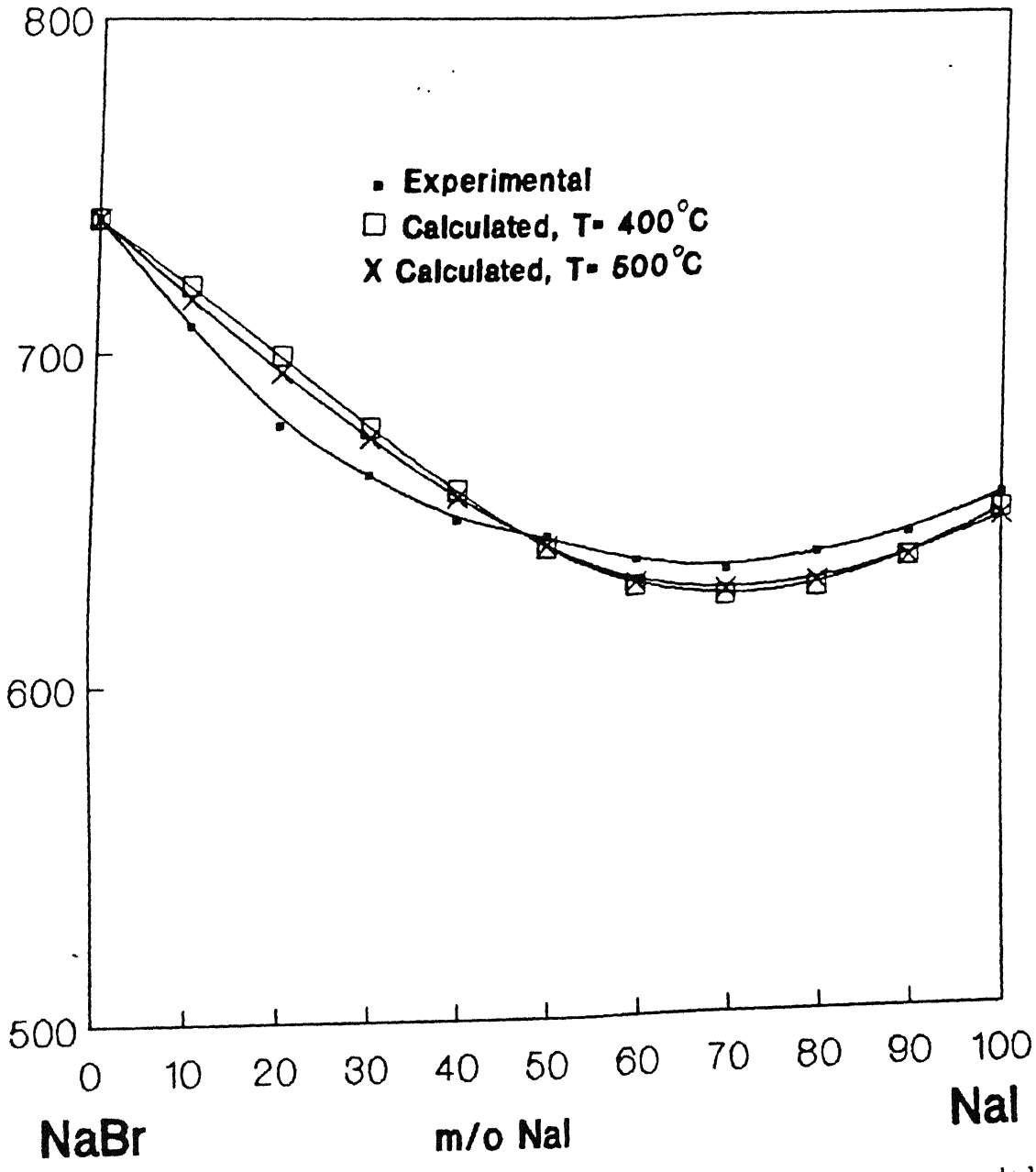

Fig.6.3 Calculated T_m (solidus curve) using LL model, Eq.(2.33) for NaBr-NaI system.

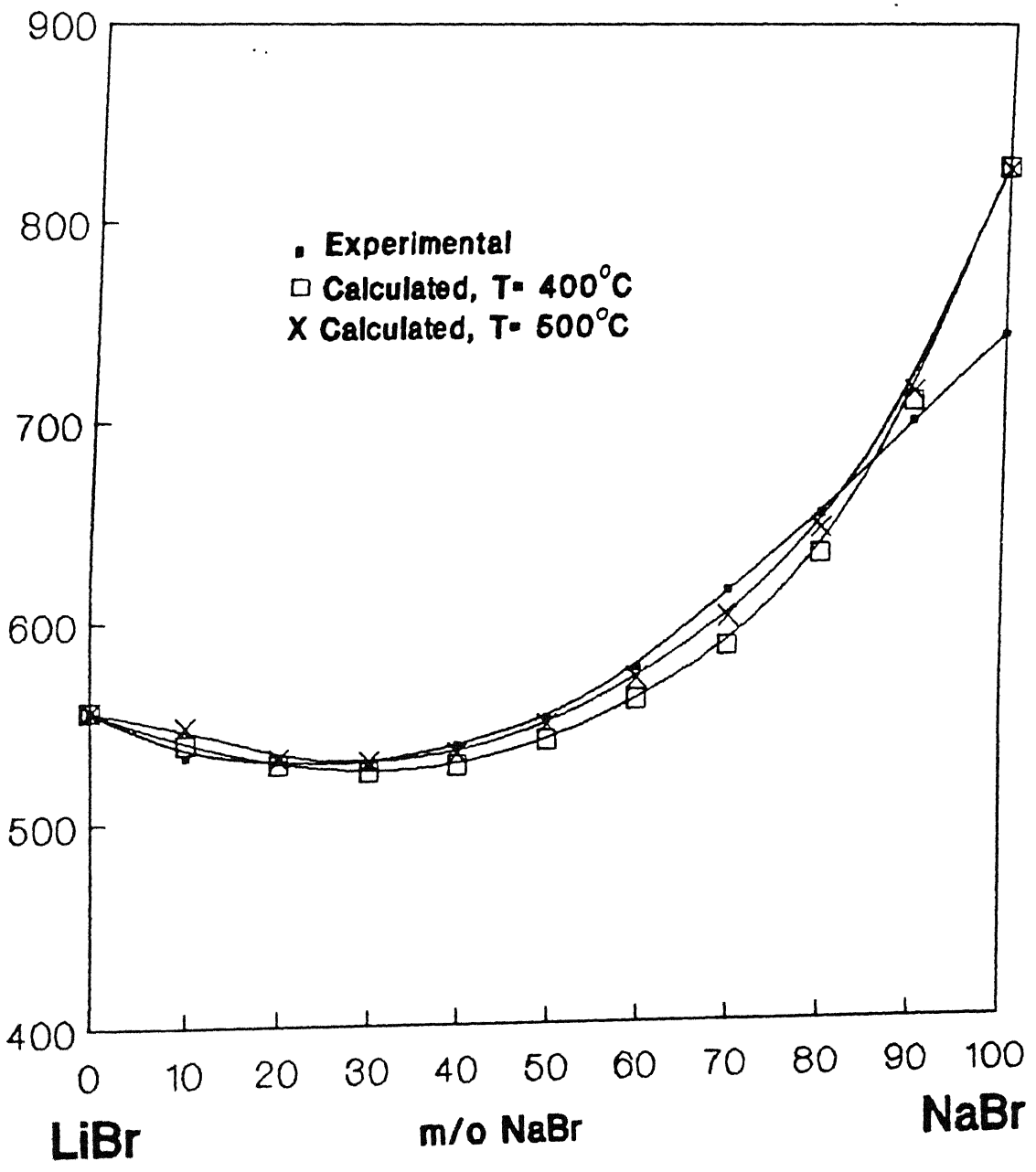

Fig.6.4 Calculated T_m (solidus curve) using LL model, Eq.(2.33) for LiBr-NaBr system.

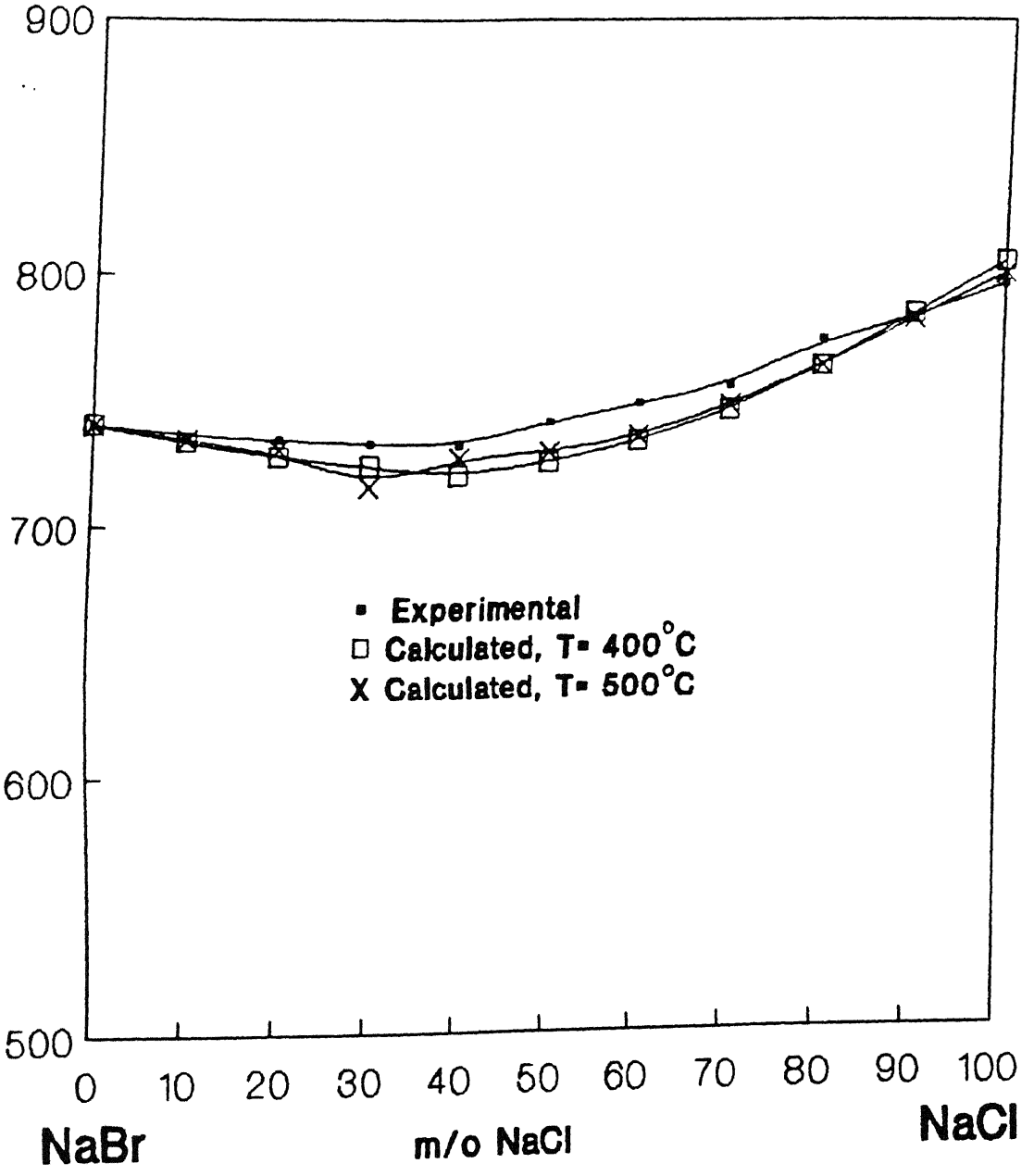

Fig.6.5 Calculated T_m (solidus curve) using LL model, Eq.(2.33) for NaBr-NaCl system.

KBr-NaBr (Fig.6.2) and LiBr-NaBr (Fig.6.4) systems at x=1 is about 50-70°C. It should be noted that a similar disagreement was also observed in the conductivity isotherm plots (Figs.5.1.8, 5.2.6 and 5.4.9), especially in the composition range x = 0.9 - 1.0, and was attributed to the fact that the formation and migration enthalpies of the defects in NaI and NaBr do not fit the empirical correlations (Eqs.2.22 and 2.28) very well.

Thus, in summary, the LL model would suggest that the solidus temperature of the phase diagram (T-x) in the alkali-halide binary system can be calculated from the conductivity data only.

6.3 The CBα Model:

Appendix A lists the input parameters involved in the eq.(2.43) which predicts the composition corresponding to the maximum conductivity in mixed crystals. Table 6.2 compares the maximum conductivity composition (x_m) obtained from the CBα model (eq.2.43) with that obtained from experiments. The fact that the CBα model which predicts the x_m for KBr-KI, KI-NaI, KI-RbI and KBr-NaBr systems satisfactorily, fails to predict the x_m accurately for KBr-NaI system may be analyzed in the following way.

In KBr-NaI system, if we consider KBr as the starting component and NaI as the dopant, eq.(2.43) predicts an absurd value of x_m = 2.12. Alternatively, if KBr is considered as a dopant in NaI, one still gets an absurd value of x_m = 1.78. The value of x_m must, of course, lie between zero and unity;

TABLE 6.2

Comparison of calculated x_m (composition corresponding to maximum conductivity) using Eq.2.43 (CBα model) with experimental x_m values.

Mixed crystal system Host-Dopant	x_m (calculated)	x_m (experimental)	Reference for experimental x_m
KI-RbI	0.88	0.85 - 0.9	Bonpunt and Haget (1974)
RbI-KI	0.1	0.1 - 0.15	Bonpunt and Haget (1974)
KI-NaI	0.56	0.55 ± 0.05	Haget et al (1975)
NaI-KI	0.36	0.45 ± 0.05	Haget et al (1975)
KCl-RbCl	0.85	0.8 - 0.85 0.7	Kantola and Lindstrom(1967) Holt et al (1969)
RbCl-KCl	0.1	0.15 - 0.2 0.3	Kantola and Lindstrom(1967) Holt et al (1969)
KBr-KI	0.62	0.64 0.7	Shahi and Wagner (1983) Johannesen and Mckelvy
KI-KBr	0.58	0.36 0.3	Shahi and Wagner (1983) Johannesen and Mckelvy (1985)
KBr-KCl	0.83	0.32	Johannesen (1987)
KCl-KBr	0.8	0.68	Johannesen (1987)
NaCl-NaBr	0.46	0.45 - 0.47 0.6	BimaSankaram and Bansigir(1978) present study
NaBr-NaCl	0.52	0.53 -0.55 0.4	BimaSankaram and Bansigir(1978) present study
KBr-NaI	2.12	0.7(and 0.4)	Present study
NaI-KBr	1.78	0.3(and 0.6)	present study
KBr-NaBr	0.37	0.42	Present study
NaBr-KBr	0.29	0.3	present study
NaBr-NaI	0.37	0.6	Present study
NaI-NaBr	0.4	0.4	present study
NaBr-LiBr	0.35	0.7	Present study
LiBr-LiI	0.14	0.3	present study

$$0 \leq \frac{(k_d/k_o) - 2}{\lambda\ (k_d/k_o)} \leq 1$$

As λ is positive by definition, we have the two inequalities

$$[(k_d/k_o) - 2]/\ (k_d/k_o) \geq 0$$

or
$$k_d/k_o \geq 2 \qquad (6.4)$$

and
$$(k_d/k_o) - 2 - \lambda\ (k_d/k_o) \leq 0 \qquad (6.5)$$

which must be satisfied by all the systems. Applying the above inequalities to KBr-NaI system, we find that eq.(6.4) is satisfied, ie., k_d/k_o for KBr-NaI is greater than 2. However, the inequation (6.5) is violated. Therefore the CBΩ model cannot be used to predict the maximum conductivity composition for KBr-NaI mixed crystal system (see Table 6.3 for other systems).

Although the inequations (6.4) and (6.5) are very well satisfied for NaBr-NaI, NaBr-LiBr, NaCl-NaBr and KCl-KBr systems, the CBΩ model still predicts inaccurate values of x_m (Table 6.2). We wish to point out here that the success of this model depends critically on the accuracy of the experimental values of the input parameters such as k_d/k_o, n etc. An uncertainity of ± 2 % in the values of dB/dP, which does not seem unrealistic (Puri and Verma 1977), leads to an error of ∓ 8 % in the values of x_m. In addition, there exists some ambiguity in the literature about the value of the Born's exponent n. Thus, the validity of the CBΩ model as such cannot be questioned just on the basis of the discrepancy pointed out above; the errors appearing in various

TABLE 6.3

The various parameters involved in the CBα model.

Mixed crystal system (Host-Dopant)	$\lambda = \frac{V_2}{V_1} - 1$	$\frac{k_d}{k_o}$	$1 - \frac{2}{k_d/k_o}$
KI-RbI	0.122	2.305	0.132
RbI-KI		2.248	0.110
KI-NaI	0.301	2.305	0.132
NaI-KI		2.241	0.108
KCl-RbCl	0.145	2.282	0.124
RbCl-KCl		2.241	0.108
KBr-KI	0.227	2.294	0.128
KI-KBr		2.305	0.132
KBr-KCl	0.154	2.294	0.128
KCl-KBr		2.282	0.124
NaCl-NaBr	0.191	2.190	0.087
NaBr-NaCl		2.222	0.100
KBr-NaI	0.061	2.294	0.128
NaI-KBr		2.241	0.108
KBr-NaBr	0.346	2.294	0.128
NaBr-KBr		2.222	0.100
NaBr-NaI	0.269	2.222	0.100
NaI-NaBr		2.241	0.108
NaBr-LiBr	0.283	2.222	0.100
LiBr-LiI		2.227	0.102

input parameters could probably be the reason for the failure of this model for some of the mixed crystal systems.

6.4 Vacancy Formation Model of Melting:

The phenomenon of melting of solids is insufficiently understood. So far there is no quantitative theory which could satisfactorily explain all the details of the melting process. However, based on the linear correlations between the (Schottky) vacancy formation enthalpy and the melting temperature (Barr and Lidiard 1970; Kostopoulos et al 1989; Varotsos and Alexopoulos 1986), we can develop a relation between these parameters. Incidentally, a similar kind of relationship has already been observed in metals (Kraftmakher 1966), ie., the Vacancy formation energy is proportional to the melting point of the metal. The correlation based on the data for 23 metals including alkali metals, Ag, Cu, Pt, Mg, Pb, Cd, Sn, etc., is

$$H = 8.33 \times 10^{-4} \quad T_m \quad eV \qquad (6.6)$$

Gorecki (1974, 1976) showed that the atomic fraction of vacancies at the melting point is $\approx 3.7 \times 10^{-3}$ which is nearly constant for all the 23 metals examined.

The existance of such critical concentration of vacancies at the melting point (x_C) is not reported for ionic solids, perhaps mainly because of the errors involved in the measured values of H. Figure 6.6 shows the concentration of Schottky defects at the melting point of some selected ionic solids. It can be seen that the concentration (mole fraction) of vacancies at the melting point lies in the range 10^{-3} - 10^{-4} which is

nearly an order of magnitude smaller than the value (3.7×10^{-3}) for the metals. It should, however, be pointed out that there exists considerable discrepancy between the reported values of the x_C for a given ionic solid. For example, the conductivity data of Dreyfus and Nowick (1962) yields an $x_C = 1.1 \times 10^{-3}$ while those of Beaumont and Jacobs (1966) gives $x_C = 3.8 \times 10^{-4}$ for KCl. The latter value, of course, is considered less reliable and hence it is not included in the plot of Fig.6.6.

It is worth mentioning here that the order - disorder (ionic - superionic) transitions that resemble the melting (solid - liquid) transitions in some respect, have been argued to be driven by a critical concentration of the defects (Shahi et al. 1986). The significant decrease in the superionic transition temperature of AgI doped with divalent (Weiss et al 1950) / homovalent impurities etc. was successfully explained on the basis of the above model. Since the critical concentration of defects in doped AgI is attained at lower temperatures, the order - disorder transition temperature is lowered.

In view of the preceding discussion, it should be interesting to determine the concentration of Schottky vacancies in the mixed crystals which would require conductivity measurements on aliovalently doped mixed crystals as well, in both intrinsic and extrinsic regions. This appears difficult in view of the fact that most of the alkali halide binary systems form solid solution (mixed crystal) only at elevated temperatures corresponding to intrinsic region. In any case, in absence of

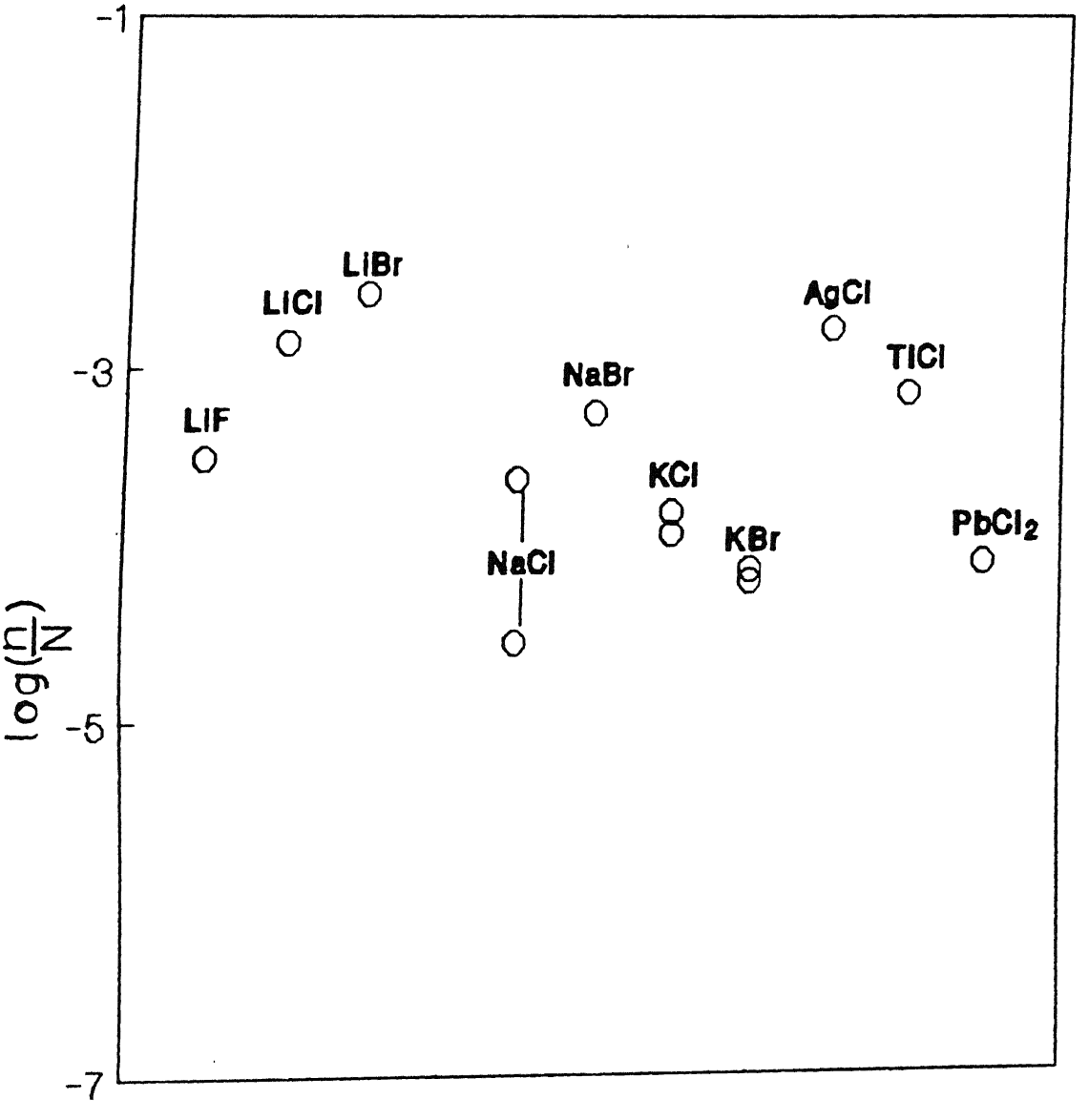

Fig.6.6 Concentration of Schottky defects of pure solids at their melting points.

such studies the ionic conductivity at the melting point, $\sigma(T_m)$, itself may be examined. Since the mobility of the various alkali ions may not be greately different (see Table 1.1, Chapter-1), it is expected, in view of the correlation between the (critical) concentration of vacancies at the melting point and the melting process, that the conductivity of the mixed crystals at the melting temperature, $\sigma(T_m)$, should be nearly constant.

Figure 6.7 shows $\sigma(T_m)$ vs composition for the five mixed crystal systems studied in this work. It is observed that the $\sigma(T_m)$ of NaCl-NaBr mixed crystals is indeed constant ($\approx 10^{-3}$ ohm^{-1} cm^{-1}), independent of composition, and that of NaBr-NaI system is constant within the reproducibility limit (a factor of 2). The $\sigma(T_m)$ of KBr-NaBr and KBr-NaI systems is lower, particularly in KBr-rich region, which may be attributed to the lower mobility (Friauf 1972) of (larger) K^+ -ions ($\approx 5 \times 10^{-4}$ cm^2 V^{-1} s^{-1} at $T_m = 728^oC$ of KBr) than that of (smaller) Na^+ -ions ($\approx 9.5 \times 10^{-4}$ cm^2 V^{-1} s^{-1} at $T_m = 741^oC$ of NaBr). Likewise, a positive deviation in the $\sigma(T_m)$ of NaBr-LiBr system as LiBr concentration increases may be due to larger mobility of Li^+ -ions ($\approx 1.9 \times 10^{-3}$ cm^2 V^{-1} s^{-1} at $T_m = 555^oC$ of LiBr) than that of Na^+ -ions.

Thus, it is reasonable to conclude that the melting process in alkali halides and their mixed crystals is activated by a critical concentration of (Schottky) vacancies that appear to lie in the range $10^{-3} \leq x_C \leq 10^{-4}$ mole fraction. Precise conductivity studies across the melting transition temperatures of alkali halides and their mixed crystals, perhaps involving

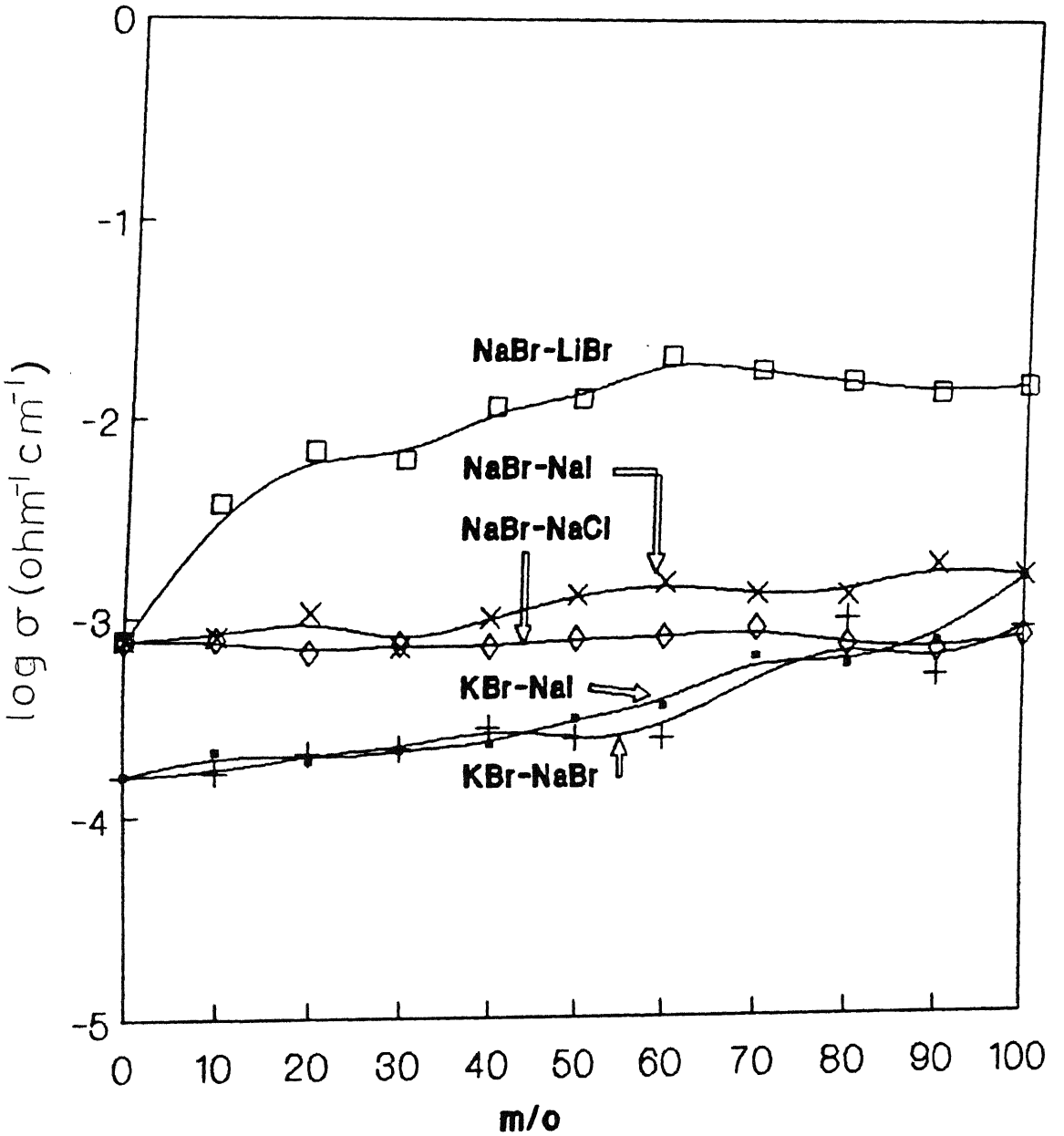

Fig.6.7 Conductivity of the mixed crystals at their melting points (solidus temperature).

sample holders suitable for molten salts (Kvist and Lunden 1965) would be required to fix the critical concentration more accurately.

Based on these results, it does appear that the melting process is linked with the degree of atomic disorder (concentration of vacancies) in ionic solids as well. Moreover, it is physically concievable that as temperature increases the concentration of vacancies increases rapidly, and as soon as the critical concentration is reached the crystalline framework becomes unstable, resulting in mass disorder or melting.

Table 6.4 shows the heat of fusion (Weast 1980) and the Schottky defect formation energy (Friauf 1972) of some of the ionic solids (alkali, silver, thallium and lead halides). It is readily noticed that the heat of fusion (H_{fusion}) is proportional to the formation energy of Schottky defects;

$$(H_{fusion}) \; / \; H = (7.1 \pm 2.5) \times 10^{22} \quad \text{per gm-mole} \qquad (6.7)$$

If we consider the melting process itself as an anamolous creation of excess number of Schotkky defects, the above relation suggests that $(7.1 \pm 2.5) \times 10^{22}$ vacancy pairs are created per gm-mole at the cost of heat of fusion. It is equivalent to an increase of the concentration of vacancy pairs by $x = 0.12 \pm 0.04$ (or 12 ± 4 %).

Interestingly, a similar kind of relation is observed for metals also (Gorecki 1974), ie.,

TABLE 6.4

Heat of fusion and Schottky defect formation energy of some selected ionic solids.

	H_{fusion}† cal/gm-mole	H (eV)	H_{fusion} / H 10^{22}(per gm-mole)
NaF	7000	2.42	7.55
NaCl	7220	2.3 - 2.75	8.2 - 6.86
NaBr	6140	1.68 - 1.72	9.54 - 9.32
NaI	5340	1.46 - 2.2	9.55 - 6.34
KF	6500	2.64 - 2.72	6.43 - 6.24
KCl	6410	2.3 - 2.6	7.28 - 6.44
KBr	5000	2.33 - 2.53	5.6 - 5.16
KI	4100	1.6 - 2.2	6.69 - 4.9
RbF	4130	1.67 - 2.5	6.47 - 4.32
RbCl	4400	2.04 - 2.12	5.63 - 5.42
RbBr	3700	1.8 - 1.98	5.37 - 4.88
RbI	2990	1.78 - 2.09	4.39 - 3.7
TlCl	4260	1.3	8.56
TlBr	5990	1.1	14.2
AgCl	3155	1.44	5.72
AgBr	2180	1.13 - 1.28	5.04 - 4.45
$PbCl_2$	5650	1.56 - 1.16	9.46 - 12.7
$PbBr_2$	4290	1.4 - 1.44	8 - 7.78
CsCl	3600	1.86	5.06

†Weast (1980).

$$(H_{fusion}) / H = 7.66 \times 10^{22} \quad \text{per gm-atom} \qquad (6.8)$$

which amounts to an increase in the concentration of Schottky vacancies by $x = 0.13$ (or 13 %).

This argument can also be verified from the volume of formation of Schottky defects and its relation with the volume change at the melting point of the solids. According to Bollmann et al (1989), the experimentally observed relative change in volume of the metals and ionic solids at their melting point is related to the Schottky defect formation volume by

$$\frac{\Delta V}{V_m} = \frac{V_s}{V_o} \times \qquad (6.9)$$

where ΔV is the change in volume of the solid at the melting, V_m is the molar volume, V_s is the Schottky defect formation volume and V_o is the volume per molecule. A compilation of the data for various metals and ionic solids exhibiting Schottky type of defects and the plot of $\Delta V/V_m$ vs V_s/V_o gives the value $x = 0.125$. This is in good agreement with the value observed by us for ionic solids (eq.6.7) and by Gorecki (1974) for metals (eq.6.8). Hence, it is concluded that the melting process itself is a process of anamolous creation of excess number of vacancies in solids exhibiting Schottky defects. In other words, an amount of $(7.1 \pm 2.5) \times 10^{22}$ vacancies in metals and vacancy pairs in ionic solids, which is constant for almost all the solids exhibiting Schottky type of defects, is created per gm-mole during the melting process which is driven by a critical concentration of vacanies (or vacancy pairs in ionic solids).

found to be too sensitive to the errors in the various input parameters. A modification of the CBΩ model in view of the present results would be desirable.

Our results provide a strong support to the theory of melting that invokes a "critical" concentration of Schottky defects.

The strong correlation between the energy of formation of defect and the heat of fusion suggests that the melting process itself could be a creation of anomalous point defects.

Lastly, an interesting finding of this study is that the two phase mixtures generally exhibit conductivities that are order(s) of magnitude higher than those of parent single phase (metastable) solid solutions. This suggests the enormous possibility of developing "aluminaless" composite solid electrolytes for various electrochemical applications.

REFERENCES

Armand.M.B, Chabagno.J.M and Duclot.M (1978) "2 nd Int. Conf. Solid Electrolytes", St. Andrews, Scotland.

Badwal.S.P.S (1988) Proc. Int. Seminar on Solid State Ionic Devises, 18-23 July 1988, Singapore, p.165.

Barr.L.W and Dawson.D.K (1971) Proc. Britt. Ceramic Soc., No.19, 151.

Barr.L.W and Lidiard.A.B (1970) In "Physical Chemistry - An advanced treatise",(Ed. Jost.W) Academic Press. New York, vol. 10, p.151.

Barret.W.T and Wallace.W.E (1954) J. Am. Chem. Soc.76, 366.

Bauerle.J.E (1969) J. Phys. Chem. Solids 30, 2657.

Beaumont.J.H and Jacobs.P.W.M (1966) J. Chem. Phys. 45, 1496.

Beniere.F, Beniere.M and Chemla.M (1969) J. Chimie 66, 898.

Beniere.F (1972) In "Physics of Electrolytes", (Ed. Hladik.J), vol.1, Academic Press, New York and London.

Beniere.F and Haribabu.V (1987) Cryst. Latt. Defects and Amorph. Mat. 15, 263.

Beniere.M, Beniere.F, Catlow.C.R.A, Shukla.A.K and Rao.C.N.R (1977) J. Phys. Chem. Solids, 38, 521.

Bhatnagar.S, Gupta.S and Shahi.K (1987) Solid State Ionics 31, 263.

Bhima Sankaram.T and Bansisir.K.G (1978) Crystal Lattice Defects, 7, 209.

Bollmann.W (1980) Phys. Stat. Solidi (a) 61, 395.

Bollmann.W, Uvarov.N.F and Hairetdinov.E.F (1989) Cryst. Res. Technology 24, 421.

Bonpunt.L, Chanh.N.B, Comberton.G, Haget.Y and Beniere.F (1983) Radiation Effects 75, 33.

Boukamp.B.A and Huggins.R.A (1976) Phys. Lett. 58A, 231.

Bradley.J.N and Greene.P.D (1967) Trans. Faraday Soc. 62, 2069.

Brune.A and Wagner.J.B.,Jr. (1987) Solid State Ionics 25, 165.

Bunde.A, Dieterich.W and Roman.H.E (1985) Phys. Rev. Lett. 55, 5.

Cain.L.S and Slifkin.L.M (1980) J. Phys. Chem. Solids 41, 173.

Catlow.C.R.A, Corish.J, Diller.K.M, Jacobs.P.W.M and Norgett.N.J (1979) J. Phys. C: Solid State Phys. 12, 451.

Chaklanobis.S, Syal.R.K and Shahi.K (1990) Solid State Ionics 44, 107.

Chandra.S and Rolfe.J (1970 a) Can. J. Phys. 48, 397.

Chandra.S and Rolfe.J (1970 b) Can. J. Phys. 48, 412.

Chandra.S and Rolfe.J (1971) Can. J. Phys. 49, 2098.

Chandra.S (1981) "Superionic Solids", North-Holland Publishing Company, Amsterdam.

Chang.M.R.W, Shahi.K and Wagner.J.B.,Jr. (1984) J. Electrochem. Soc. 131, 1213.

Coleman.D.S and Lacy.P.D.A (1967) Mat. Res. Bull. 2, 935.

Cullity.B.D (1956) "Elements of X- Ray Diffraction", Addition - Wesley Publishing Company Inc.

Dawson.D.K and Barr.L.W (1967) Phys. Rev. Lett. 19, 844.

Deshpande.V.K, Raghuwanshi.F.C and Singh.K (1986) Solid State Ionics 18/19, 378.

Dreyfus.R.W and Nowick.A.S (1962) J. Appl. Phys. 33, 473.

Dudney.N.J (1985) J. Am. Ceram. Soc. 68, 538.

Dudney.N.J (1987) J. Am. Ceram. Soc. 75, 65.

Erofeev.V.N and Hartmann.E (1988) Solid State Ionics 28-30, 241.

Farrington.G.C and Briant.J.L (1978) Mater. Res. Bull. 13, 763.

Fineman.M.A and Wallace.W.E (1948) J. Am. Chem. Soc. 70, 4165.

Frenkel.J (1926) Z. Physik 35, 652.

Friauf.R.J (1972) In "Physics of Electrolytes", (Ed. Hladik.J), vol.1 and 2, Academic Press, New York and London.

Funke.K (1976) Prog. Solid State Chem. 11, 345.

Furton.D.E, Parker.J.M and Wright.P.V (1973) Polymer 14, 589.

Geller.S (1977) In "Solid Electrolytes", (Ed. Geller.S), Springer - Verlag, Berlin.

Ginnings.D.C and Phipps.T.E (1930) J. Am. Chem. Soc. 52, 1340.

Glyde.H.R (1967) Rev. Mod. Phys. 39, 373.

Gorecki.T (1974) Z. Metallkde 65, 426.

Gorecki.T (1974) Z. Metallkde 67, 269.

Gupta.S, Patnaik.S, Chaklanobis.S and Shahi.K (1988) Solid State Ionics 31, 5.

Gupta.S (1988) M.Tech. Thesis, Indian Institute of Technology, Kanpur (India).

Haget.Y, Chanh.N.B, Garin.P and Bonpunt.L (1975) Acta Metall.23, 724.

Haven.Y (1950) Rec. Trav. Chim. Pays-Bas. 69, 1471.

Haven.Y (1957) In "Report of the Conference on Defects in Crystalline Solids held at Bristol in July 1954", p.261, London.

Havesey.von.G and Seith.W (1929) Z. Physik 51, 790.

Holt.J.B, Sockel.H.G and Schmalzried.H (1969) J. Am. Ceram. Soc. 52, 375.

Hong.H.Y (1976) Mat. Res. Bull.11, 173.

Hoodless.I.M, Strange.J.H and Wylde.L.E (1971) J. Phys. C: Solid State Phys. 4, 2737.

Hooper.A (1984) In "Solid State Batteries" (Ed. Sequeira.C.A.C and Hooper.A) Nato ASI series.

Hoshino.H and Shimoji.M (1967) J. Phys. Chem. Solids 28, 1169.

Hu.Y.W, Raistrick.I.D and Huggins.R.A (1976) Mat. Res. Bull. 11, 1227.

Ihara.S, Warita.Y and Suzuki.K (1984) Phys. Stat. Solidi (a)86, 729.

International Critical Tables (1928) vol.IV, p.40-72, McGraw-Hill Book Co. Inc., New York.

Johannesen.O and Mckelvy.M (1985) Solid State Ionics 17, 251.

Johannesen.O and Mckelvy.M (1986) J. Phys. Chem. Solids 47, 265.

Johannesen.O (1987) Proc. of the 6th Int. Conf. on Solid State Ionics, Garmisch- Partenkirchen, FRG, Sept. 6-11, p.1310.

Jow.T and Wagner.J.B.,Jr. (1979) J. Electrochem. Soc. 126, 1963.

Kelting.H and Witt.H (1949) Z. Physik 126, 697.

Kiukkola.K and Wagner.C (1957 a) J. Electrochem. Soc. 104, 308.

Kiukkola.K and Wagner.C (1957 b) J. Electrochem. Soc. 104, 379.

Koch.E and Wagner.C (1937) Z. Phys. Chem. Abt. B38, 295.

Kostopoulos.D, Varotsos.P and Mourikis.S (1975) Can. J. Phys. 53, 1318.

Kurnick.S.W (1952) J. Chem. Phys. 20, 218.

Kurosawa.T (1957) J. Phys. Soc. Japan 12, 338.

Kvist.A and Lunden.A (1965) Z. Naturf. 20a, 235.

Kvist.A (1967) Z. Naturf. 22a, 208.

Laskar.A.L (1984) Materials Science Forum, vol.1, p.59. "Diffusion in solids" (Ed. Murch.G.E), Proc. of the Indo-US Binational workshop, Bombay, Jan. 9-12, 1984.

Laskar.A.L (1989) "Diffusion in Materials" (Ed. Laskar.A.L, Bocquet.J.L, Brebec.G, Monty.C) p.459, Nato ASI series.

LeClaire.A.D (1970) In "Physical Chemistry - An advanced treatise",(Ed. Jost.W) Academic Press. New York, vol. 10.

Liang.C.C (1973) J. Electrochem. Soc. 120, 1289.

Lidiard.A.B (1957) In "Handbuch der physik", (Ed. Flugge.S) vol.20, p.246, Springer-verlag, Berlin.

Lunden.A, Bengtzelius.A, Kaber.R, Nilsson.L, Schroeder.K and Tärneberg.R (1983) Solid State Ionics 9 & 10, 89.

Lunden.A (1986) In "Materials for Solid State Batteries" (Ed. Chowdari.B.V.R and Radhakrishna.S) p.149. World Scientific Publishing Co. Singapore.

Mahan.G.D (1976) Phys. Rev.b14, 780.

Maier.J (1985 a) J. Phys. Chem. Solids 46, 309.

Maier.J (1985 b) Mat. Res. Bull. 20, 383.

Maier.J (1988) Solid State Ionics 28-30, 1465.

Maier.J (1989) In "Science and Technology of Fast ion Conductors", (Ed. Tuller.H.L and Balkanski.M), Plenum Press, p.89.

Malugani.J.P, Wasniewski.A, Doreau.M, Robert.G and Al Rikabi.A (1978) Mat. Res. Bull. 13, 427.

Mapother.D, Crooks.H.N and Maurer.R.J (1950) J. Chem. Phys. 18, 1231.

March.N.H (1980) Phys. Chem. Liq. 10, 1.

Mercier.R, Tachz.M, Malguani.J.P and Robert.G (1985) Solid State Ionics 15, 109.

Mott.N.F and Littleton.M.J (1938) Trans. Faraday Soc. 34, 485.

Nakamura.O, Kodama.T, Ogino.I and Miyake.Y (1976) Jap. Patent 76/106, 683 as cited in Chandra (1981).

Nakamura.O and Goodenough.J.B (1982) Solid State Ionics 7, 119.

Owens.B.B and Argue.G.R (1967) Science 157, 308.

Owens.B.B (1971) In "Advances in Electrochemistry and Electrochemical Engineering" vol.8 (Ed. Tobias.C.W) John Wiley, New York.

Pack.S (1979) Paper 133. Presented at the Electrochemical Society meeting, Los Angeles, California, Oct. 14-19.

Patnaik.S (1987) M.Tech. Thesis, Indian Institute of Technology, Kanpur (India).

Phase Diagram for Ceramists (1964) (Ed. Resser.M.K) Am. Ceram. Soc., Columbus, Ohio (1964) and (1969).

Phipps.T.E and Partridge.E.G (1929) J. Am. Chem. Soc. 51, 1331.

Prakash.G and Shahi.K (1987) Solid State Ionics 23, 151.

Puri.D.S and Verma.M.P (1977) Phys. Rev. B15, 2337.

Reuter.B and Hardel.K (1961) Naturwissenschaften 48, 161.

Reuter.B and Hardel.K (1966) Ber. Bunsenges. Phys. Chem. 70, 82.

Rice.M.J and Roth.W.L (1972) J. Solid State Chemistry 4, 294.

Roberts.R.W and Smith.C.S (1970) J. Phys. Chem. Solids 31, 619.

Roman.H.E, Bunde.A and Dieterich.W (1986) Phys. Rev. B34, 3439.

Roman.H.E and Yossouff.M (1987) Phys. Rev. B36, 7285.

Schamp.H.W and Katz.E (1954) Phys. Rev. 94, 828.

Schiraldi.A, Pezzati.E and Chiodelli.G (1978 a) Z. Physik. Chem. (N.F) 110, 1.

Schiraldi.A, and Pezzati.E (1978 a) Z. Physik. Chem.(N.F) 110, 1.

Schlaikjer.C.R and Liang.C.C (1971) J. Electrochem. Soc. 118, 1447.

Schlaikjer.C.R and Liang.C.C (1971) In "Fast Ion Transport in Solids" (Ed.von Gool.W) p.685, North-Holland.

Schottky.W (1935) Z. Phys. Chem. Abst. B29, 335.

Singh.K, Chandrayan.V.R and Deshpande.V.K (1988) Solid State Ionics 28-30, 228.

Shahi.K (1977) Phys. Stat. Solidi (a)41, 11.

Shahi.K and Wagner.J.B.,Jr. (1981 a) J. Electrochem. Soc. 128, 6.

Shahi.K and Wagner.J.B.,Jr. (1981 b) Phys. Rev. B12, 6417.

Shahi.K and Wagner.J.B.,Jr. (1982 a) J. Phys. Chem. Solids 43, 713.

Shahi.K and Wagner.J.B.,Jr. (1982 b) J. Solid State Chemistry 42, 107.

Shahi.K and Wagner.J.B.,Jr. (1983) J. Phys. Chem. Solids 44, 89.

Shahi.K, Weppner.W and Rabenau.A (1986) Phys. Status. Solidi (a)93, 171.

Shulze.H (1952) Ph.D Thesis, University of Göttingen, as cited by Lidiard (1957).

Smith.C.S and Roberts.R.W (1968) In "Generalised Born Model", Atomic Energy Commision Tech. Rep. No. 1 (contract No. AT 40-I-3802).

Smith.C.S and Roberts.R.W (1968) In "Note on the Murnaghan Equation of State", Atomic Energy Commision Tech. Rep. No. 3 (contract No. AT 40-I-3802).

Smith.C.S and Cain.L.S (1975) J. Phys. Chem. Solids 36, 205.

Süptitz.P and Teltow.J (1967) Phys. Stat. Solidi 23, 9.

Takahashi.T and Yamamoto.O (1966 a) Electrochim. Acta 11, 779.

Takahashi.T and Yamamoto.O (1966 b) Electrochim. Acta 11, 911.

Takahashi.T, Ikeda.S and Yamamoto.O (1972) J. Electrochem. Soc. 119, 477.

Takahashi.T, Yamamoto.O and Ikeda.S (1973) J. Electrochem. Soc. 120, 1431.

Takahashi.T, Yamamoto.O, Yamada.S and Hayashi.S (1979) J. Electrochem. Soc. 126, 1654.

Teltow.J (1949) Ann. Phys. Lpz. 5, 63, 71.

Tubandt.C (1920). Z. Anorg. Allgem. Chem. 110, 234 and 115, 105. as cited by Beniere (1972).

Tuller.H.L (1981) "Mixed conduction in Nonstoichiometric Oxides", p.271, Academic Press, New York.

Uvarov.N.F, Hairetdinov.E.F and Bollmann.W (1989) Cryst. Res. Technology 24, 413.

Varotsos.P, Ludwig.W and Alexopoulos.K (1978) Phys. Rev. B18, 2683.

Varotsos.P (1981) J. Phys.Chem. Solids 42, 405.

Varotsos.P.A, and Alexopoulos.K.D (1986) "Thermodynamics of point defects and their relations with bulk properties", North-Holland, Amsterdam.

Von Alpen.U, Rabenau.A and Talat.G.H (1977) App. Phys. Lett 30, 621.

Wallace.W.E and Flinn.R.A (1953) Nature 172, 681.

Weast.R.C (1980) Handbook of Physics and Chemistry, CRC Press, Boca-Rabon, Florida.

Weiss.K, Jost.W and Oel.J.J (1958) Z. Phys. Chem (N.F) 15, S 429.

Wiedersich.H and Geller.S (1971) In "The Chemistry of Extended Defects in Non-Metallic Solids", (Ed. Eyring.L and O'Keeffe.M) North-Holland, Amsterdam.

Yao.Y.F.Y and Kummer.J.T (1967) J. Inorg. Nucl. Chem. 89, 2453.

APPENDIX A

Input parameters involved in Eq.2.43 to calculate the composition corresponding to the maximum conductivity in the mixed alkali-halide crystals.

	V 10^{-24} cm^3 /molecule	dB/dP	n	k_d/k_o
LiCl	33.941	4.95*	7.85	2.221
LiBr	41.623	5.12*	8.37	2.227
LiI	54.325	5.34*	9.03	2.232
NaCl	44.852	5.38	8.73	2.190
NaBr	53.408	5.44	9.21	2.222
NaI	67.773	5.58	9.79	2.241
KCl	62.274	5.46	9.86	2.282
KBr	71.874	5.47	10.01	2.294
KI	88.198	5.56	10.39	2.305
RbCl	71.288	5.86*	10.57	2.241
RbBr	81.771	5.94*	10.82	2.243
RbI	98.943	6.08*	11.26	2.248

Data were taken from Smith and Cain (1975) and Roberts and Smith (1970).

*Values calculated from the relation dB/dP = (n + 7) / 3 (Smith 1968; Smith and Roberts 1968).

LIST OF PUBLICATIONS

1. "Fast ion transport and phase diagram of the KBr-NaBr system" J. Phys. Chem. Solids, vol. 52, p. 527-536 (1991).

2. "Phase diagram and enhanced electrical transport in KBr-NaBr mixed crystals".
Solid State Ionics, vol. 45, p. 83-91 (1991).

3. "Comments on CBΩ model: Prediction of composition corresponding to maximum conductivity in mixed crystals".
Solid State Communication (in Press).

4. "Effect of iodide ion substitution on the ionic conductivity and the melting point of NaBr".
Communicated to J. Solid State Chemistry.

PHY-1991-D-MAN-ENH